Physiological Chemistry and Physics and Medical NMR Volume 40, 2008

Addresses of Chief Editor and Editorial College

Toshihiko Ubuka
Department of Clinical Nutrition
Kawasaki University of Medical Welfare
Kurashiki, Okayama, 701-0193, Japan

Denys Wheatley
BioMedES
Leggat House, Keithall
Inverurie
Aberdeen AB51 OLX
United Kingdom

EDITORIAL AND BUSINESS OFFICE

Physiological Chemistry and Physics
and Medical NMR
P.O. Box 1452
Melville, New York 11747

Editor In Chief, Dr. Gilbert N. Ling
Managing Editor, Margaret M. Ochsenfeld

SCOPE: PCP provides a forum for the review and publication of reports of original research in a broad range of subjects in biophysics, biochemistry and cellular physiology. Reports of direct applications of basic knowledge to human studies are invited; examples would include the measurements of relaxation times as part of NMR imaging. Single experiments, conclusions based on inadequate statistics, purely speculative papers, and clinical case reports are not accepted.

POLICY: The pages of PCP are accessible to competing viewpoints, interpretations, theories and opinions. Debate is invited via Editorial Comments and Letters to the Editor. Criteria for evaluating submissions include soundness of the study and clarity of presentation, and papers are not rejected on the basis of interpretation or theory, however controversial. PCP believes that scientific issues should be settled by investigation and open debate, not by an appeal to anonymous authority.

PCP attempts to achieve a balance between freedom of expression and constructive peer review. All papers are refereed by reviewers who may remain anonymous, but the Chief Editors make all final decisions, and will handle appeals from authors who feel their papers are unfairly reviewed.

The Editors endeavor to make decisions regarding acceptance or rejection of manuscripts quickly, and have set self-imposed deadlines for doing so. Referees also are given deadlines.

TYPES OF PAPERS: *Regular papers* may be experimental or theoretical. *Short notes, Priority notes* and *Letters* in response to published papers are invited. *Reviews* are desired, but authors are urged to contact an Editor before sending a finished review manuscript. *Symposia* may be published as regular or supplemental issues.

SUBSCRIPTIONS: Price is US$160.00 per volume in the United States and US$170.00 outside the United States. *Physiological Chemistry and Physics and Medical NMR* is published annually, the volume numbered yearly. New subscriptions will start with the first issue of the volume in progress, unless the subscriber directs otherwise. Most back issues are available

Instructions to Authors

SUBMISSIONS: An original and two copies of all material are requested. The original must be typewritten on one side only. Papers should be sent to Dr. Gilbert N. Ling, Editor, P.O. Box 1452, Melville, New York 11747 U.S.A. Manuscripts should be submitted only to this journal and not have been published in part or whole in another publication, except as short preliminary notes, abstracts, or as unpublished work in reviews or symposia. Be sure to keep a copy of your manuscript.

NOTE: Referees will be instructed to destroy their copies of the manuscript after reviewing them. We will return only the original manuscript to you for revision or if rejected.

MANUSCRIPTS: All material should be typed double-spaced with margins at least one inch wide and pages numbered consecutively beginning with the title page. In addition to a paper copy, send an IBM- or Macintosh-compatible file on a CD, in Word or Wordperfect. *Title Page* should include title (of at most 100 characters and spaces), full names of authors as you wish them to be published, names and cities of institutional affiliation(s) of authors and of institution(s) where the studies were performed, and name, full address, telephone number, fax number and e-mail address of the person to whom correspondence, proofs, and reprint requests are to be sent. Four to six *key words* should be listed on the title page. These words will assist indexers. Also, at bottom of title page include a short running title of 40 characters or less.

Abstract should be concise and no longer than 225 words. *Body* may or may not be divided into Introduction, Materials and Methods, Results and Discussion, depending on the length and nature of the paper. Introductory remarks should indicate clearly the significance of the work presented. *References* may be indicated in the text and listed in the reference list in whatever style the author prefers, but we prefer that titles of articles be omitted.

TABLES: Tables should be typewritten on separate sheets and identified by roman numerals (eg. Table III) and titles. Table notes should be keyed by superscript italic lower-case letters (eg. [a]Control). The approximate locations of *tables* and *figures* should be indicated in the margins of the manuscript.

ILLUSTRATIONS: Original artwork or glossy photostatic prints, together with two photocopies (like Xerox copies) should be provided. Each illustration should be numbered on the back in pencil, along with the authors' names. It is preferred that line drawings be made on paper that is not larger than 8½ by 13 inches, and that the drawing be its intended size in the printed paper. Most figures will occupy ½ to full column, that is 5 inches wide. Lines and lettering should be thick enough to allow reduction. A drawing of overall dimension of 8 by 10 inches that will be reduced to ¼ of its original size should be lettered with 18-point (capitals 6 mm high, lower-case 4 mm high) or larger lettering. Glossy photostatic prints are acceptable, and should be attached firmly to a sheet of paper the same size as the manuscript. Postacceptance: If possible send figures as an image file using TIFF or JPEG formatting scanned at a resolution of 600 dpi.

PHOTOGRAPHS: High-quality black and white glossy prints should be provided in triplicate, and may be provided as one print plus two photocopies if the photocopies are sufficiently clear to portray the original to referees. Photographs should be attached firmly to a sheet of paper the same size as the manuscript. Photographs that have been scanned and stored as a TIFF file with a resolution of 300 dpi may also be submitted.

REFEREES: Two anonymous referees will be sought for each paper. Authors are encouraged to suggest names and addresses of suitable referees. Referees will be given deadlines for mailing manuscripts back or phoning reviews in, and will be invited to provide editorial statements or Letters that deal with issues raised by submitted papers.

REPRINTS: An order form is enclosed with proofs sent to authors.

PAGE CHARGES: Page charge is $20.00 per published page. It may be waived in the case of severe international exchange difficulties. An additional charge of $15.00 will be levied for photographs that require screening (eg., E.M's, chromatograms, scans).

Physiol. Chem. Phys. & Med. NMR (2008) *40*: 1–42

Water Proton Relaxation Times of Pathological Tissues

Syed Farooq Akber

Department of Radiation Oncology
Case Western Reserve University
Cleveland, Ohio 44106
Email: Sakber@aol.com

Abstract: The spin-lattice relaxation time (T1) and spin-spin relaxation time (T2) of pathological human and animal tissues are archived to update those already published. The mechanisms for water proton relaxation times of pathological tissues and the dissimilarities in relaxation times between normal and pathological tissues are also briefly reviewed.

KEY WORDS: spin-lattice relaxation time, spin-spin relaxation time, magnetic resonance imaging, water, tissue characterization, paramagnetic ions.

HAZLEWOOD in 1979 (83) compiled very comprehensive data on relaxation times of water protons followed by reports by Bottomley *et al* (37, 38) and Akber (12). In this paper, relaxation data of pathological human and animal tissues are compiled from 1987–2007.

Damadian and his group (54–56) showed that the relaxation times of normal and tumorous tissues are different. Several models, theories and hypotheses were put forth to account for the dissimilarities in relaxation times between normal and malignant tissues. The cause of dissimilarities in normal and pathological tissue relaxation times are not clear but nevertheless, have been attributed to water content, paramagnetic ions, protein content and oxygen content.

Bottomley *et al* (37, 38) have discussed in detail the relaxation rate dependence on frequency, temperature, and excision time, *in vitro* and *in vivo* measurements; therefore, these parameters will not be discussed in this report. Hazlewood (83) has discussed in great detail the relaxation time models to account for the dissimilarities in relaxation time between normal and pathological tissues. Water proton relaxation data of pathological tissues of liver, breast, muscle, heart, brain, kidney, lung, spleen, and miscellaneous tissues are given in Tables II–X. Table I, lists the abbreviations used in tables and text.

TABLE I. ABBREVIATIONS USED IN TABLES AND TEXT

ADD	—	Adductors
AGUSPIO	—	Ultra small supermagnetic iron oxide
ALL	—	Acute Lymphoblastic leukemia
AMI-25	—	Large supermagnetic iron oxide
AML	—	Acute myelogenous leukemia
BCAO	—	Bilateral common carotid artery occlusion
Co	—	Cobalt
$CC1_4$	—	Carbon tetrachloride
Cu	—	Copper
DH	—	Diffuse histiocytic
DLPD	—	Diffuse lymphocytic poorly differentiated
DMD	—	Duchenne muscular dystrophy
DENA	—	Diethylnitrosamine
DTPA	—	Diethylenetriaminepentacetic acid
DVT	—	Deep venous thrombi
EAE	—	Encephalomyelitis
v	—	Frequency at which relaxation times were measured
Fe	—	Iron
Gd	—	Gadolinium
GRA	—	Gracilis
GAS	—	Gastrocnemius
Glu	—	Gluteus maximus
GM	—	Gray matter
Gy	—	Gray
HD	—	Hodgkin's disease
HCC	—	Hepatocelluar carcinima
HCL	—	Hairy cell leukemia
IV	—	In vivo (body temperature of 37 °C)
L	—	Left
M	—	Male
MCA	—	Middle cerebral artery
MLH	—	Mixed lynmpocytic histocytic
MM	—	Multiple Myeloma
Mn	—	Manganese
MnDPDP	—	Manganese-dipyridoxal diphosphate
MS	—	Multiple Sclerosis
MSM	—	Microspheres
N	—	Number of samples
NAA	—	N-acetyl aspartate
NABT	—	Normal Appearing brain tissue
NAWM	—	Normal Appearing White Matter
NHL	—	Non-Hodgkins Lymphoma
NLPD	—	Nodular poorly differentiated lymphocytic
PV	—	Polycythemia Vera
QUAD	—	Vastus taleralis of quadriceps femoris
R	—	Right
RBM	—	Red Bone Marrow
REF	—	Reference
RT	—	Room temperature
SAR	—	Sartorius
SCC	—	Squamous cell carcinoma
SD	—	Standard Deviation
SLE	—	Systemic lupus erythematosus
SPIO-AG	—	Superparamagnetic iron oxide particles
T	—	Temperature at which relaxation measurements were made (°C)
T1	—	Spin-lattice relaxation time in ms
T2	—	Spin-spin relaxation time in ms
TD	—	Tardive dyskinesia
TPPS4	—	Tetraphenylporphine sulfonate
TS	—	Tourette's Syndrome
WM	—	White Matter

TABLE II. LIVER

T1 ± SD (ms)	T2 ± SD (ms)	v (MHz)	N	T	Species	Pathology	Ref	Comments
223		3.4	2	IV	Human	Hepatitis	175	
226		3.4	2	IV	Human	Hepatitis	175	
805		6.3	1	IV	Human	Non Hodgkins lymphoma	194	DLPD (Focal areas)
752		6.3	1	IV	Human	Non Hodgkins lymphoma	194	NLPD
585 ± 160	54 ± 4	15	12	1V	Human	Amyloidosis	27	Before Therapy
690 ± 70	57 ± 6	15	1	1V	Human	Amyloidosis	27	Before Therapy
770 ± 120	55 ± 9	15	1	1V	Human	Amyloidosis	27	Before Therapy
690 ± 85	50 ± 4	15	1	1V	Human	Amyloidosis	27	Before Therapy
760 ± 125	50 ± 6	15	1	1V	Human	Amyloidosis	27	Before Therapy
380 ± 30	58 ± 5	15	1	1V	Human	Amyloidosis	27	After Therapy
410 ± 70	50 ± 8	15	1	1V	Human	Amyloidosis	27	After Therapy
540 ± 75	49 ± 5	15	1	1V	Human	Amyloidosis	27	After Therapy
510 ± 60	48 ± 5	15	1	1V	Human	Amyloidosis	27	After Therapy
512 ± 114	55 ± 7	15	10	IV	Human	Lymphoma	156	Malignant
297 ± 21	42.1 ± 1.6	20	1	1V	Rat	Fibrosis	173	$CC1_4$ Induced
288 ± 28	35.9 ± 3	20	1	1V	Rat	Fibrosis	173	Benign
289 ± 9.9	38.2 ±.9	20	1	1V	Rat	Fibrosis	173	D-galactosamine
309 ± 27	46.8 ± 5.9	20	1	1V	Rat	Fibrosis	173	$CC1_4$ Induced
267 ± 17	44.4 ± 59	20	16	RT	Rat	Hepatitis	201	3 hrs $CC1_4$ induced
321 ± 15	52.3 ± 6.6	20	22	RT	Rat	Hepatitis	201	24 hr $CC1_4$ induced
326 ± 24	51.1 ± 5.9	20	16	RT	Rat	Hepatitis	201	48 hr $CC1_4$ induced
260		20	16	22	Rat	Hepatocarcinoma (Days 30)	167	DENA induced
230		20	14	22	Rat	Hepatocarcinoma (Days 58)	167	DENA induced
300		20	12	22	Rat	Hepatocarcinoma (Days 118)	167	DENA induced
550		20	10	22	Rat	Hepatocarcinoma (Days 131)	167	DENA induced
744 ± 9.0	82.7 ± 2.3	20	8	37	Mice	Hepatoma 129	152	
777 ± 41	75.1 ± 8.7	20	1	IV	Rat	Tumor	173	R3230
655 ± 13	63 ± 1.4	20	1	IV	Rat	Tumor	173	Rat HCC
835 ± 32	63.1 ± 3.1	20	1	IV	Rat	Tumor	173	WR6 lymphoma
655 ± 13	63 ± 2	20	3	37	Rat	Tumor (H-4-II-E)	172	
657 ± 11.2	64.2 ± 3.7	20	3	37	Rat	Tumor (H-4-II-E)	172	After 5 umol of AGUSPIO Administered
657 ± 12.9	63.1 ± 7.5	20	3	37	Rat	Tumor (H-4-II-E)	172	After 5 umol of AMI-25 Administered

TABLE II. LIVER (*continued*)

T1 ± SD (ms)	T2 ± SD (ms)	v (MHz)	N	T	Species	Pathology	Ref	Comments
657 ± 14.1	65.6 ± 4.4	20	3	37	Rat	Tumor (H-4-II-E)	172	After 10 umol of AGUSPIO Administered
651 ± 16.5	63.6 ± 3.5	20	3	37	Rat	Tumor (H-4-II-E)	172	After 10 umol of AMI-25 Administered
803 ± 49.5	75.7 ± 8.1	20	3	37	Rat	Tumor (R3230AC)	172	5 m mol adm. AGUSPIO
796 ± 43.2	75.6 ± 5.8	20	3	37	Rat	Tumor (R3230AC)	172	5 m mol adm AM1-25
777 ± 17.2	76.2 ± 6.0	20	3	37	Rat	Tumor (R3230AC)	172	10 m mol adm AGUSPIO
782 ± 17.6	77.6 ± 6.2	20	3	37	Rat	Tumor (R3230AC	172	10 m mol adm AMI-25
777 ± 41.3	75.1 ± 8.3	20	3	37	Rat	Tumor (R3230 AC)	172	
	90	20	4	IV	Rat	Tumor	139	Implanted tumor
	78	20	4	IV	Rat	Tumor	139	Implanted tumor with dextran magnetite
662 ± 60	44.7 ± 4.5	20	3	IV	Rat	Tumor	178	7 days after implantation
549 ± 128	42.8 ± 4.6	20	3	IV	Rat	Tumor	178	14 days after implantation
753 ± 102	76.7 ± 6.7	20	3	IV	Rat	Tumor	178	21 days after implantation
664 ± 221	67.1 ± 6.3	20	3	IV	Rat	Tumor	178	28 days after implantation
	96.37 ± 31.86	21	15	IV	Human	Cystic Fibrosis	210	
	59.9 ± 13.3	21	31	IV	Human	Diffuse disease	28	
262 ± 16		21	5	IV	Rat	Hepatatis	141	24 h after $CC1_4$ administration
329 ± 14		21	5	IV	Rat	Hepatatis	141	48 h after $CC1_4$ administration
112 ± 10		21	5	IV	Rat	Hepatatis	141	Aministration of 0.25 mmol/kg Gadebonate
108 ± 4		21	5	IV	Rat	Hepatatis	141	Aministration of 0.25 mmol/kg Gadebonate
	57.8 ± 11.3	21	28	IV	Human	Malignant	28	
662 ± 44	45 ± 10	21	10	IV	Human	Malignant	156	Lymphoma
	91.5 ± 4.5	21	7	IV	Rat	Tumor	49	Saline
	92.1 ± 4.4	21	7	IV	Rat	Tumor	49	Mitomycin C
	26.1 ± 3.1	21	7	IV	Rat	Tumor	49	Saline+AMI 25
	23.6 ± 1.2	21	7	IV	Rat	Tumor	49	Mitomycin + AMI 25
1156	78	21	8	IV	Human	Tumor	13	
425 ± 25	41.3 ± 3.7	21.1	3	IV	Rat	Lymphoma	222	
197 ± 34	12.6 ± 1.8	21.1	3	IV	Rat	Lymphoma	222	50 umol Fe/kg (ferrite) administered

835 ± 32	63.1 ± 3.1	21.1	3	IV	Rat	Lymphoma	222	
780 ± 34	59.3 ± 4.9	21.1	3	IV	Rat	Lymphoma	222	50 umol Fe/kg (ferrite) administered
1010 ± 497	143 ± 51	25.1	21	IV	Human	Hemanangioma	61	
569 ± 133	87 ± 17	25.1	13	IV	Human	Hepatoma	61	
691 ± 100	71 ± 21	25.1	24	IV	Human	Metestases	61	
832 ± 234	84 ± 16	25.1	8	IV	Human	Lymphoma	221	Focal
638 ± 184	83 ± 6	25.1	8	IV	Human	Lymphoma	221	Diffuse
876 ± 334	78 ± 32	25.1	8	IV	Human	Lymphoma	221	Mixed
499 ±34	53.4 ±34	40	5	IV	Rat	Hepatitis	207	
205 ±19	35.5 ±1.2	40	4	IV	Rat	Hepatitis	207	MnDPDP
304 ±16	24.7 ±2.5	40	5	IV	Rat	Hepatitis	207	SPIO-AG
437 ±87	93.4 ±2.7	40	5	IV	Rat	Tumor	207	
464 ±77	82.5 ±10.5	40	4	IV	Rat	Tumor	207	MnDPDP
917 ±106	93.6 ±86	40	5	IV	Rat	Tumor	207	SPIO-AG
933 ± 57	90.7 ± 10.6	40	6	40	Rat	Tumor	122	
847 ± 86	91.5 ± 10.8	40	6	40	Rat	Tumor	122	200 umol/kg$MnCl_2$ administered
931 ± 192	58 ± 11	63	15	1V	Human	Cirrohosis	208	
	44.2 ± 8.3	63	10	1V	Human	Diffuse Disease	28	
	142 ± 40	63	50	IV	Human	Hemangioma	146	
	85.6	63	15	IV	Human	Hemangioma	137	
341 ± 38		63	50	IV	Human	Malignant	146	
	43.0 ± 7.6	63	40	1V	Human	Malignant	28	
	61.4 ± 18.5	63	15	IV	Human	Metastases	137	
1191 ± 196	92 ± 6	63	3	IV	Human	Metastases	215	
	71.9 ± 12.01	63	7	IV	Rat	Necrosis	128	Coaglative
	51.03 ± 8.72	63	7	IV	Rat	Necrosis	128	Liquefactive
	76 ± 11	63	50	IV	Human	Tumor	146	
	57.8 ± 6.3	63	7	IV	Rat	Tumor	128	Viable
695 ± 76		86	17	IV	Rat	Fibrosis	2	Induced by C $C1_4$

TABLE III. BREAST

T1 ± SD (ms)	T2 ± SD (ms)	v (MHz)	N	T	Species	Pathology	Ref	Comments
336 ± 60		2.12	1	21	Human	Metastasis	109	
749	57	20	1	IV	Human	Malignant	140	
768	56	20	1	IV	Human	Malignant	140	
645	62	20	1	IV	Human	Malignant	140	
622	67	20	1	IV	Human	Malignant	140	
759	61	20	1	IV	Human	Malignant	140	
764	70	20	1	IV	Human	Malignant	140	
854	80	20	1	IV	Human	Malignant	140	
693	79	20	1	IV	Human	Malignant	140	
444	69	20	1	IV	Human	Malignant	140	
610	50	20	1	IV	Human	Malignant	140	
634	52	20	1	IV	Human	Malignant	140	
685 ± 105	64 ± 9	20	11	34	Human	Malignant	140	Mean value
632	128	20	1	27	Human	Tumor	15	Grade II
699	172	20	1	27	Human	Tumor	15	Grade III
807	296	20	1	27	Human	Tumor	15	Grade III
705	109	20	1	27	Human	Tumor	15	Grade II
504	146	20	1	27	Human	Tumor	15	Grade II
848	120	20	1	27	Human	Tumor	15	Grade II
840	170	20	1	27	Human	Tumor	15	Grade II
642	140	20	1	27	Human	Tumor	15	Grade II
778	94	20	1	27	Human	Tumor	15	Grade II
721	88	20	1	27	Human	Tumor	15	Grade II
574	123	20	1	27	Human	Tumor	15	Grade II
656	112	20	1	27	Human	Tumor	15	Grade III
680	91	20	1	27	Human	Tumor	15	Grade II
611	108	20	1	27	Human	Tumor	15	Grade II
628	92	20	1	27	Human	Tumor	15	Grade III
765	135	20	1	27	Human	Tumor	15	Grade II
616	147	20	1	27	Human	Tumor	15	Grade III
504	202	20	1	27	Human	Tumor	15	Grade II
780	129	20	1	27	Human	Tumor	15	Grade II
678	124	20	1	27	Human	Tumor	15	Grade II
863	107	20	1	27	Human	Tumor	15	Grade II
524	87	20	1	27	Human	Tumor	15	
798	189	20	1	27	Human	Tumor	15	
689 ± 106	135 ± 46	20	23	27	Human	Tumor	15	Mean of 23 patients

TABLE VI. MUSCLE

T1 ± SD (ms)	T2 ± SD (ms)	v (MHz)	N	T	Species	Pathology	Ref	Comments
367 ± 151	84.8 ±	2.6	24	IV	Rat	Tumor	47	
250 ± 35	67.5 ±7.5	2.6	24	IV	Rat	Tumor	47	Viable
339 ± 3		4.5	1	1V	Human	Duchenne Muscular Dystrophy	144	GLU (3-6)
269 ± 20		4.5	4	1V	Human	Duchenne Muscular Dystrophy	144	GLU (7-10)
211 ± 35		4.5	10	1V	Human	Duchenne Muscular Dystrophy	144	GLU (11-14)
185 ± 13		4.5	5	1V	Human	Duchenne Muscular Dystrophy	144	
348 ± 8		4.5	1	1V	Human	Duchenne Muscular Dystrophy	144	QUAD (3-6)
295 ± 13		4.5	4	1V	Human	Duchenne Muscular Dystrophy	144	QUAD (7-10)
270 ± 31		4.5	10	1V	Human	Duchenne Muscular Dystrophy	144	QUAD (11-14)
217 ± 19		4.5	5	1V	Human	Duchenne Muscular Dystrophy	144	ADD (3-6)
300 ± 11		4.5	4	1V	Human	Duchenne Muscular Dystrophy	144	ADD (7-10)
260 ± 31		4.5	10	1V	Human	Duchenne Muscular Dystrophy	144	ADD (11-14)
200 ± 19		4.5	5	1V	Human	Duchenne Muscular Dystrophy	144	
304 ± 14		4.5	4	1V	Human	Duchenne Muscular Dystrophy	144	SAR (3-6)
284 ± 22		4.5	10	1V	Human	Duchenne Muscular Dystrophy	144	SAR (7-10)
284 ± 45		4.5	5	1V	Human	Duchenne Muscular Dystrophy	144	SAR (11-14)
291 ± 15		4.5	4	1V	Human	Duchenne Muscular Dystrophy	144	GRA (3-6)
287 ± 16		4.5	10	1V	Human	Duchenne Muscular Dystrophy	144	GRA (7-10)
278 ± 32		4.5	5	1V	Human	Duchenne Muscular Dystrophy	144	GRA (11-14)
347 ± 4		4.5	1	1V	Human	Duchenne Muscular Dystrophy	144	GAS
301 ± 19		4.5	4	1V	Human	Duchenne Muscular Dystrophy	144	GAS (3-6)
280 ± 23		4.5	10	1V	Human	Duchenne Muscular Dystrophy	144	GAS (7-10)
250 ± 44		4.5	5	1V	Human	Duchenne Muscular Dystrophy	144	GAS (11-14)
793 ± 36	186 ± 76	6.3	4	1V	Human	Aneurysm	164	Bone cyst
890 ±263	92 ± 41	6.3	11	1V	Human	Malignant	164	Fibrous histocytoma
726 ±179	120 ± 15	6.3	4	1V	Human	sarcoma	164	
816 ±285	75 ± 26	6.3	15	1V	Human	sarcoma	164	Osteogenic
803 ±223	61 ± 13	6.3	7	1V	Human	Tumor	164	Gaint cell
1150 ±419	129 ± 55	6.3	8	1V	Human	Tumor	164	
727 ± 121	83.0 ±	7.1	26	IV	Rat	Tumor	47	
632 ±87	65.7	7.1	26	IV	Rat	Tumor	47	Viable

TABLE IV. MUSCLE (*continued*)

	T2 ± SD (ms)	v (MHz)	N	T	Species	Pathology	Ref	Comments
679 ±16	136 ± 3	10	5	IV	Mice	Tumor	42	10 mg/kg Dexamethasone
678 ±18	136 ± 3	10	5	IV	Mice	Tumor	42	10 mg/kg Dexamethasone
610 ±13	116 ± 3	10	5	IV	Mice	Tumor	42	Anesthetized – 4h with Dexmethasone
578 ±18	108 ± 9	10	5	IV	Mice	Tumor	42	Anesthetized – 8h with Dexmethasone
595 ± 14	117 ± 3	10	5	IV	Mice	Tumor	42	Not anesthetised
580 ± 25	102 ± 4	10	5	IV	Mice	Tumor	42	Not anesthetised
780	70	10.7		37	Mice	Tumor	68	
299	58	10.7		37	Mice	Tumor	68	200 mg/kg Mn (III) TPPS4 administered
638 ± 56	56 ± 9	20	3	34	Human	Adenocarcinoma	140	Neck
670		20	5	37	Mice	Adenocarcinoma	120	
790		20	5	37	Mice	Adenocarcinoma	120	
125		20	5	37	Mice	Adenocarcinoma	120	
772 ± 182	59 ± 10	20	6	34	Human	Carcinoma	140	Cheek
978	56	20	1	34	Human	Fibrosarcoma	140	Forearm
975 ± 217	83 ± 23	20	2	34	Human	Fibrosarcoma	140	Leg
445	12	20	1	34	Human	Liposarcoma	140	Forearm
824	77	20	1	34	Human	Sarcoma	140	Wrist
	43.2 ± 6.5	21	31	1V	Human	Diffuse Disease	28	
1013 ± 170	73 ± 30	21	5	IV	Rat	Inflamation	159	Carrageanan-induced
665 ± 127	67 ± 12	21	5	IV	Rat	Inflamation	159	Carrageanan-induced with Gd-DTPA
	44.9 ± 11.7	21	28	1V	Human	Malignant	28	
	33.0 ± 5.6	63	10	1V	Human	Diffuse Disease	28	
	35.9 ± 7.6	63	40	1V	Human	Milignant	28	
860 ± 50	33.3 ± 2.6	63	11	1V	Human	Ischemia	211	Soleus
839 ± 72	32.4 ± 2.4	63	11	1V	Human	Ischemia	211	Gastroemuis
797 ± 47	32.0 ± 2.4	63	11	1V	Human	Ischemia	211	Tibialisanterior
859 ± 68	32.7 ± 2.9	63	11	1V	Human	Ischemia	211	Peroneus Longus
849 ± 59	32.7 ± 2.1	63	11	1V	Human	Ischemia	211	Leg

1660 ± 109		86	6	RT	Chicken	Atrophic	148	
1400 ± 150		86	8	RT	Chicken	Hypertrophic	148	
2044 ± 201	66.8 ± 1.1	124	25	IV	Rat	Tumor	47	
1885 ± 16	54.9 ± 5.3	124	25	IV	Rat	Tumor	47	Viable
898 ± 32	45 ± 0.1	200.1	1	RT	Mice	Tumor	135	
910 ± 4	36 ± 0.1	200.1	1	RT	Mice	Tumor	135	
923 ± 5	35 ± 0.1	200.1	1	RT	Mice	Tumor	135	
969 ± 31	41 ± 0.3	200.1	1	RT	Mice	Tumor	135	
1127 ± 9	39 ± 0.2	200.1	1	RT	Mice	Tumor	135	
956 ± 48	49 ± 0.1	200.1	1	RT	Mice	Tumor	135	0.5 h after photodynamic therapy
1026 ± 11	36 ± 0.1	200.1	1	RT	Mice	Tumor	135	1.5 h after photodynamic therapy
1003 ± 14	39 ± 0.1	200.1	1	RT	Mice	Tumor	135	2.0 h after photodynamic therapy
1359 ± 2	42 ± 0.1	200.1	1	RT	Mice	Tumor	135	4.0 h after photodynamic therapy
1504 ± 3	39 ± 0.2	200.1	1	RT	Mice	Tumor	135	6.0 h after photodynamic therapy
2631 ± 233	47.9 ± 6.1	204	24	IV	Rat	Tumor	47	
2483 ±109	45.4 ± 2.9	204	24	IV	Rat	Tumor	47	Viable

TABLE V. HEART

T1 ± SD (ms)	T2 ± SD (ms)	v (MHz)	N	T	Species	Pathology	Ref	Comments
388 ± 17	65 ± 3	6.38	9	RT	Dog	Ischemic	57	
148 ± 30	44 ± 4	6.38	28	RT	Dog	Ischemic	57	
93 ± 36	43 ± 9	6.38	41	RT	Dog	Ischemic	57	
423 ± 51	44 ± 2	15	6	IV	Dog	Hypoperfused	183	
314 ± 69	45 ± 4	15	6	IV	Dog	Hypoperfused	183	
521 ± 51	49 ± 9	15	3	IV	Dog	Reperfused	182	
794 ± 203	57 ± 6	15	4	IV	Dog	Reperfused	182	
450 ± 52	62 ± 12	15	4	IV	Dog	Reperfused	182	
644 ± 142	53 ± 6	15	6	IV	Dog	Reperfused	182	
386 ± 56	57 ± 6	15	3	IV	Dog	Reperfused	182	
691 ± 49	60.2 ± 9.7	20	8	40	Dog	Infarction	185	
308 ± 82.1	52.6 ± 4	21	6	37	Pig	Infarction	223	
	64 ± 14	25.1	8	1V	Human	Angina	1	Unstable Angina Reversible
	67 ± 21	25.1	7	1V	Human	Angina	1	Unstable Angina Irreversible
	43 ± 11	25.1	5	1V	Human	Angina	1	Stable Angina Reversible
	40 ± 9	25.1	3	1V	Human	Angina	1	Stable Angina Irreversible
	62 ± 18	25.1	4	1V	Human	Infarction	1	Acute MI Reversible
	66 ± 11	25.1	7	1V	Human	Infarction	1	Acute MI Irreversible
1387 ± 63		63.0	4	IV	Human	Amyloidosis	121	
1340 ± 81	81 ± 12	63	9	IV	Hunan	Amyloidosis	91a	
1146 ± 71	72 ± 9	63	9	IV	Human	Amyloidosis	91a	

TABLE VI. BRAIN

T1 ± SD (ms)	T2 ± SD (ms)	v (MHz)	N	T	Species	Pathology	Ref	Comments
348 ± 44		0.84	1	IV	Human	Infarction	138	Onset 1 week
424 ± 62		0.84	1	IV	Human	Infarction	138	Onset 1 week
428 ± 68		0.84	1	IV	Human	Infarction	138	Onset 1 week
428 ± 76		0.84	1	IV	Human	Infarction	138	Onset 1 week
444 ± 98		0.84	1	IV	Human	Infarction	138	Onset 1 week
380 ± 76		0.84	1	IV	Human	Infarction	138	Onset 1 week
488 ± 88		0.84	1	IV	Human	Infarction	138	Onset 1 week
456 ± 68		0.84	1	IV	Human	Infarction	138	Onset 1 week
360 ± 56		0.84	1	IV	Human	Infarction	138	Onset 1 week
534 ± 76		0.84	1	IV	Human	Infarction	138	Onset 1 week
432 ± 52		0.84	10	IV	Human	Infarction	138	Onset 1 week (Mean of 10 patient)
412 ± 64		0.84	1	IV	Human	Infarction	138	Onset 2 week
444 ± 56		0.84	1	IV	Human	Infarction	138	Onset 2 week
452 ± 92		0.84	1	IV	Human	Infarction	138	Onset 2 week
516 ± 148		0.84	1	IV	Human	Infarction	138	Onset 2 week
452 ± 48		0.84	1	IV	Human	Infarction	138	Onset 2 week
556 ± 84		0.84	1	IV	Human	Infarction	138	Onset 2 week
472 ± 53		0.84	6	IV	Human	Infarction	138	Onset 2 week (Mean of 6 patients)
532 ± 156		0.84	1	IV	Human	Infarction	138	Onset 5 week
492 ± 120		0.84	1	IV	Human	Infarction	138	Onset 5 week
460 ± 160		0.84	1	IV	Human	Infarction	138	Onset 5 week
500 ± 148		0.84	1	IV	Human	Infarction	138	Onset 5 week
678 ± 154		0.84	1	IV	Human	Infarction	138	Onset 5 week
576 ± 124		0.84	1	IV	Human	Infarction	138	Onset 5 week
540 ± 78		0.84	6	IV	Human	Infarction	138	Onset 5 week (Mean of 6 patients)
355		0.84	1	IV	Human	Infarction	138	5 month old infarct
435		0.84	1	IV	Human	Infarction	138	3 years old infarct
524		0.84	1	IV	Human	Infarction	138	5 years old infarct
635		0.84	1	IV	Human	Infarction	138	8 years old infarct
928 ± 128		0.84	1	IV	Human	Infarction	138	8 month old infarct
748 ± 320		0.84	1	IV	Human	Infarction	138	1 years old infarct
928 ± 141		0.84	1	IV	Human	Infarction	138	5 years old infarct
836 ± 196		0.84	1	IV	Human	Infarction	138	8 years old infarct

TABLE VI. BRAIN (*continued*)

T1 ± SD (ms)	T2 ± SD (ms)	v (MHz)	N	T	Species	Pathology	Ref	Comments
861 ± 87		0.84	1	IV	Human	Infarction	138	Mean value of 8 month–8 years infarct
441 ± 62	161 ± 13	0.84	14	IV	Human	Tumor	217	
692 ± 92	232 ± 31	0.84	13	IV	Human	Tumor	217	
349		2.12	1	IV	Human	Abscess	226	
116		2.12	1	IV	Human	Abscess	226	With Gd-DTPA administered
446		2.12	1	IV	Human	Glioblastoma	225	
315		2.12	1	IV	Human	Glioblastoma	225	
187		2.12	1	IV	Human	Glioblastoma	225	With Gd-DTPA administered
46		2.12	1	IV	Human	Glioblastoma	225	With Gd-DTPA administered
315 ± 6		2.12	1	21	Human	Meningioma	109	Transitional
551 ± 36		2.12	1	21	Human	Meningioma	109	Angioplastic
382 ± 11		2.12	1	21	Human	Meningioma	109	Hemangiopericytic
311		2.12	1	IV	Human	Meningioma	225	
323		2.12	1	IV	Human	Meningioma	225	
376		2.12	1	IV	Human	Meningioma	225	
281		2.12	1	IV	Human	Meningioma	225	
147		2.12	1	IV	Human	Meningioma	225	With Gd-DTPA administered
71		2.12	1	IV	Human	Meningioma	225	With Gd-DTPA administered
136		2.12	1	IV	Human	Meningioma	225	With Gd-DTPA administered
73		2.12	1	IV	Human	Meningioma	225	With Gd-DTPA administered
369		2.12	1	IV	Human	Metastasis	225	
353		2.12	1	IV	Human	Metastasis	225	
263		2.12	1	IV	Human	Metastasis	225	
34		2.12	1	IV	Human	Metastasis	225	With Gd-DTPA administered
82		2.12	1	IV	Human	Metastasis	225	With Gd-DTPA administered
79		2.12	1	IV	Human	Metastasis	225	With Gd-DTPA administered
285 ± 23		2.12	1	21	Human	Neurioma	109	
354 ± 5		3.4	6	IV	Human	Schizophrenics without TD	29	Basal ganglia (R)
360 ± 5		3.4	6	IV	Human	Schizophrenics without TD	29	Basal ganglia (L)
335 ± 4		3.4	15	IV	Human	Schizophrenics with TD	29	Basal ganglia (R)
330 ± 5		3.4	15	IV	Human	Schizophrenics with TD	29	Basal ganglia (L)
510 ± 200		4.2	5	IV	Human	adenomas	125	Pituitary
480		4.2	1	IV	Human	adenoma	124	Pituitary

310		4.2	1	IV	Human	adenoma	124	Pituitary
390		4.2	1	IV	Human	cyst	125	Colloid
580 ± 100		4.2	11	IV	Human	gliomas	125	High grade
750 ± 140		4.2	4	IV	Human	gliomas	125	Low grade
590		4.2	1	IV	Human	Glioblastoma	124	
360		4.2	1	IV	Human	Glioblastoma	124	
680		4.2	1	IV	Human	Glioblastoma	124	
310		4.2	1	IV	Human	Glioblastoma	124	With Gd-DTPA
740		4.2	1	IV	Human	Hemangioblastoma	125	
470 ± 60		4.2	9	IV	Human	Meningiomes	125	
500		4.2	1	IV	Human	Meningioma	124	
520		4.2	1	IV	Human	Meningioma	124	
350		4.2	1	IV	Human	Meningioma	124	
320		4.2	1	IV	Human	Meningioma	124	With Gd-DTPA
470		4.2	1	IV	Human	Meningioma	124	
290		4.2	1	IV	Human	Meningioma	124	With Gd-DTPA
520		4.2	1	IV	Human	Metastasis	124	
320		4.2	1	IV	Human	Metastasis	124	With Gd-DTPA
570		4.2	1	IV	Human	Neurinoma	124	Acoustic
510		4.2	1	IV	Human	Neurinoma	124	Acoustic
200		4.2	1	IV	Human	Neurinoma	124	Acoustic With Gd-DTPA
610 ± 140		4.2	4	IV	Human	Neurinoma	124	Acoustic
520 ± 80		4.2	1	IV	Human	Tumor	124	
300 ± 80		4.2	1	IV	Human	Tumor	124	With Gd-DTPA
	98.6 ± 7.8	6.3	19	IV	Human	Multiple Sclerosis	14	
500	120	6.4	1	IV	Monkey	Encephalomyelitis	197	Postmortem
460	110	6.4	1	IV	Monkey	Encephalomyelitis	197	Postmortem
540	260	6.4	1	IV	Monkey	Encephalomyelitis	197	Postmortem
600	270	6.4	1	IV	Monkey	Encephalomyelitis	197	Postmortem
1221		10.7	1	22	Human	Astrocytoma	103	
1634		10.7	1	22	Human	Astrocytoma	103	
523 ± 36	71 ± 6	10.7	18	20	Pig	Cord	110	Acute EAE
495 ± 45	70 ± 7	10.7	18	20	Pig	Cord	110	Relapsing EAE
469 ± 30	68 ± 4	10.7	18	20	Pig	Cord	110	Remitting EAE
580 ± 44	67 ± 5	10.7	18	20	Pig	Brain stem	110	Acute EAE
557 ± 45	69 ± 7	10.7	18	20	Pig	Brain stem	110	Relapsing EAE
556 ± 36	70 ± 3	10.7	18	20	Pig	brain stem	110	Remitting EAE
489 ± 33	66 ± 4	10.7	18	20	Pig	Cerebellium	110	Acute EAE
467 ± 30	62 ± 4	10.7	18	20	Pig	Cerebellium	110	Relapsing EAE
473 ± 22	67 ± 5	10.7	18	20	Pig	Cerebellium	110	Remitting EAE
1445		10.7	1	22	Human	Glioma	103	

TABLE VI. BRAIN (*continued*)

T1 ± SD (ms)	T2 ± SD (ms)	v (MHz)	N	T	Species	Pathology	Ref	Comments
1591		10.7	1	22	Human	Glioma	103	
1660		10.7	1	22	Human	Hemangioblastoma	103	
578 ± 41	68 ± 4	10.7	18	20	Pig	Encephalomyelitis	110	Acute EAE
542 ± 34	69 ± 7	10.7	18	20	Pig	Encephalomyelitis	110	Relapsing EAE
544 ± 22	73 ± 3	10.7	18	20	Pig	Encephalomyelitis	110	Remitting EAE
725 ± 40	218 ± 34	12	10	IV	Human	Adenoma	105	Pituitary
728 ± 54	175 ± 21	12	15	IV	Human	Adenoma	104	Pituitary
869 ± 125	218 ± 34	12		IV	Human	Astrocytoma	105	
886	210	12	1	IV	Human	Angiomatus	104	
933 ± 69	515 ± 78	12	6	IV	Human	Cramiopharyngioma	104	
884 ± 93	218 ± 34	12		IV	Human	Craniopharyngioma	105	
745 ± 80	218 ± 34	12		IV	Human	edema	105	
730 ± 91	287 ± 72	12	17	IV	Human	edema	104	Perifocal
728 ± 54	175 ± 21	12	15	IV	Human	edenoma	104	Pituitary
768 ± 78	167 ± 31	12	15	IV	Human	Endotheliomatous	104	
780 ± 60	218 ± 34	12		IV	Human	Ependymona	105	
698 ± 78	135 ± 26	12	2	IV	Human	Fibrous	104	
766+60	218 ± 34	12		IV	Human	Glioblastoma	105	
442 ± 94	218 ± 34	12		IV	Human	Hematoma	105	
765 ± 95	165 ± 35	12	32	IV	Human	Meningioma	104	
767 ± 93	218 ± 34	12		IV	Human	Meningioma	105	
696 ± 91	176 ± 23	12	12	IV	Human	Metastases	105	
895 ± 65	207 ± 25	12	15	IV	Human	Neuroma	105	
816 ± 170	238 ± 57	12	4	IV	Human	Obligoastrocytoma	105	
714	176	12	1	IV	Human	Psammoma	104	
959 ± 88	210 ± 27	12	7	IV	Human	Regressive	104	
723 ± 84	143 ± 37	12	4	IV	Human	Transitional	104	
1142 ± 206	99 ± 13	15	7	IV	Human	meningioma	219	
450 ± 79	93 ± 7	15	7	IV	Human	meningioma	219	After Gd-DTPA administration
1778 ± 832	113 ± 16	15	5	IV	Human	Neuroma	219	
425 ± 83	91 ± 16	15	5	IV	Human	Neuroma	219	After Gd-DTPA administration
735 ± 124	188 ± 77	21	22	IV	Human	Tumor	92	
670 ± 189	276 ± 214	21	22	IV	Human	Tumor	92	
709 ± 151	229 ± 159	21	22	IV	Human	Tumor	92	Mean value

980 ±80		41	5	21	Cat	Edema	67	
	396 ± 20	63	10	IV	Human	Adenoma	114	Pituitary
	337 ± 16	63	10	IV	Human	Adenoma	114	Pituitary
	60.52 ± .15	63	14	IV	Human	Amygdala (L)	163	
	62.25 ± 4.18	63	14	IV	Human	Amygdala (R)	163	
	363 ± 12	63	10	IV	Human	Astrocytoma I-II	114	
	180 ± 5	63	10	IV	Human	Astrocytoma I-II	114	
	155 ± 5	63	10	IV	Human	Astrocytoma I-II	114	
	105 ± 3	63	10	IV	Human	Astrocytoma III-IV	114	
	172 ± 10	63	10	IV	Human	Astrocytoma III-IV	114	
	57.42 ± 4.02	63	14	IV	Human	Caudate-TS	163	
	59.8 ± 4.46	63	14	IV	Human	Caudate-TS	163	
	51.91 ± 4.28	63	14	IV	Human	corpus callosum	163	Anterior
	55.31 ± 4.18	63	14	IV	Human	corpus callosum	163	Posterior
	55.49 ± 5.09	63	14	IV	Human	cingulate gray (L)	163	
	59.06+5.41	63	14	IV	Human	cingulate gray (R)	163	
	52 ± 5.74	63	14	IV	Human	cingulate white (L)	163	
	55.72 ± 7.99	63	14	IV	Human	Cingulate white (R)	163	
	260 ± 11	63	10	IV	Human	Craniopharyngioma	114	
	366 ± 15	63	10	IV	Human	Craniopharyngioma	114	
1314	145	63	1	IV	Human	Edema	36	
1032	158	63	1	IV	Human	Edema	36	
1649	218	63	1	IV	Human	Edema	36	
1249	140	63	1	IV	Human	Edema	36	
1116	163	63	1	IV	Human	Edema	36	
1130	165	63	1	IV	Human	Edema	36	
1220	145	63	1	IV	Human	Edema	36	
	46.37 ± 4.5	63	14	IV	Human	Globus pallidus (L)	163	
	49.11 ± 3.65	63	14	IV	Human	Globus pallidus (R)	163	
	81.7 ± 7.15	63	54	IV	Human	Gray Matter	189	SLE
	59.16 ± 2.81	63	14	IV	Human	Insular cortex (L)	163	
	65.58 ± 5.96	63	14	IV	Human	Insular cortex (R)	163	
	107.2 ± 12.1	63	31	IV	Human	Lesions reversible	189	SLE
	84.67 ± 10.6	63	133	IV	Human	Lesions not reversible	189	SLE
	139 ± 4	63	10	IV	Human	Meningioma	114	
1213 ± 258	271 ± 61	64	12	IV	Human	Edema	181	
972 ± 124	109 ± 17	64	12	IV	Human	GM	181	With brain tumor
599 ± 90	87 ± 7	63	12	IV	Human	WM	181	With brain tumor
1168 ± 212	191 ± 95	64	12	IV	Human	Tumor	181	
	144.4 ± 38.9	63		IV	Human	Multiple sclerosis	196	Posterior fosa
	153.7 ± 15.8	63		IV	Human	Multiple sclerosis	196	Cord

TABLE VI. BRAIN (*continued*)

T1 ± SD (ms)	T2 ± SD (ms)	v (MHz)	N	T	Species	Pathology	Ref	Comments
	253.7 ± 78.7	63		IV	Human	Multiple sclerosis	196	periventicular
	60.34 ± 3.1	63	34	IV	Human	Multiple sclerosis	73	NAWM
1103 ± 93.6	104 ± 18.4	63	4	IV	Human	Multiple sclerosis	18	Total white matter
1022 ± 132.4	97 ± 12.1	63	4	IV	Human	Multiple sclerosis	18	NAWM
1428 ± 266	139 ± 16.9	63	4	IV	Human	Multiple sclerosis	18	Abnormal WM
1201 ± 78.2	123 ± 9.9	63	4	IV	Human	Multiple sclerosis	18	Abnormal WM
	55.85 ± 4.36	63	14	IV	Human	Occipital white Matter (L)	163	
	60.27 ± 4.29	63	14	IV	Human	Occipital white Matter (R)	163	
	51.16 ± 3.3	63	14	IV	Human	Putamen (L)	163	TS
	54.86 ± 4.09	63	14	IV	Human	Putamen (R)	163	TS
1168 ± 212	191 ± 90	63	12	IV	Human	Tumor	181	
3036	317	63	1	IV	Human	Tumor	36	glioblastoma
1159	103	63	1	IV	Human	Tumor	36	anaplastic astrozytom
1718	205	63	1	IV	Human	Tumor	36	glioblastoma
1135	133	63	1	IV	Human	Tumor	36	Oligodendroglioma
1500	174	63	1	IV	Human	Tumor	36	Anaplastic astrozytoma
	47.67 ± 2.32	63	14	IV	Human	Red nucleus (L)	163	
	48.27 ± 3.23	63	14	IV	Human	Red nucleus (R)	163	
	45.22 ± 4	63	14	IV	Human	Substantia nigra (L)	163	
	48.66+4.05	63	14	IV	Human	Substantia nigra (R)	163	
	54.18 ± 2.62	63	14	IV	Human	Thalamus (L)	163	posterior
	53.67 ± 3.57	63	14	IV	Human	Thalamus (R)	163	posterior
	53.67 ± 2.71	63	14	IV	Human	Thalamus (L)	163	anterior
	56.01 ± 3.36	63	14	IV	Human	Thalamus (R)	163	anterior
595 ± 19		63	13	IV	Himan	NWH –MS	18b	NAA conc 6.93+0.63
710 ± 87		63	14	IV	Human	NAWM-MS	18b	NAA conc 6.15+0.56
848 ± 64		63	9	IV	Human	MS	18b	Hypointensive
985 ± 64		63	2	IV	Human	MS	18b	Acute Hypointensive
1043 ± 186			15	IV	Human	MS	18b	Severely Hypointensive
	52.24 ± 2.67	63	14	IV	Human	Left frontal white	163	
	55.3 ± 4.1	63	14	IV	Human	Right frontal white	163	
	81.7 ± 7.15	63	54	IV	Human	Systemic lupus erythematosus	189	GM
	66.72 ± 2.7	63	54	IV	Human	Systemic lupus erythematosus	189	WM-subcortical
	67.06 ± 3.48	63	54	IV	Human	Systemic lupus erythematosus	189	WM-deep

	107.2 ± 12.1	63	31	IV	Human	Systemic lupus erythematosus	189	Reversible lession
	84.67 ± 10.6	63	133	IV	Human	Systemic lupus erythematosus	189	Non reversible lession
	181.6 ± 63.6	63	12	IV	Human	Systemic lupus erythematosus	189	Infarct
617		63		IV	Human	Cysterical cyst	97a	
161		63		IV	Human	Tuberculomad	97a	
490 ± 20		64	32	IV	Human	WM obsessive compulsive	80	
463.4 ± 11.04	94.0 ± 2.79	80.0	9	IV	Rats	Allergic encephalo Acute	226	
425.5 ± 8.73	82.7 ± 0.98	80.0	6	IV	Rats	Asymptomatic	226	
466.7 ± 12.8	87.1 ± 1.85	80.0	7	IV	Rats	Asymptomatic	226	
418.6 ± 6.6	83.0 ± 1.13	80.0	5	IV	Rats	Demyelinating Early	226	
467.3 ± 6.11	89.9 ± 1.19	80.0	13	IV	Rats	Demyelinating Acute	226	
479.4 ± 17.75	91.0 ± 2.92	80.0	5	IV	Rats	EAE Early	226	
462.4 ± 4.05	88.0 ± 2.07	80.0	5	IV	Rats	Myelitis Late	226	
468 ± 6.61	90.7 ± 1.01	80.0	12	IV	Rats	Asymptomatic	226	
467.7 ± 8.46	94.2 ± 2.06	80.0	12	IV	Rats	Symptomatic	226	
	133 ± 4	197.0	12	37	Cat	Edema	87	
	94 ± 4	197.0	12	37	Cat	Tumor	87	
1200 ± 1	58 ± 2	197.4	9		Rat	C6 glioma	168	
1312 ± 107	89 ± 3	197.4	5	IV	Human	Glioma	224	
1284 ± 86	87 ± 7	197.4	5	IV	Human	Neuroblastoma	224	
1338 ± 85	86 ± 9	197.4	5	IV	Human	Schwannoma	224	
1311 ± 98	87 ± 7	197.4	5	IV	Human		225	
	144 ± 2.2	200	1	IV	Human	Astrocytoma	174	grade IV
1770 ± 131	97 ± 12	200	4	RT	Rat	GM	143	24 h after cold injury
1625 ± 75	83 ± 6.1	200	4	RT	Rat	GM	143	1 week after cold injury
	140 ± 2.1	200	1	IV	Human	Multiple Sclerosis	174	Chronic plaque
1725 ± 199	92.8 ± 8.8	200	4	RT	Rat	WM	143	24 h after cold injury
1604 ± 114	83.4 ± 2.7	200	4	RT	Rat	WM	143	1 week after cold injury
2020 ± 51		360	20	25	Rat	T9 glioma	95	
1820 ± 68	120 ± 23	360		25	Rat	Ischemic @ 30 min	96	BCAO
1770 ± 51	114 ± 22	360		25	Rat	Ischemic @ 60 min	96	BCAO
1820 ± 85	111 ± 16	360		25	Rat	Ischemic @ 120 min	96	BCAO
1800 ± 143	104 ± 19	360		25	Rat	Ischemic @ 180 min	96	BCAO
2030 ± 80	62 ± 20	360		IV	Mouse	U87 High grade glial tumor	198a	
2062 ± 60		294	4	IV	Rat	Ipsilateral cortex	18a	MCA occlusion
1811 ± 28		294			Rat	Ischemia onset + 1 hr	18a	
2600 ± 38		294		IV	Rat	Contralateral	18a	
1007 ± 18		294		IV	Rat	Ischemia onset + 2 hr	18a	
1027 ± 74				IV	Rat	NABT	79a	

TABLE VII. KIDNEY

T1 ± SD (ms)	T2 ± SD (ms)	v (MHz)	N	T	Species	Pathology	Ref	Comments
446.5 ± 90.6	115.9 ± 61.5	4.2	7	IV	Human	Angiomyolipoma	200	
468.5 ± 96.3	165.8 ± 52.1	4.2	12	IV	Human	cancer	200	Renal cell
362.8 ± 40.5	92.5 ± 21.8	4.2	8	IV	Human	cancer	200	Renal pelvic
352.2	81.2	4.2	1	IV	Human	Tumor	200	
386 ± 12	58 ± 3	6.38	24		Dog	Ischemic	57	4 day occlusion
388 ± 17	65 ± 3	6.38	24		Dog	Ischemic	57	4 day occlusion
433 ± 20	75 ± 6	6.38	24		Dog	Ischemic	57	4 day occlusion
352 ± 29		15.0	10	37	Rat	Diabetes	136	Cortex - On set 8 days
415 ± 25		15.0	6	37	Rat	Diabetes	136	Outer Medular - On set 8 days
598 ± 56		15.0	8	37	Rat	Diabetes	136	Inner Med On set 8 days
337 ± 12		15.0	16	37	Rat	Diabetes	136	Cortex - On set 12 days
404 ± 36		15.0	12	37	Rat	Diabetes	136	Outer Medular On set 12 days
553 ± 46		15.0	10	37.	Rat	Diabetes	136	Inner Med - On set 12 days
638 ± 168	109 ± 41	20	25	IV	Human	Carcinoma	199	
1182 ± 164 (R)	112 + 18	86	10	IV	Mice	Polycystic disease	212	
1098 ± 69 (L)	98 ± 18	86	10	IV	Mice	Polycystic disease	212	
772 (R)	62	86	2	IV	Mice	Polycystic disease	212	Age 9 days
784 ± 63 (R)	122 ± 34	86	4	IV	Mice	Polycystic disease	212	Age 30 days
797 ± 157 (L)	122 ± 12	86	4	IV	Mice	Polycystic disease	212	Age 30 days
1048 ± 71 (R)	86 ± 30	86	4	IV	Mice	Polycystic disease	212	Age 60 days
1279 ± 408 (L)	94 ± 18	86	4	IV	Mice	Polycystic disease	212	Age 60 days

TABLE VIII. LUNG

T1 ± SD (ms)	T2 ± SD (ms)	v (MHz)	N	T	Species	Pathology	Ref	Comments
328 ± 28		2.12	1	21	Human	Metastasis	109	Cancer
950 ± 59		2.12	1	21	Human	Metastasis	109	Cancer
566+117	92+29	20	99	40	Human	Lymphnodes	76	Benign
640+138	105+26	20	99	40	Human	Lymphnodes	76	Malignant
605 ± 133.7	32.3 ± 2.95	20	8	RT	Mice	Bleomycin induced fibrosis	204	
668 ± 105.7	36.2 ± 3.75	20	4	RT	Mice	Bleomycin induced fibrosis	204	
613 ± 126.36	54.6 ± 20.71	20	18	RT	Mice	Bleomycin Chronic fibrosis	204	
884+28 (R)	64.2+3.1	64	8	RT	Rat	Radiation induced phneumonitis	153	0.8 days after irradiation
871+22 (L)	63.0+2.6	64	8	RT	Rat	Radiation induced phneumonitis	153	0.8 days after irradiation
875 ± 11 (R)	60.9 ± 2.2	64	9	RT	Rat	Radiation induced phneuomits	153	2 days after irradiation
871 ± 22 (L)	61.1 ± 2.6	64	9	RT	Rat	Radiation induced phneuomits	153	2 days after irradiation
877 ± 9 (R)	63.7 ± 3.4	64	8	RT	Rat	Radiation induced phneuomits	153	7 days after irradiation
881 ± 2 (L)	60.9 1.7	64	8	RT	Rat	Radiation induced phneuomits	153	7 days after irradiation
866 ± 25 (R)	65.8 ± 2.9	64	8	RT	Rat	Radiation induced phneuomits	153	14 days after irradiation
864 ± 14 (L)	64.0 ± 3.5	64	8	RT	Rat	Radiation induced phneuomits	153	14 days after irradiation
844 ± 22 (R)	71.6 ± 3.4	64	8	RT	Rat	Radiation induced phneuomits	153	28 days after irradiation
878 ± 16 (L)	64.9 ± 2.4	64	8	RT	Rat	Radiation induced phneuomits	153	28 days after irradiation
852 ± 25 (R)	70.4 ± 3.4	64	8	RT	Rat	Radiation induced phneuomits	153	56 days after irradiation
883 ± 27 (L)	65.5 ± 2.3	64	8	RT	Rat	Radiation induced phneuomits	153	56 days after irradiation
892 ± 19 (R)	66.8 ± 2.3	64	8	RT	Rat	Radiation induced phneuomits	153	84 days after irradiation
909 ± 23 (L)	63.9 ± 1.9	64	8	RT	Rat	Radiation induced phneuomits	153	84 days after irradiation
874 ± 26 (R)	62.9 ± 1.1	64	8	RT	Rat	Radiation induced phneuomits	153	140 days after irradiation
902 ± 24 (L)	61.4 ± 1.2	64	8	RT	Rat	Radiation induced phneuomits	153	140 days after irradiation
812 ± 19 (R)	62.1 ± 4.1	64	8	RT	Rat	Radiation induced phneuomits	153	182 days after irradiation
872 ± 18 (L)	62.4 ± 2.2	64	8	RT	Rat	Radiation induced phneuomits	153	182 days after irradiation
815 ± 128		64	32	IV	Human	SCC	216a	Sqamous cell carcinoma
712 ± 117		64	32	IV	Human	SCC	216a	Following Radiation & Chemo
787 ± 139		64	29	IV	Human	SCC	216a	Second Rad & Chemo
549 ± 18		64		IV	Human	Hyperblastic lymphones	216a	
924+116		64		IV	Human	Malignant SCC lymphonodes	216a	
854 ± 23				IV	Human	Inflamation	216a	

TABLE VIII. LUNG (*continued*)

T1 ± SD (ms)	T2 ± SD (ms)	v (MHz)	N	T	Species	Pathology	Ref	Comments
785 ± 116		64		IV	Human	Residual Lymphonodes	216a	Following First Rad & Chem Tx
731 ± 71		64		IV	Human	Residual Lymphonodes	216a	Following Second Rad & Chem Tx
	66.3 ± 2.3	64		IV	Rat	3 days after Tx	192	Co-60 (20 Gy)
	155 ± 11	64		IV	Rat	1 day after Tx	192	Co-60 (20 Gy)
1430 ± 21	109.9 ± 4.1	100	3	25	Human	Adenocarinoma	190	Poorly differentiated
973 ± 36	83.8 ± 18.5	100	5	25	Human	Adenocarinoma	190	Well differentiated
1389	95.0	100	1	25	Human	Carcinoid	190	
1273 ± 33	112.6 ± 39.8	100	3	25	Human	Small cell carcinoma	190	
1280 ± 79	104.7 ± 28.9	100	12	25	Human	Squamous cell carcinoma	190	

TABLE IX. SPLEEN

T1 ± SD (ms)	T2 ± SD (ms)	v (MHz)	N	T	Species	Pathology	Ref	Comments
409		6.3	1	IV	Human	Diffuse Histiocytic	194	DH :Nodular poorly differentiated
682		6.3	1	IV	Human	Diffuse lymphocytic	194	poorly differentiated (DLPD)
849	60	6.3	1	IV	Human	Hodgkins disease	194	
784	30	6.3	1	IV	Human	Hodgkins disease	194	
381	65	6.3	1	IV	Human	Hodgkins disease	194	
515	66	6.3	1	IV	Human	Hodgkins disease	194	
592	100	6.3	1	IV	Human	Hodgkins disease	194	
786		6.3	1	IV	Human	Mixed lymphocytic histiocytic	194	MLH
952		6.3	1	IV	Human	NLDP	194	
971 ± 146	76 ± 8	15	9	IV	Human	Malignant lymphoma	156	
791 ± 159	64 ± 10	15	9	IV	Human	Malignant lymphoma	156	
787	77	15	9	IV	Human	Malignant lymphoma	156	Low intensity image
896 ± 68	95 ± 3	15	9	IV	Human	Malignant lymphoma	156	Surrounding spleen tissue
1100 ± 36	74 ± 9	15	12	IV	Human	Amyloidis	27	
609 ± 15	62.2 ± 1.6	20	7	37	Mice	L1210 Leukemia	152	
1662 ± 981	58+11	21	7	IV	Human	Malignant Lymphoma	156	
1179 ± 360	55+10	21	7	IV	Human	Malignant Lymphoma	156	
1181	54	21	7	IV	Human	Malignant Lymphoma	156	
1737 ± 138	64 ± 1	21	7	IV	Human	Malignant Lymphoma	156	
691 ± 50.4	51 ± 2.5	40	10	40	Rat	Lymphoma	123	1 h after 20umol/kg MSM administered
1017 ± 86.4	79.9 ± 5	40	10	40	Rat	Flank tumors	123	1 h after 20umol/kg MSM administered
1045 ± 59.6	94.4 ±.2	40	10	40	Rat	Tumors	123	1 h after 20umol/kg MSM administered
1148 ± 243	90 ± 17	63	5	IV	Human	Hyperplasia	209	Benign
1385 ± 370	68 ± 21	63	5	IV	Human	Hypertension	209	Portal
1484 ± 144	91 ± 8	63	5	IV	Human	Lymphoproliferative	209	
1079 ± 46	70 ± 28	63	5	IV	Human	Myeloproliferative	209	

TABLE X. MISCELLANEOUS TISSUE

T1 ± SD (ms)	T2 ± SD (ms)	v (MHz)	N	T	Species	Pathology	Ref	Comments
					ADRENAL			
	88 ± 21	21	30	IV	Human	Adenomas	79	
	110 ± 19	21	18	IV	Human	Malignant	79	
					APPENDIX			
527 ± 15	68 ± 5	10	10	37	Human	Appendicitis	97	
					BONE MARROW			
971	85	63	8	IV	Human	Polycythemia	99	
499 ± 75	103 ± 25	6..3	16	IV	Human	Malignant	198	
439 ± 17	119 ± 23	6.3	10	IV	Human	Malignant	198	
633 ± 66	57 ± 4	15	1	IV	Human	HD	155	
1246 ± 17	56 ± 8	15	1	IV	Human	HCL	155	
325 ± 51	51 ± 6	15	1	IV	Human	Malignant	155	After irradiation (20–40 Gy)
242 ± 25	51 ± 7	15	1	IV	Human	Malignant	155	Mean Value
493 ± 117	55 ± 4	15	3	IV	Human	Malignant	155	Mean Value
879 ± 324	59 ± 4	15	3	IV	Human	Malignant	155	
759 ± 144	63 ± 5	15		IV	Human	NHL	155	
477 ± 148	57 ± 3	15		IV	Human	NHL	155	60–70% cellurity
518 ± 117	52 ± 1	15		IV	Human	RBM	155	60% cellurity
1093 ± 316	80 ± 10	21	2	IV	Human	ALL	155	
975 ± 67	68 ± 10	21	2	IV	Human	AML	155	
916 ± 220	85 ± 9	21	1	IV	Human	HCL	155	
722 ± 102	78 ± 13	21	1	IV	Human	MM	155	50% cellurity
287 ± 50	55 ± .7	21	21	IV	Human	Malignant	155	
1048 ± 212	72	21	17	IV	Human	Malignant	155	Mean value
574 ± .l40	61 ± 8	21	6	IV	Human	Malignant	155	Mean value
349±29	63 ± 3	21	3	IV	Human	Malignant	155	After irradiation (20–40 Gy)
110 ± 215	76 ± 15	21	8	IV	Human	NHL	155	
553 ± 86	59 ± 4	21	2	IV	Human	NHL	155	50–60% cellurity
1198 ± 355	62 ± .7	21	1	IV	Human	PV	155	
920 ± 289	60 ± 4	21	3	IV	Human	RBM	155	
590 ± 222	57±.l	21	1	IV	Human	RBM	155	50–60% cellurity
438 ± 67	58 ± 3	21	1	IV	Human	RBM	155	40% cellurity
336 ± .42	61 ± .8	63	1	IV	Human	AML	203	

363 ± 15	64 ± 3	63	1	IV	Human	AML	203	
379.± 23	84 ± 3	63	1	IV	Human	AML	203	
365. ± 10	76 ± 7	63	1	IV	Human	AML	203	
423 ± 11	62 ± .6	63	1	IV	Human	AML	203	
314 ± 35	61 ± 4	63	1	IV	Human	AML	203	
413 ± 48	47.7 ± 6.7	63	4	IV	Human	Anemia	195	
935		63	1	IV	Human	Aplasia	100	
1790		63	1	IV	Human	Aplasia	100	
1530.1	38.6	63	17	IV	Human	Epiphysis	76a	Anorexia Nervosa
1469.1	45.2	63	12	IV	Human	Femur Diaphysis	76a	Anorexia Nervosa
1068.1	40.4	63	18	IV	Human	Lumbar spine	76a	Anorexia Nervosa
1137		63	1	IV	Human	Aplona	100	
910		63	1	IV	Human	Aplona	100	
1085		63	1	IV	Human	Aplona	100	
771 ± 164	43.4 ± 6.3	63	15	IV	Human	Bone Marrow disorder	195	Mean value
2341 ± 514	51.3 ± 3.7	63	3	IV	Human	Hodgkins disease	195	
1209		63	1	IV	Human	Leukemia	100	
60		63	1	IV	Human	Leukemia	100	
1025		63	1	IV	Human	Leukemia	100	Partial Remission
935		63	1	IV	Human	Leukemia	100	
1145		63	1	IV	Human	Leukemia	100	
598		63	1	IV	Human	Leukemia	100	
495		63	1	IV	Human	Leukemia	100	Complete remission
1090		63	1	IV	Human	Leukemia	100	Complete remission
672		63	1	IV	Human	Leukemia	100	
1355		63	1	IV	Human	Leukemia	100	
945		63	1	IV	Human	Leukemia	100	
1160		63	1	IV	Human	Leukemia	100	
569		63	1	IV	Human	Leukemia	100	Partial Remission
1040		63	1	IV	Human	Leukemia	100	
1790		63	1	IV	Human	Leukemia	100	
1160		63	1	IV	Human	Leukemia	100	
569		63	1	IV	Human	Leukemia	100	Partial Remission
1040		63	1	IV	Human	Leukemia	100	
1020		63	1	IV	Human	Leukemia	100	
830		63	1	IV	Human	Leukemia	100	
655		63		IV	Human	Leukemia	100	
550		63	1	IV	Human	Leukemia	100	
910		63	1	IV	Human	Leukemia	100	
1275		63	1	IV	Human	Leukemia	100	

TABLE X. MISCELLANEOUS TISSUE (*continued*)

T1 ± SD (ms)	T2 ± SD (ms)	v (MHz)	N	T	Species	Pathology	Ref	Comments
865		63	1	IV	Human	Leukemia	100	
1095		63	1	IV	Human	Leukemia	100	
1135		63	1	IV	Human	Leukemia	100	
883		63	1	IV	Human	Leukemia	100	
1040		63	1	IV	Human	Leukemia	100	
980		63	1	IV	Human	Leukemia	100	
960		63	1	IV	Human	Leukemia	100	
1006		63	1	IV	Human	Leukemia	100	
810		63	1	IV	Human	Leukemia	100	
690		63	1	IV	Human	Leukemia	100	
651		63	1	IV	Human	Leukemia	100	
1055		63	1	IV	Human	Leukemia	100	
1020		63	1	IV	Human	Leukemia	100	
1100		63	1	IV	Human	Leukemia	100	
840		63	1	IV	Human	Leukemia	100	Partial Remission
1100		63	1	IV	Human	Leukemia	100	
640		63	1	IV	Human	Leukemia	100	Partial remission
1000		63	1	IV	Human	Leukemia	100	
900		63	1	IV	Human	Leukemia	100	
735		63	1	IV	Human	Leukemia	100	Partial remission
940		63	1	IV	Human	Leukemia	100	
975		63	1	IV	Human	Leukemia	100	
595		63	1	IV	Human	Leukemia	100	
700		63	1	IV	Human	Leukemia	100	
900		63	1	IV	Human	Leukemia	100	
1200		63	1	IV	Human	Leukemia	100	
940		63	1	IV	Human	Leukemia	100	
900		63	1	IV	Human	Leukemia	100	
1100		63	1	IV	Human	Leukemia	100	
1236		63	1	IV	Human	Leukemia	100	Partial remission
1455		63	1	IV	Human	Leukemia	100	
1070		63	1	IV	Human	Leukemia	100	
990		63	1	IV	Human	Leukemia	100	
1100		63	1	IV	Human	Leukemia	100	

700		63	1	IV	Human	Leukemia	100	
1619 ± 629	53.7 ± 7.6	63	4	IV	Human	Lymphoblastic disorders	195	
1030 ± 70	74 ± 6	63	6	IV	Human	Lymphoma	213	
1043 ± 26	40.8 ± 3.0	63	6	IV	Human	Lymphoma	213	
961 ± 209	47.9 ± 9.0	63	6	IV	Human	Lmphoproliferature disorders	195	
1021 ± 56	81 ± 5	63	6	IV	Human	Metastasis	213	
922 ± 87	56 ± 10	63	6	IV	Human	Metastasis	213	
1150		63	1	IV	Human	Moderate Hyperplasia	100	
900		63	1	IV	Human	Moderate Hyperplasia	100	
1200		63	1	IV	Human	Moderate Hyperplasia	100	
1250		63	1	IV	Human	Moderate Hyperplasia	100	
900		63	1	IV	Human	Max Hyperplasia	100	
1250		63	1	IV	Human	Max Hyperplasia	100	
850		63	1	IV	Human	Max Hyperplasia	100	
1156		63	1	IV	Human	Max Hyperplasia	100	
1276 ± 353	51.0 ± 10.7	63	8	IV	Human	Myleoproliferature disease	195	
1091 ± 244	46.3 ± 3.6	63	5	IV	Human	Myeloid Leukemia	195	
895 ± 38	68 ± 5	63	11	IV	Human	Osteoporosis	213	
917 ± 28	40.7 ± 1.4	63	11	IV	Human	Osteoporosis	213	
					CERVIX			
674	62	20	1	34	Human	Malignant	140	
1055	58	20	1	34	Human	Malignant	140	
726	79	20	1	34	Human	Malignant	140	
992	80	20	1	34	Human	Malignant	140	
550	26	20	1	34	Human	Malignant	140	
610	56	20	1	34	Human	Malignant	140	
554	38	20	1	34	Human	Malignant	140	
737 ± 190	57 ± 18	20	7	34	Human	Malignant	140	Mean of 7 patients
1002		21	1	IV	Human	Carcinoma	178a	
607		21	1	IV	Human	Carcinoma	178a	
809		21	1	IV	Human	Carcinoma	178a	
779		21	1	IV	Human	Carcinoma	178a	
598		21	1	IV	Human	Carcinoma	178a	
574		21	1	IV	Human	Carcinoma	178a	
731		21	1	IV	Human	Carcinoma	178a	
764		21	1	IV	Human	Carcinoma	178a	
754		21	1	IV	Human	Carcinoma	178a	
788		21	1	IV	Human	Carcinoma	178a	
747		21	1	IV	Human	Carcinoma	178a	

TABLE X. MISCELLANEOUS TISSUE (*continued*)

T1 ± SD (ms)	T2 ± SD (ms)	v (MHz)	N	T	Species	Pathology	Ref	Comments
574		21	1	IV	Human	Carcinoma	178a	
1083		21	1	IV	Human	Carcinoma	178a	
755		21	13	IV	Human	Carcinoma	178a	Mean of 13 patients
723		21	1	IV	Human	Carcinoma	178a	During Radiation Treatment
504		21	1	IV	Human	Carcinoma	178a	During Radiation Treatment
635		21	1	IV	Human	Carcinoma	178a	During Radiation Treatment
549		21	1	IV	Human	Carcinoma	178a	During Radiation Treatment
322		21	1	IV	Human	Carcinoma	178a	During Radiation Treatment
622		21	1	IV	Human	Carcinoma	178a	During Radiation Treatment
727		21	1	IV	Human	Carcinoma	178a	During Radiation Treatment
822		21	1	IV	Human	Carcinoma	178a	During Radiation Treatment
763		21	1	IV	Human	Carcinoma	178a	During Radiation Treatment
634		21	9	IV	Human	Carcinoma	178a	Mean of 9 patients
819		21	1	IV	Human	Carcinoma	178a	After RT (1–4 months)
663		21	1	IV	Human	Carcinoma	178a	After RT (1–4 months)
619		21	1	IV	Human	Carcinoma	178a	After RT (1–4 months)
802		21	1	IV	Human	Carcinoma	178a	After RT (1–4 months)
650		21	1	IV	Human	Carcinoma	178a	After RT (1–4 months)
781		21	1	IV	Human	Carcinoma	178a	After RT (1–4 months)
578		21	1	IV	Human	Carcinoma	178a	After RT (1–4 months)
618		21	1	IV	Human	Carcinoma	178a	After RT (1–4 months)
663		21	1	IV	Human	Carcinoma	178a	After RT (1–4 months)
598		21	1	IV	Human	Carcinoina	178a	After RT (1–4 months)
653		21	1	IV	Human	Carcinoma	178a	After RT (1–4 months)
598		21	1	IV	Human	Carcinoma	178a	After RT (1–4 months)
1071		21	1	IV	Human	Carcinoma	178a	After RT (1–4 months)
701								Mean of 13 patients
673		21	1	IV	Human	Carcinoma	178a	After RT (5–8 months)
705		21	1	IV	Human	Carcinoma	178a	After RT (5–8 months)
738		21	1	IV	Human	Carcinoma	178a	After RT (5–8 months)
561		21	1	IV	Human	Carcinoma	178a	After RT (5–8 months)
680		21	1	IV	Human	Carcinoma	178a	After RT (5–8 months)
671		21	5	IV	Human	Carcinoma	178a	Mean of 5 patients
612		21	1	IV	Human	Carcinoma	178a	After RT (9–18 months)

610	21	1	IV	Human	Carcinoma	178a	After RT (9–18 months)
446	21	1	IV	Human	Carcinoma	178a	After RT (9–18 months)
680	21	1	IV	Human	Carcinoma	178a	After RT (9–18 months)
560	21	1	IV	Human	Carcinoma	178a	After RT (9–18 months)
685	21	1	IV	Human	Carcinoma	178a	After RT (9–18 months)
599	21	6	IV	Human	Carcinoma	178a	Mean of 6 patients
611	21	1	IV	Human	Carcinoma	178a	After RT (>18 months)
679	21	1	IV	Human	Carcinoma	178a	After RT (9–18 months)
565	21	1	IV	Human	Carcinoma	178a	After RT (9–18 months)
620	21	1	IV	Human	Carcinoma	178a	After RT (9–18 months)
670	21	1	IV	Human	Carcinoma	178a	After RT (9–18 months)
820	21	1	IV	Human	Carcinoma	178a	With residual pelvic tumor
701	21	1	IV	Human	Carcinoma	178a	With residual pelvic tumor
755	21	1	IV	Human	Carcinoma	178a	With residual pelvic tumor
558	21	1	IV	Human	Carcinoma	178a	With residual pelvic tumor
324	21	1	IV	Human	Carcinoma	178a	With residual pelvic tumor
630	21	1	IV	Human	Carcinoma	178a	With residual pelvic tumor
470	21	1	IV	Human	Carcinoma	178a	With residual pelvic tumor
677	21	1	IV	Human	Carcinoma	178a	With residual pelvic tumor
794	21	1	IV	Human	Carcinoma	178a	With residual pelvic tumor
635	21	9	IV	Human	Carcinoma	178a	Mean of 9 patients
593	21	1	IV	Human	Carcinoma	178a	With pelvic tumor :During RT
615	21	1	IV	Human	Carcinoma	178a	With pelvic tumor :During RT
300	21	1	IV	Human	Carcinoma	178a	With pelvic tumor :During RT
562	21	1	IV	Human	Carcinoma	178a	With pelvic tumor :During RT
710	21	1	IV	Human	Carcinoma	178a	With pelvic tumor :During RT
716	21	1	IV	Human	Carcinoma	178a	With pelvic tumor :During RT
770	21	1	IV	Human	Carcinoma	178a	With pelvic tumor :During RT
609	21	7	IV	Human	Carcinoma	178a	Mean of 7 patients
670	21	1	IV	Human	Carcinoma	178a	With pelvic tumor : After RT (1–4 months)
655	21	1	IV	Human	Carcinoma	178a	With pelvic tumor : After RT (1–4 months)
536	21	1	IV	Human	Carcinoma	178a	With pelvic tumor : After RT (1–4 months)
641	21	1	IV	Human	Carcinoma	178a	With pelvic tumor : After RT (1–4 months)
599	21	1	IV	Human	Carcinoma	178a	With pelvic tumor : After RT (1–4 months)
777	21	1	IV	Human	Carcinoma	178a	With pelvic tumor : After RT (1–4 months)

TABLE X. MISCELLANEOUS TISSUE (*continued*)

T1 ± SD (ms)	T2 ± SD (ms)	v (MHz)	N	T	Species	Pathology	Ref	Comments
903		21	1	IV	Human	Carcinoma	178a	With pelvic tumor : After RT (1–4 months)
855		21	I	IV	Human	Carcinoma	178a	With pelvic tumor : After RT (1–4 months)
900		21	1	IV	Human	Carcinoma	178a	With pelvic tumor : After RT (1–4 months)
726		21	9	IV	Human	Carcinoma	178a	Mean of 9 patients
992		21	1	IV	Human	Carcinoma	178a	With pelvic tumor : After RT (5–9 months)
560		21	I	IV	Human	Carcinoma	178a	With pelvic tumor : After RT (5–9 months)
1035		21	1	IV	Human	Carcinoma	178a	With pelvic tumor : After RT (5–9 months)
794		21	I	IV	Human	Carcinoma	178a	With pelvic tumor : After RT (5–9 months)
845		21	4	IV	Human	Carcinoma	171 178a	Mean of 4 patients
					COLON			
2000 ± 40	30 ± O.3	400	3	23	Mice	Carcinoma	179	
					GUM			
880 ± 1 0	52 ± 2	20	2	34	Human	Carcinoma	140	
					INTESTINE			
869	67	20	1	34	Human	Adenocarcinoma	140	Large intestines
753 ± 10		20	2	37	Human	Tumor	66	Adenocarcinoma
705 ± 10		20	2	37	Human	Tumor	66	Adenocarcinoma
726 ± 10		20	2	37	Human	Tumor	66	Adenocarcinoma
841 ± 10		20	2	37	Human	Tumor	66	Adenocarcinoma
					LYMPHOMA			
992 ± 107	74 ± 5	15	4	IV	Human	NHL	156	Low grade
924 ± 147	73 ± 6	15	5	IV	Human	NHL	156	High grade
1599 ± 609	68 ± 1	21	7	IV	Human	NHL	156	Low grade
1366 ± 506	67 ± 13	21	9	IV	Human	NHL	156	High grade

					LARYNX			
900 + 11	70 ± 5	20	3	34	Human	Carcinoma	140	
728 ± 20	61 ± 13	20	3	34	Human	Carcinoma	140	Hypopharynx
					ORAL DISSECTION			
883	63	20	1	34	Human	Carcinoma	140	
					OPHARYNX			
560 ± 46	40 ± 5	20	2	34	Human	Carcinoma	140	
					PANCREAS			
495 ± 4	118 ± 15	6.25	5	37	Mice	Adenocarcinoma	42	
460 ± 13	117 ± 6	6.25	5	37	Mice	Adenocarcinoma	42	10 mglkg Dexamethasone @t=0 h
385 ± 13	94 ± 2	6.25	5	37	Mice	Adenocarcinoma	42	10 mglkg Dexamethasone @t=4 h
376 ± l3	67 ± 4	6.25	5	37	Mice	Adenocarcinoma	42	10 mglkg Dexamethasone @t=8 h
600 ± l7	115 ± 3	10	5	37	Mice	Adenocarcinoma	42	10 mglkg Dexamethasone @t=0 h
518 ± l0	98 ± 3	10	5	37	Mice	Adenocarcinoma	42	10 mglkg Dexamethasone @t=4 h
456 ± l3	89 ± 4	10	5	37	Mice	Adenocarcinoma	42	10 mglkg Dexamethasone @t=8 h
	92.35 ± l0.7	21	15	IV	Human	Cystic Fibrosis	210	
					PENIS			
753 ± 105	58 ± 17	20	7	34	Human	Carcinoma	140	
					POPLITEAL			
1043	80	20	1	34	Human	Malignant Synonioma	140	Poplited (R)
					PAROTID GLANDS			
2070 ± 897	80 ± 23	63	5	IV	Human	Adenoid cystic	216	
3900 ± 1749	101 ± 41	63	9	IV	Human	Adenoma	216	
2592 ± 1375	50 ± 11	63	5	IV	Human	Adenocarcinoma	216	
907 ± 213	113 ± 27	63	3	IV	Human	Cyst	216	
517 ± 326	61 ± 17	63	3	IV	Human	Cystadeno lymphoma	216	
2950 ± 1585	76 ± 37	63	5	IV	Human	Lymphoma	216	
1190 ± 403	61 ± 26	63	5	IV	Human	Post operative fibrosis	216	
1467 ± 431	84 ± 26	63	5	IV	Human	Squamous cell carcinoma	216	
1310 ± 328	58 ± 19	63	5	IV	Human	Tumor recurrence	216	
					RECTUM			
561 ± 153	50 ± 5	20	34	RT	Human	Adenocarcinoma	140	

TABLE X. MISCELLANEOUS TISSUE (*continued*)

T1 ± SD (ms)	T2 ± SD (ms)	v (MHz)	N	T	Species	Pathology	Ref	Comments
					SKIN			
657 ± 18	60 ± 14	20	34	RT	Human	Carcinoma	140	
1801.2 ±41	27.4 ± 0.8	395	20	RT	Human	Carcinoma	60	Basal cell
1087.9 ±-29.3	19.2±1	395	48	RT	Human	Tumor	60	Dermis
1152.7 ± 32.8	23.3 ± 0.8	395	28	RT	Human	Tumor	60	Epidermis
1445.6 ± 130.	34.3 ± 0.8	395	7	RT	Human	Tumor	60	Melonoma
13091 ± 25.5	26.4 ± 0.4	395	12	RT	Human	Tumor	60	Nevocellular nevus
1417 ± 68.9	24.6 ± 0.6	395	6	RT	Human	Tumor	60	Seborrheic Keratosis
455.1 ± 32.04	48.6 ± 1.4	395	46	RT	Human	Tumor	60	Subcutis
					SPINE			
1399		10.7	1	22	Human	Astrocytoma	103	Fluid spine
1660		10.7	1	22	Human	Astrocytoma	103	Fluid spine
1263		10.7	1	22	Human	Ganglioma	103	Fluid spine
1504		10.7	1	22	Human			Fluid spine
633		10.7	1	22	Human	Astrocytoma	103	Solid spine
986		10.7	1	22	Human	Astrocytoma	103	Solid spine
704		10.7	1	22	Human	Astrocytoma	103	Solid spine
756		10.7	1	22	Human	Astrocytoma	103	Solid spine
560		10.7	1	22	Human	Ganglioma	103	Solid spine
461 ± 12.0		10.7	58	IV	Human	Vertebrate	98	Degenerate disc
756	93	21	1	37	Human	Craniopharyngioma	107	
1239	395	21	1	37	Human	Meningioma	107	
805	193	21	1	37	Human	Neurinoma	107	
690	395	21	1	37	Human	Subdural hematoma	107	
					STOMACH			
873	67	20	1	34	Human	Adenocarcinoma	140	
					THROMBOSE			
	32 ± 1.2	20	1	IV	Human	Deep Venous Thrombis	19	11 days onset
	43.3 ± 3.4 3.4	20	1	IV	Human	Deep Venous Thrombis	19	DVT - Intermediate
	40.3 ± 0.8	20	1	IV	Human	Deep Venous Thrombis	19	23 days onset
	59.0 ± 5.7	20	1	IV	Human	Deep Venous Thrombis	19	Intermediate

	38.7 ± 6.0	20	1	IV	Human	Deep Venous Thrombis	19	5 days onset
	44.8	20	1	IV	Human	Deep Venous Thrombis	19	13 days onset
	48.4 ± 6.7	20	1	IV	Human	Deep Venous Thrombis	19	Intennediate
	36.2 ± 11.7	20	1	IV	Human	Deep Venous Thrombis	19	Intennediate
894 ± 176	43.7 ± 2.9	20	1	IV	Human	Deep Venous Thrombis	19	I day onset
1069 ± 16	57.1 ± 2.7	20	I	IV	Human	Deep Venous Thrombis	19	3 days onset
777 ± 70	35.4 ± 1.7	20	1	IV	Human	Deep Venous Thrombis	19	6 days onset
1083 ± 395	33.4 ± 5.6	20	1	IV	Human	Deep Venous Thrombis	19	1 day onset
	41.4 ± 10.1	20	1	IV	Human	Deep Venous Thrombis	19	Intennediate
					THYROID			
618 ± .66	59 ± 19	20	10	34	Human	Tumor	140	
526 ± 61		20.4	IV	50	Human	Benign	102	
576 ± 42		20.4	IV	10	Human	Adenoma	102	.
634 ± 28		20.4	IV	14	Human	Cancer	102	
					TESTIS			
776	53	20	1	34	Human	Cancer	140	
2002 ± 13	33.6 ± 4.9	270	8	23	Hamster	Ligation	157	10–20 days after ligation
1930 ± 2	22.5 ± 2.0	270	23	23 .	Hamster	Ligation	157	41 days after ligation
					TONGUE			
783 ± 97	67 ± 10	20	3	34	Human	Carcinoma	140	

Relaxation Time and Water Content

In general water content relates well with the relaxation times in normal tissues and between normal and malignant tissues. However in specific cases, a lack of correlation can nevertheless, be explicitly demonstrated. Thus, the literature is replete with reports proclaiming a relationship and questioning a correlation between relaxation times and water content (15–17, 20–26, 30–35, 39–41, 43–46, 50, 58, 59, 62, 63, 69–72, 77, 78, 80, 81, 83–91, 93, 94, 101, 105–109, 111–113, 115, 118, 119, 129, 130, 136, 142, 145, 147, 149–152, 160–162, 165, 166, 169, 171, 176, 180, 184, 186–188, 191, 205, 206, 214, 218, 220, 227, 228).

Normal and Malignant Tissues

Kiricuta *et al* (113) proposed that the main cause of relaxation time dissimilarities between normal and malignant tissues is due to greater tissue hydration in the malignant tissues. Ling *et al* (130) calculated that the water content difference between normal and cancer cells is less than 10% and therefore cannot account for the relaxation time dissimilarities. Shah *et al* (187, 188) reported the T1 values of normal and malignant tissues in Swiss and ICRC mice. Shah *et al* (187,188) made an interesting observation in which the Swiss mice normal liver T1 value is 426 ± 12 ms with 70.8 ± 0.25 % water, and in the liver tumor bearing mice a T1 value of 615 ± 17 ms and 72.5 ± 0.42 % water. This indeed bodes well for the water content theory. However, in normal spleen the T1 value is 712 ± 26 ms with 77.5 ± 1.2 % water and in tumor bearing spleen, a T1 value of 782 ± 19 ms and 77.4 ± 0.9 % water (187, 188). Similarly, normal kidney yield a T1 value of 581 ± 25 ms with 75.2 ± 1.3 % water content and tumor bearing kidney yield a T1 value of 669 ± 24 with 75.4 ± 1.1 % water. Furthermore, in ICRC mice, normal liver T1 is 375 ± 29 ms with 68.8 ± 2.4 % water and liver with tumor bearing animal T1 value is 366 ± 17 ms with 70.8 ± 0.75 % water (187,188). Given so many inconsistencies, the exact mechanism of relaxation times is still debated with pro and con arguments.

In Negendank *et al* (152) work, they reported T1 and T2 values of liver in C3H mice as 306 ± 12 ms and 39.9 ± 0.4 ms with 70.7 ± 0.3 % water and hepatoma T1 and T2 values as 744 ± 9.0 ms and 82.7 ± 2.3 ms with 82.5 ± 0.6 % water. Again, this bodes well that an increase in water content in cancerous tissue is responsible for elevated relaxation times. However, AKR spleen (normal) yields a T1 and T2 value of 425 ± 45 ms and 62.7 ± 3.5 ms with 79.1 ± 0.5 % water whereas T cell lymphoma yields T1 and T2 values of 587 ± 15 ms and 74.5 ± 2.0 ms with 79.3 ± 0.1 % water content (152). Furthermore, DBA spleen (normal) T1 and T2 values are 503 ± 12 ms and 51.2 ± 1.3 ms and 78.3 ± 0.7 % water and L1210 leukemia T1 and T2 values are 609 ± 15 ms and 62.2 ± 1.6 ms with 78.8 ± 0.7 % water (152). This provides inconsistencies in relating relaxation time with water content.

Cancerous Tissues

Kiricuta *et al* (113) found that Walker carcinoma yield T1 and T2 values of 1093 ms and 77 ms with 83.2 ± 0.47 % water whereas lymph nodes metastases of Walker carcinoma

yield T1 and T2 values of 916 ± 45 ms and 65 ± 0.06 ms with 83.7 ± 0.9 % water. With the same water content, the T1 values are significantly different.

Ling *et al* (130) measured the T1 and T2 values of Sarcoma 180 and Ehrlich carcinoma and found them to be 803 ± 15.5 ms and 61.6 ± 1.87 ms and 815 ± 7.07 ms and 86.3 ± 3.20 ms whereas the water content is 81.7 ±1.6 and 80.8 %. However, inspite of water content differences, the relaxation time values nevertheless, remain the same.

Shah *et al* (187) found that mice fibrosarcoma and adenocarcinoma yield a T1 value of 944 ± 26 ms and 653 ± 18 ms, whereas the water content is 79.1 ± 0.7 and 79.0 ± 0.5 %. Interestingly, the water content is the same but the T1 is significantly different. To provide further assessment, Negendank *et al* (152) measured the T1 and T2 values of L1210 leukemia and T-cell lymphoma (609 ± 15, 62.2 ± 1.6 ms, and 587 ± 15, 74.5 ± 2.0 ms) (and the % water content was 78.8 ± 0.7 and 79.3 ± 0.1). T-cell lymphoma has lower T1 and higher water content compared to L1210 leukemia. This does not bode well for the hypotheses that an increase in T1 corresponds to an increase in water content. These dissimilarities in relaxation times and water content between normal and malignant tissues and from one cancer type to the other raises questions about the validity of water content and its influence on relaxation times. For example, cell nuclear fractions isolated from normal and malignant tissues yield significantly higher T1's relative to the tissue, suggesting that cell water content may not be able to unfold the mystery of relaxation times (15, 35, 187, 188).

Edematous Tissue

Many investigators have shown that an increase in T1 in edematous tissue is due to an increase in water content (16, 32, 40, 70, 77, 91, 96, 107–108, 115, 119, 129, 150, 151, 181, 191). The increase in T1 reported by investigators in edematous tissue has been attributed to water-membrane, and / or water protein interactions and by interactions with salt ions and paramagnetic ions or due to oxygen concentration (10–12, 82, 202, 214).

It is noted that other investigators show a lack of correlation between T1 and water content in edematous tissue. For example, Iwama *et al* (96) observed that there is no significant difference between T1 for edematous brain and control brain tissues. The T1 values Iwama *et al* (96) observed were 1.87 ± 0.056 s and 1.85 ± 0.041 s respectively. However, the T1 for T9 glioma tissue was 2.02 ± 0.051 s, which indeed was significantly longer than that of the edematous tissue or of control brain. Knight *et al* (115) observed: "Our findings, however, indicate that proton density ratios in regions 1 through 4 reach maximum values at 48 hours after MCA occlusion, therefore, increased tissue water content alone cannot account for the elevated relaxation times observed at 24 hours."

However, the most interesting observation noted was Boesiger *et al* (36). They found that in seven patients, tumors yield the longest T1 followed by edema, normal tissue near edema and normal tissue of the contralateral site. The questions are: "Why edema T1 is shorter than that of tumor and why the normal tissue near edema yields a longer relaxation time than that of the contralateral hemisphere of normal tissue?" Akber (8) has provided an explanation of the variation of T1 from tumor to edema to normal based on oxygen diffusion and concentration. Akber (3–7) suggested that the relaxation time dissimilarities in tissues (normal, malignant and edematous) are due to oxygen content. Gatenby *et al* (74, 75) has shown that oxygen tension in human tumors at the center is

low and there exists a gradient of oxygen tension from tumor to normal tissue. It is also well known that normal tissue close to tumors exhibit longer T1 than normal tissue without tumor (23).

Relaxation Time and Paramagnetic Ions

The possibility that the paramagnetic ions in the biological systems might unfold the mystery of relaxation times mechanisms have been argued with pro and con arguments (8, 11, 31, 34, 44, 48, 51, 52, 53, 64, 65, 83, 88, 126, 131–134, 127, 152, 154, 170, 184, 187, 188).

Normal and Cancerous Tissues

Regarding paramagnetic ions and the dissimilarities in T1 values between normal and malignant tissues; an interesting paradox can be assessed from the work of Shah *et al* (187). In Swiss mice normal tissues (non-tumor bearing (NTB)) and mouse fibrosarcoma tumor bearing (TB) tissues, non-tumor bearing (NTB) spleen has higher paramagnetic ions (Fe=965 ± 64; Cu = 20 ± 1; Mn = 8.7 ± 1.8 ug/g) than tumor bearing spleen (Fe = 454; Cu 14.3 ± 3.1; Mn = 4.1 ± 0.9 ug/g) and the T1 values in non-TB spleen (712 ± 19 ms) is not much different than TB spleen (782 ± 19 ms). In non-TB spleen, Fe and Mn ions are twice the amount compared to TB spleen. This defies all the arguments put forth by investigators that such large amount of Fe and Mn in non-TB spleen fails to lower T1 value. Furthermore, in Shah's work, the T1 values of ICRC mice liver in non-tumor bearing mice is 375 ± 29 ms while the paramagnetic ions are (Fe = 715 ± 78, Cu + 11.6 ± 2.0, and Mn = 2.3 ± 0.23 ug/g) while the T1 value in tumor bearing liver is 366 ± 17 ms while the paramagnetic ion contents are (Fe = 809, Cu = 24.5 ± 1.21, and Mn = 5.0 ± 1.1 ug/g). Inspite of the higher paramagnetic ion content in tumor bearing liver, the T1 is almost the same.

Negendank *et al* (152) observed that in DBA spleen (normal) the T1 value is 511 ± 67 ms, T2 value is 61.3 + 3.0 ms and spleen leukemia (L1210) is 542 ± 12 ms T2 is 61.7 ± 1.3 ms whereas the paramagnetic ion contents are (Mn = 10.7 ± 0.2, Cu = 45.7 ± 1.3, Fe = 13.3 ± 3.40 umol / kg) and (Mn = 10.2 ± 2.6, Cu = 44.5 ± 3.5, Fe = 7.6 ± 0.18 umol/kg). Inspite of lower paramagnetic ion content in spleenic leukemia, the T1 values are not significantly different.

Cancerous Tissues

Ling *et al* (131, 132, 134) measured the T1 values of Sarcoma 180 and Ehrlich carcinoma and found them to be 803 ± 15.5 ms and 815 ± 7.07 ms whereas the paramagnetic ion content in Sarcoma 180 is (Fe 124 ± 4.32; Cu = 29.1, Mn = 0.0 umol/kg) and Ehrlich carcinoma is (Fe = 29.5 ± 12.6, Cu = 23.5 ± 2.4, Mn ± 0.8 umol/kg). Inspite of several fold increase in Fe ion content of Sarcoma 180, the T1 values of the two cancerous tissues remain the same. Furthermore, Ling *et al* (131, 132, 134) also observed that AS 30 D

hepatoma yield a T1 value of 843.6 ± 16.4 ms and paramagnetic ion content of (Mn = 0.03 ± 0.03, Cu = 40.0 ± m8.7, Fe = 126 ± 11.7 umol / kg). Comparing with either the Ehrlich carcinoma or Sarcoma 180, the AS-30 D hepatoma has much higher Fe and Cu content than either of the other two cancer tissues but AS-30 D hepatoma yields a longer T1 than the other two cancer tissues.

Negendank *et al* (152) on the other hand, observed the T1 values in AKR spleen lymphoma and DBA spleen L1210 leukemia and the T1 values are 587 ± 15 ms and 609 ± 15 ms respectively. The paramagnetic ions are (Mn = 8.6 ± 1.1, Cu = 20.2 ± 2.4, Fe = 6.6 ± 14 umol / kg) and (Mn = 7.7 ± 3, Cu = 32.8 ± 12, Fe = 10.7 ± 6.8 umol / kg). It is interesting to observe that leukemia has higher Cu, and Fe content and still yields a longer T1 than lymphoma.

Relaxation Time and Protein Content

It is often conjectured that since a fraction of the cell water is bound to the protein surface, the mere presence or absence of protein in a cell may dictate the relaxation time of water protons (41, 43, 44, 48, 62, 78, 83, 85, 93, 116, 117, 158, 171, 177).

Ranade (171) determined the protein content of the involved and uninvolved human tissues with different types of cancer. According to Ranade: “Estimated levels of the protein content of normal and malignant tissues by themselves did not correlate with elevation of T1 values.”

In spite of claim and counter claim of relaxation time correlation with protein content, protein content has not been proven to elucidate the relaxation mechanism.

Conclusion

It appears from the published data that generally malignant tissues yield a longer relaxation time compared to normal tissues. The exact mechanism to elucidate the relaxation time dissimilarities between normal and malignant tissue still remains elusive. As discussed in this paper, explanations have ranged — increase in water content, influence of paramagnetic ions, presence of protein in a cell and oxygen content. The assessment that can be drawn from the preceding discussion, is that as of yet, we do not have an understanding / mechanisms to account for the relaxation time dissimilarities in normal tissues, normal and malignant tissues or among malignant tissues.

References

1. Ahmad, M., Johnson, R.F., Fawcett, H.D., Screiber, M.H. (1988) *MRI* 6:527.
2. Aisen, P.M., Doi, K., Swanson, S.D. (1994) *Magn Reson Med* 31:551.
3. Akber, S.F. (1987) *Med Phys* 14:1090.
4. Akber, S.F. (1988) *Med Hypotheses* 26:187.
5. Akber, S.F. (1989) *Europ J Radiol* 9:56.
6. Akber, S.F. (1989) *Europ J Radiol* 9:198.
7. Akber, S.F. (1990) *Acta Radiologica* 31:541.

8. Akber, S.F. (*1992*) *Physiol Chem Phys & Med NMR 24:71.*
9. Akber, S.F. (1992) *Physiol Chem Phys & Med NMR* 24:329.
10. Akber, S.F. (1992) *Med Hypotheses* 37:24.
11. Akber, S.F. (1993) *Nuklearmedizin* 32:52.
12. Akber, S.F. (1996) *Physiol Chem Phys & Med NMR* 28:205.
13. Anderson, T., Ericksson, A., Eriksson, B., Hernmingsson, A., Lindh, E., Nyman, R., Oberg, K. (1989) *Br J Radiol* 62:433.
14. Armspach, J.P., Gounot, D., Rurmbach, L., Charnbron, J. (1991) *MRI* 9:107.
15. Arulmozhi, V., Narayanan, S., Krishnan, B., Rao, A.S., Veliath, A.J., Ratnakur, C. (1988) *Physiol Chem Phys & Med NMR* 20:337.
16. Bakay, L., Kurland, R.J., Parrish, R.G., Lee, J.C., Peng, R.J., Bartkowski, H.M. (1975) *Exp Brain Research* 23:241.
17. Bakker, C.J., Vriend, J. (1984) *Phys Med Biol* 29:509.
18. Barbosa, S., Blumhardt, L.D., Roberts, N., Lock, T., Edwards, R.H.T. (1994) *MRI* 12:33.
18a. Barbier, E.L., Liu, L., Grillone, E., Payen, J.F., Lebas, J.F., Segebarth, C., Remy, C. (2005) *NMR in Biomedicine* 18:499.
18b. Barkhof, F., Van Walderveen, M. (1999) *Phil Trans R Soc London* B354:1675.
19. Bass, J.C., Hedlund, L.W., Sostman, H.D. (1990) *MRI* 8:631.
20. Beall, P.T., Hazlewood, C.F., Rao, P.N. (1974) *Science* 192:904.
21. Beall, P.T., Asch, B.B., Chang, D.C., Medina, D., Hazlewood, C.F. (1980) *J Natl Cancer Inst* 64:335.
22. Beall, P.T., Brinkley, B.R., Chang, D.C., Hazlewood, C.F. (1982) *Cancer Res* 42:4124.
23. Beall, P.T., Hazlewood, C.F. (1983) Distinction of the normal, preneoplastic, and neoplastic states by water proton NMR relaxation times. In: *Nuclear Magnetic Resonance (NMR) Imaging*. (C. L. Partain, E. James and F.D. Rollo, eds), W.B. Saunders, Philadelphia, p. 312.
24. Bederson, J.E., Bartkowski, R.B., Moon, K., Halks-Miller, M., Nishimura, M.C., Brant-Zawadski, M., Pitts, L.H. (1986) *J Neurosurg* 64:795.
25. Belton, P.S., Jackson, R.R., Packer, K.J. (1972) *Biochim Biophys Acta* 286: 16.
26. Belton, P., Packer, K. (1974) *Biochim Biophys Acta* 354: 305.
27. Benson, L., Hemmingsson, A., Ericsson, A., Jung, B., Sperber, G., Thuomas, K.A., Westermark, P. (1987) *Acta Radiol* 28 :13.
28. Bernardino, M.E., Chaloup, J.C., Malko, J.A., Chezmar, J.L., Nelson, R.C. (1989) *MRI* 7:363.
29. Besson, J.A.O., Corrigan, F.M., Cherryman, G.R., Smith, F.W. (1987) *Br J Psychiatry* 150:161.
30. Besson, J.A.O., Greentree, S.G., Foster, M.A., Remmington, J.E. (1989) *MRI* 7:141.
31. Blicharska, B., Florkowski, Z., Hennel, J.W., Held, G., Noak, F. (1970) *Biochem Biophys Acta*. 207:381.
32. Biosvert, D.P., Handa, Y., Allen, P.D. (1990) Proton relaxation in acute and subacute ischemic brain edema. In: *Brain Edema Pathogenesis, Imaging and Therapy* (D.M. Long, ed.), Raven Press, New York.
33. Block, R.E. (1973) *FEBS Lett* 34:109.
34. Block, R.E., Maxwell, G.P. (1974) *J Magn Reson* 14:329.
35. Block, R.E., Maxwell, G.P., Branam, D.L. (1971) *J Natl Cancer Inst* 59:1731.
36. Boesiger, P., Greiner, R., Schoepflin, R.E., Kann, R., Kuenzi, U. (1990) *MRI* 8:491.
37. Bottomley, P.A., Foster, T.I., Argesinger, R.E., Pfeirfer, L.M. (1984) *Med Phys* 11: 425.
38. Bottomley, P.A., Foster, T.I., Argesinger, R.E., Pfeirfer, L.M. (1987) *Med Phys* 14:1.
39. Bovee, W., Huisman, P., Smidt, J. *(*1974) *J Natl Cancer Inst* 52:595.
40. Boxt, L.M., Hsu, D., Katz, J., Detweiler, P., McLaughlin, S., Kolb, T.J., Spotnitz, H.M. (1993) *MRI* 11:375.
41. Bratton, C.B., Hopkins, A.L., Weinberg, J.W. (1965) *Science* 147:738.
42. Braunschweiger, P.C., Reynolds, K., Nelson, T.R., Maring, E. (1987) *MRI* 5:483.
43. Brown, M.F., Ellena, J.F., Trindle, C., Williams, G.D. (1986) *J Chem Phys* 84:1.

44. Cameron, I.L., Virgina, A., Ord, B.A., Fullerton, G.D. (1984) *MRI* 2:97.
45. Cerdan, S., Lotscher, H.R., Kunnecke, B., Seelig, J. (1989) *Magn Reson Med* 12:151.
46. Chang, D.C., Rorschach, H.E., Hazlewood, C.F., Nichols, B.L. (1973) *Ann NY Acad Sci* 704:434.
47. Chen, J.H., Avram, H.E., Crooks, L.E., Arakawa, M., Kaufman, L., Brito, A.C. (1992) *Radiology* 184:427.
48. Civan, M.M., Shporer, M. (1975) *Biophys J* 15:299.
49. Clement, O., Frija, G., Charnbon, C., Schouman-Clayes, E. (1992) *Invest Radiol* 27:230.
50. Clifford, J. (1968) In: *Membrane Models and the Function of Biological Membranes*. (Bolis L, Pethica BA, eds.), Amsterdam: Proc Int Conf Bio Membr, NATO Advanced Study Institute, North Holland Publishing Co., p. 19.
51. Cooke, R., Wein, R. (1973) *Ann NY Acad Sci* 204:197.
52. Cope, F.W. (1969) *Biophys J* 9:303.
53. Cottom, G.L., Vasek, A., Lusted, D. (1972) *Res Comm Chem Pathol Pharmacol* 4: 495.
54. Damadian, R. (1971) *Science* 171:1151.
55. Damadian, R., Zaner, K., Hor, D. (1973) *Physiol Chem Phys & Med NMR* 5:381.
56. Damadain, R., Zaner, K., Hor, D., DiMaio, T. (1974) *Proc Natl Acad Sci* 71:1471.
57. Diesbourg, L.D., Prato, F.S., Wisenberg, G., Drost, D.J., Marshall, T.P., Carroll, S.E., O'Neill, B. (1992) *Magn Reson Med* 23:239.
58. Ebara, M., Josephsen, P., Karle, H., Juhl, E., Soresen, P.G., Henrickson, O. (1986) *Radiology* 159:371.
59. Eggleston, C., Saryan, L.A., Hollis, D.P. (1975) *Cancer Research* 35:1326.
60. el Gammal, S., Hartwig, R., Aygen, S., Bauermann, T., el Gammal, C., Altmeyer, P. (1996) *J Invest Dermatol* 106:1287.
61. Egglin, T.K., Rummeny, E., Stark, D.D., Wittenberg, J., Saini, S.F., Ferrucci, J.T. (1990) *Radiology* 176:107.
62. Escanye, J.M., Canet, D., Robert, J. (1982) *Biochim Biophys Acta* 721:305.
63. Escanye, J.M., Canet, D., Robert, J. (1984) *J Magn Reson* 58:118.
64. Fahlvik, A.E., Holtz, E., Klaveness, J.O. (1990) *MRI* 8:363.
65. Fahlvik, A.E., Holtz, E., Leander, P., Schroder, U., Klaveness, J. (1990) *Invest Radiol* 25: 113.
66. Fantazzini, P., Sarra, A. (1996) *Magma* 4:157.
67. Fatorous, P.P., Marmarou, A., Kreft, K.A., Schwaz, P.P. (1991) *Magn Reson Med* 17:402.
68. Fiel, R.J., Button, T.M., Gilani, S., Mark, E.H., Musser, D.A., Henkelman, R.M., Bronskill, M.J., Van-Heteren, J.G. (1987) *MRI* 5: 149.
69. Fowler, P.A., Casey, C.E., Cameron, G.G., Foster, M.A., Knight, C.R. (1990) *Br J Obst Gynaecol* 97:595.
70. Fu, Y., Tanaka, K., Nishimura, S. (1990) Evaluation of brain edema using magnetic resonance proton relaxation times. In: *Brain Edema Pathogenesis. Imaging and Therapy* (D.M. Long, ed.), Raven Press, New York.
71. Fung, B.M. (1977) *Biochim Biophys Acta* 497:317.
72. Fung, B.M, Wassil, D., Durham, D.L., Chestnut, R.W., Durham, N.N., Berlin, K.D. (1975) *Biochim Biophys Acta* 385:180.
73. Gasperini, C., Horsfield, M.A., Thorpe, J.W., Kidd, D., Barker, G.J., Tofts, P.S., MacManus, D.G., Thompson, A.J., Miller, D.H., McDonald, W.I. (1996) *J Magn Reson Imaging* 6:580.
74. Gatenby, R.A., Coia, L.R., Katz, H., Moldofsky, P.J., Engstrom, P., Brown, D.Q., Brookland, R., Broder, G.J. (1985) *Radiology* 156:211.
75. Gatenby, R.A., Kessler, A.H.B., Rosenblum, J.S., Coia, L.R., Moldofsky, P.J., Hartz, W.H., Broder, G.J. (1988) *Intl J Rad Oncol Biol Phys* 14:831.
76. Glazer, G.M., Orringer, M.B., Chenevert, T.L., Borrello, J.A., Penner, M.W., Quint, L.E., Li, K.C., Aisen, A.M. (1988) *Radiology* 168:429.
76a. Geiser, F., Murtz, P., Lutterberg, G., Traber, F., Block, W., Imbierowicz, K., Schilling, G., Schild, H., Liedtke, R. (2001) *Psychosomatic Med* 63:631.

77. Go, K.G., Edzes, H.T. (1975) *Arch Neurol* 17:462-465.
78. Gore, J.C. (1983) Pathophysiological significance of relaxation. In: *Nuclear Magnetic Resonance (NMR) Imaging*. (C. L. Partain, E. James and F.D. Rollo, eds.). W.B. Saunders, Philadelphia.
79. Gruss, L.P., Newhouse, J.H. (1996) *JCAT* 20:792.
79a. Griffin, C.M., Dehmehski, J., Chard, D.T., Parker, C.J., Barker, G.J., Thompson, A.J., Miller, D.H. (2002) *Mult Scler* 8:211.
80. Haacke, E.M., Mitchell, J., Lee, D. (1990) *MRI* 8:79.
81. Hansen, J.R. (1971) *Biochim Biophys Acta* 230:482.
82. Hausser, R., Noack, F.Z. (1965) Naturforschg 20a:1668.
83. Hazlewood, C. (1979) In: *Cell Assocaited Water*. (W. Drost-Hansen, and J.S. Clegg, eds.). Academic Press, NY pp. 165–259.
84. Hazlewood, C., Chang, D.C., Nichols, B.L., Woessner, D.E. (1974) *Biophys J* 14:583.
85. Hazlewood, C.F., Nichols, B.L., Chamberlain, N.F. (1969) *Nature* 222: 747.
86. Hazlewood, C.F., Nichols, B.L., Chang, D.C., Brown, B. (1971) *Johns Hopkins Med J* 128:117.
87. Hoehn-Berlage, M., Tolxdorff, T., Bockhorst, K., Okada, Y., Ernestus, R.I. (1992) *MRI* 10:935.
88. Hollis, D.P., Economou, J.S., Parks, L.C., Eggleston, J.C., Saryan, L.A., Czeisler, J.L. (1973) *Cancer Res* 33:2156.
89. Hollis, D.P., Saryan, L.A., Economou, J.S., Eggleston, J.C., Czeisler, J.L., Morris, H.P. (1974) *J Natl Cancer Inst* 53:807.
90. Hollis, D.P., Saryan, L.A., Eggleston, J.C., Morris, H.P. (1975) *J Natl Cancer Inst* 54: 1469.
91. Horikawa, Y., Naruse, S., Tanaka, C., Harikawa, K., Nishikawa, H. (1975) *Stroke* 17:1149.
91a. Hosch, W., Block, M., Libicher, M., Ley, S., Hegenbart, U., Dengler, T.J., Kahus, H., Kauczor, H.U., Kauffmann, G.W., Kristen, A.V. (2007) *Invest Radiol* 42:636.
92. Houdek, P.V., Landy, H.J., Quencer, R.M., Sattin, W., Polle, C.A., Harmon, C.A., Pisciotta, V., Schwade, J.G. (1988) *Intl J Rad Oncol Biol Phys* 15:213.
93. Huggert A, Odeblad E. (1958) *Acta Radiol* 51:385.
94. Inch, W.R., McCredie, J.A., Knispel, R.R., Thompson, R.T., Pintar, M.M. (1974) *J Natl Cancer Inst* 52:353.
95. Iwama, T., Yamada, H., Era, S., Sogami, M., Andoh, T., Sakai, N., Kato, K., Kuwata, K., Watari, H. (1992) *Magn Reson Med* 24:53.
96. Iwama, T., Yamada, H., Andoh, T., Sakai, N., Era, S., Sogami, M., Kuwata, K., Watari, H. (1992) *Magn Reson Med* 25:78.
97. Jacobs, D.O., Settle, R.G., Clarke, J.R., Trerotola, S.O., Sachdeva, A.K., Wolf, G.L., Rombeau, J.L. (1990) *J Surg Res* 48:107.
97a. Jayakumar, P.N., Srikanth, S.G., Chandrashekar, H.S., Subbakrishna, D.K. (2007) *Clinical Radiology* 62:370.
98. Jenkins, J.P.R., Stehling, M., Sivewright, G., Hickey, D.S., Isherwood, I. (1989) *MRI* 7:17.
99. Jensen, K.E., Grube, T., Thomson, C., Sorrenson, P.G., Christoffersen, P., Karle, H., Henriksen, O. (1988) *MRI* 6:291.
100. Jensen, K.E., Sorensen, P.G., Thomsen, C., Christofferson, P., Henricksen, O., Karle, H. (1990) *Acta Radiologica* 31:361 & 31:445.
101. Jezernik, M., Sentjurc, M., Schara, M. (1983) *Acta Neurochir-Wien* 67:1.
102. Johnson, M., Selinsky, B., Davis, M., Lawrence, T.L., Cleveland, G., Perry, J.R., Thomas, C.G. (1989) *Invest Radiol* 24: 666.
103. Jungreis, C.A., Chandra, R., Kricheff, I., Chuba, J.V. (1988) *Invest Radiol* 23:12.
104. Just, M., Higer, H.P., Schwarz, M., Bohl, J., Fries, G., Pfannenstiel, P., Thelen, M. (1988) *MRI* 6:463.
105. Just, M., Thelen, M. (1988) *Radiology* 169:779.
106. Kallman, R.F., DeNardo, G.L., Stasch, M.J. (1972) *Cancer Res* 32:483.
107. Kamman, R.L., Go, K.G., Brouwer, W., Berendson, H.J.C. (1988) Magn Reson Med 6:265.

108. Kamman, R.L., Go, K.G., Berendsen. (1990) Proton magnetic resonance relaxation times in brain edema. In: *Brian Edema Pathogenesis. Imaging and Therapy* (D.M. Long, ed.), Raven Press, New York.
109. Kaneoke, Y., Furuse, M., Inao, S., Saso, K., Yoshida, K., Motegi, Y., Mizuno, M., Izawa, A. (1987) *MRI* 5:415.
110. Karlik, S.J., Wong, C., Gilbert, J.J., Noseworthy, J.R. (1989) *MRI* 7:463.
111. Kasturi, S.R. (1985) *Physiol Chem Phys & Med NMR* 17:387.
112. Kato, H., Kogure, K., Ohtomo, H., Izumiyama, M., Tobita, M., Matsui, S. (1986) *J Cereb Blood Flow Metab* 6:212.
113. Kiricuta, I.C., Simplaceanu, V. (1975) *Cancer Res* 35:1164.
114. Kjaer, L., Thomsen, C., Gjerris, F., Mosdal, B., Henricksen, O. (1991) *Acta Radiologica* 32:498.
115. Knight, R.A., Dereski, Mo, Halpern, J.A., Ordidge, R.J., Chopp, M. (1994) *Stroke* 25:1252.
116. Koenig, S.H., Brown, R.D., Adams, D., Emerson, D., Harrison, C.G. (1984) *Biol Chem* 244:3283.
117. Koenig, S.H., Brown, R.D. III (1985) *Invest Radiol* 20:297.
118. Komu, M., Baba, Y., Tanimoto, A., Finn, J.P., Stark, D.D. (1992) *MRI* 10: 35.
119. Kotwica, Z., Thuomas, K.A., Persson, L. *Radiol Diagn* (1989) 30:307.
120. Kovalikda, Z., Hoehn-Berlage, M.H., Gersonde, K., Porschen, R., Mitter, C., Franke, R.P. (1987) *Radiology* 164:543.
121. Krombach, G.A., Hahn, C., Tomars, M., Buecker, A., Grawe, A., Gunther, R.W., Kuhl, H.P. (2007) *J Magn Reson Imaging* 25:1283.
122. Kreft, B.P., Baba, Y., Tanimoto, A., Finn, J.P., Stark, D.D. (1993) *Radiology* 186:543.
123. Kreft, B.P., Tanimoto, A., Leffler, S., Finn, J.P., Oksendal, A.N., Stark, D.D. (1994) *J Magn Reson Imaging* 4:373.
124. Kurki, T., Komu, M. (1995) *MRI* 13:379.
125. Kurki, T., Lundbom, N., Kormano, M. (1996) *J Magn Reson Imaging* 6:573.
126. Lewa, C.J., Zbytniewski, Z. (1977) *Bull Cancer* 64:37.
127. Li, D., Haacke, E.M., Tarr, R.W., Venkatesan, R., Lin, W., Wielopolski, P. (1996) *J Magn Reson Imaging* 6:415.
128. Li, K.C.P., Jefferey, R.B., Ning, Sc, Kandil, A., Hahn, G.M., Pike, B., Glover, G., Kosek, J. (1993) *Invest Radiol* 28:896.
129. Lin, W., Paczynsyski, R.P., Venkatesan, R., He, Y.Y., Powers, W.J., Hsu, Cy, Haacke, E.M. (1997) *Magn Reson Med* 38:303.
130. Ling, G.N., Tucker, M. (1980) *J Natl Cancer Inst* 64:1199.
131. Ling, G.N. (1983) *Physiol Chem Phys & Med NMR* 15:511.
132. Ling, G.N. (1989) *Physiol Chem Phys & Med NMR* 21:15.
133. Ling, G.N. (1983) *Physiol Chem Phys & Med NMR* 15:505,
134. Ling, G.N. (1990) Kolebic T, Damadian R. *Physiol Chem Phys & Med NMR* 22:1.
135. Liu, Y.H., Hawk, R.M., Ramaprasad, S. (1995) *MRI* 13:251.
136. Lohr, J., Mazurchuk, R.J., Acara, M.A., Nickerson, P.A., Fiel, R.J. (1991) *MRI* 9:93.
137. Lombardo, D.M., Baker, M.E., Spritzer, C.E., Blinder, R., Meyers, W., Herfkens, R.J. (1990) *AJR* 155:55.
138. Lundbom, N., Katevuo, K., Komu, M., Kurki, T., Kormano, M. (1992) *Invest Radiology* 27:673.
139. Magin, R.L., Bacic, G., Niesman, M.R. (1991) *Magn Reson Med* 20: 1.
140. Mariappan, S.V.S., Subramanian, S., Chandrakumar, N., Rajalakshmi, K.R., Sukumaran, S.S. (1988) *Magn Reson Med* 8:119.
141. Marzola, P., Maggionit, F., Vicinanza, E., Dapra, M., Cavagna, F.M. (1996) *J Magn Reson* 7:147.
142. Mathur-DeVre, R. (1984) *Br J Radiol* 57:955.
143. Matsumura, M. (1987) *Child's* Nerv Syst 3:2.
144. Matsumura, K., Nakano, I., Fukuda, N., Ikehira, H., Tateno, Y., Aoki, Y. (1988) *Muscle and Ner*ve 11:97.

145. McDouall, J.E.L., Evelhoch, J.L. (1990) *Cancer Res* 50:363.
146. McFarland, E.G., Mayo-Smith, W.W., Saini, S., Hahn, P.F., Goldberg, M.A., Lee, M.J. (1994) *Radiology* 193:43.
147. Miller, D.H., Johnson, G., Tofts, P.S., MacMamus, D., McDonald, W.I. (1989) *Magn Reson Med* 11: 331.
148. Misra, L.K., Narayana, P.A. (1989) *MRI* 7: 277.
149. Moser, E., Orr, J.S., Podo, F., Lendinara, L., Canese, R. (1993) *MRI* 11:865.
150. Naruse, S., Horikawa, Y., Tanaka, C., Hirakawa, K., Nishikawa, H., Yoshizaki, K. (1982) *J Neurosurg* 56:747.
151. Naruse, S., Horikawa, Y., Tanaka, C., Hirakawa, K., Nishikawa, H., Yoshizaki, K. (1986) *MRI* 4:293.
152. Negandank, W., Corbett, T., Crowley, M., Kellog, C. (1991) *Magn Reson Med* 18: 280.
153. Newcomb, C.H., Van Dyk, J., Hill, R.P. (1994) *Intl J Radiat Oncol and Phys* 30:125.
154. Niemi, P.T., Komu, M.K.E.S., Koskinen, S.K. (1992) *J Magn Reson Imaging* 2: 197.
155. Nyman, R., Rhen, S., Glimelius, B. (1987) *Acta Radiologica* 28:199.
156. Nyman, R., Rhen, S., Ericsson, A., Glimeliud, B., Hagberg, H., Hemmingsson, A., Sundstrom, C. (1987) *Acta Radiologica* 28:527.
157. Ogawa, E., Ninomiya, H., Yamazaki, K. (1993) *J Vet Med Sci* 55:683.
158. Odeblad, E., Lindstrom, G. *Acta Radiologica* (1955) 43:469.
159. Paajanen, H., Brasch, R.C., Schmiedel, U., Ogan, M. (1987) *Acta Radiologica* 28:79.
160. Paanjanen, H., Grodd, W., Revel, S., Engelstad, B., Brasu, R.C. (1987) *MRI* 5: 109.
161. Parish, R.G., Kurland, R.J., Janese, W.W., Bakay, L. (1974) *Science* 83:438.
162. Pearson, R.T., Duff, I.D., Derbyshire, W., Blanshard, J.M.V. (1974) *Biochim Biophys Acta* 362:188.
163. Peterson, B.S., Gore, J.C., Riddle, M.A., Cohen, D.J., Leckman, J.F. *Psychiatry Research* 55:205, 1994)
164. Petterson, H., Slone, R.M., Spanier, S., Gillespy, T. III, Fitzsimmons, J.R., Scott, K.N. (1988) *Radiology* 167:783.
165. Pocsik, I., Furo, I., Tompa, K., Neumark, T., Takacs, J. (1986) *Biochim Biophys Acta* 880:1.
166. Polak, J.F., Jolesz, F.A., Adams, D.F. (1988) *Invest Radiol* 23: 107.
167. Pouliquen, D., Rivet, P., Gallier, J., LeJeune, J.J., deCertaines, J.D. (1993) *Anti Cancer Res* 13:49.
168. Quesson, B., Bouzier, A.K., Thiaudiere, E., Delalande, C., Merle, M., Canioni, P. (1997) *J Magn Reson Imaging* 7:1076.
169. Rajanaygan, V., Febry, M.E., Gore, J.C. (1991) *MRI* 9:621.
170. Rannade, S.S., Shingatgeri, V.M. (1992) *Physiol Chem Phys & Med NMR* 24:165.
171. Rannade, S.S. (1988) Histopathological correlation. In: *Nuclear Magnetic Resonance (NMR) Imaging.* Vol. II, (C. L. Partain, E, James and F.D. Rollo, eds.) W.B. Saunders, Philadelphia, p.1101.
172. Reimer, P., Weissleder, R., Lee, A.S., Wittenberg, J., Brady, T.J. (1990) *Radiology* 177: 729.
173. Reimer, P., Weissledar, R., Nickeleit, V., Brady, T.J. (1992) *Invest Radiol* 27:390.
174. Rinck, P.A., Fisher, H.W., Elst, L.V., Haverbeke, Y.V., Muller, R.N. (1988) *Radiology* 168:843.
175. Richards, M.A., Webb, J.A.W., Reznek, R.H., Davis, S.F., Jewell, S.E., Gregory, W.M, (1988) *Br J Radiol* 61: 34.
176. Rofstad, E.K., Howell, L.R., DeMuth, P., Ceckler, T.L., Sutherland, R.M. (1988) *Intl J Rad Biol* 54:635.
177. Rorschach, H.E., Hazlewood, C. (1986) *J Mag Reson* 70:79.
178. Saini, S., Stark, D.D., Wittenberg, J., Vici, L.G., Brown, A.S., Ferruci, J.T. (1987) *Invest Radiol* 22:149.
178a. Santoni, R., Bucciolini, M., Chriostrinic, C., Cionini, L., Renzi, R. (1991) *Br J Radiol* 64:498.
179. Sarkar, S.K., Clark, R.K., Rycyna, R.E., Mattingly, M.A., Greig, R. (1989) *Magn Reson Med* 12: 268.

180. Saryan, L.A., Hollis, D.P., Economou, J.S., Eggelston, J.C. *(*1974) *J Natl Cancer Inst* 52:599.
181. Schad, L.R., Brix, G., Harele, W., Lorenz, W.J., Semmler, W. (1989) *J Compt Assist Tomagra* 13:577.
182. Schaefer, S., Malloy, C.R., Katz, J., Parkey, R.W., Buja, M., Willerson, J.T., Peshock, R.M. (1988) *J Am Coll Cardiol* 12:1064.
183. Schaefer, S., Lange, R.A., Gutekunst, D.P., Parkey, R.W., Willerson, J.T., Peshock, R.M. (1991) *Invest Radiol* 26: 551.
184. Schmumacher, J.H., Matys, E.R., Clorius, J.H., Hauser, H., Wesch, H., Maier-Borst, W. (1985) *Invest Radiol* 20:601.
185. Scholz, T.D., Vandenberg, B.F., Fleagle, S.R., Collins, S.M., Kerber, R.E., Skorton, D.J. (1990) *Invest Radiol* 25:1120.
186. Sergeev, A.I., Murza, L.I., Vexler, V.S. (1988) *Studia Biophysica* 125:77.
187. Shah, S., Ranade, S.S., Phadke, R.S., Kasturi, S.R. (1982) *MRI* 1:9.
188. Shah, S., Ranade, S.S., Phadke, R.S., Kasturi, S.R. (1982) *MRI* 1: 155.
189. Sibbitt, W..L., Brooks, W.M., Haseler, L.J., Griffey, R.H., Frank, L.M., Hart, B.L., Sibbitt, R.R. (1995) *Arthritis & Rheumatism* 38:810.
190. Shioya, S., Haida, M., Yosiaki, O., Fukuzaki, M., Yamabayashi, H. (1988) *Radiology* 167:105.
191. Shioya, S., Haida, M., Fukuzaki, M., Ono, Y., Tsuda, M., Ohta, Y., Yamabashi, H. (1990) *Magn Reson Med* 14:358.
192. Shioya, S., Tsuji, C., Kurita, D., Katoh, H., Tsuda, M., Haida, M., Kawana, A., Ohta, Y. (1997) *Radiat Res* 148:359.
193. Shuter, B., Tofts, P.S., Pope, J.M. (1995) *MRI* 13:563.
194. Skillings, J.R., Bramwell, V., Nicholson, R.L., Prato, F.S., Wells, G. (1991) *Cancer* 67:1838.
195. Smith, S.R., Williams, C.E., Davies, J.M., Edwards, R.H.T. (1989) *Radiology* 172:805.
196. Stevenson, V.L., Gawne-Cain, M.L., Barker, G.J., Thompson, A.J., Miller, D.H. (1997) *J Neurol* 244:119.
197. Stewart, W.A., Alvord, E.C., Hruby, S., Hall, L.D., Paty, D.W. (1991) *Brain* 114: 1096.
198. Sugimura, K., Yamasaki, K., Kitagaki, H., Tanako, Y., Kono, M. (1987) *Radiology* 165:541.
198a. Sun, Y., Mulkern, R.V., Schmidt, K., Doshi, S., Albert, M.S., Schmidt, N.O., Ziu, M., Black, P., Carrol, R., Kieran, M.W. (2004) *NMR in Biomedicine* 17:399.
199. Suzuki, M., Kishi, H., Aso, Y., Yashiro, N., Iio, M. (1988) *Rad Med* 6:263.
200. Takeda, M., Katayama, Y., Tsutsui, T., Komeyama, T., Mizusawa, T., Kazuhide, S., Takahashi, H., Sato, S. (1993) *NMR in Biomedicine* 6:329.
201. Tanimoto, A., Stark, D.D. (1991) *Invest Radiol* 26:S139.
202. Tannock, I. (1976) Oxygen distribution in tumors: Influence on cell proliferation and implications for tumor therapy. In: *Oxygen Transport to Tissues* (Gorte J,Reneau D, and Thews G., eds.) Plenum Press, New York. pp. 599.
203. Tanner, S.F., Clarke, J., Leach, Mo, Mesbahi, M., Nicolson, V., Powles, R., Husband, J.E., Tait, D. (1996) *Br J Radiol* 69:1145.
204. Taylor, C.R., Sostman, H.D., Gore, J.C., Smith, G.W. (1987) *Invest Radiol* 22:621.
205. Terrier, F., Revel, D., Alpers, C.E., Reinhold, C.E., Levine, J., Genant, H.K. (1985) *Invest Radiol* 20:813.
206. Terrier, F., Revel, D., Hricack, H., Alpers, C.E., Reinhold, C.E., Levine, J., Higgins, C.B. (1986) *Invest Radiol* 21: 221.
207. Tanimoto, A., Kuribayashi, S. (2005) *Magn Reson Med Sciences* 4:53.
208. Thomsen, C., Josephsen, P., Karle, H., Juhl, E., Sorrensen, P.G., Hericksen, O. (1990) *MRI* 8:39.
209. Thomsen, C., Josephsen, P., Karle, H., Juhl, E., Sorrensen, P.G., Henricksen, O. (1990) *MRI* 8:39.
210. Tham, R.T., Heyerman, H.G., Falke, T.H., Zwinderman, A.H., Bloem, J.L., Bakker, W., Lamers, C.B.H.W. (1991) *Radiology* 179:183.
211. Tousaint, J.F., Kwong, K.K., Mkprau, F., Weisskoff, R.M., Laraia, P.J., Kantor, H.L. (1996) *Magn Reson Med* 32:62.

212. Towner, R.A., Yamaguchi, T., Philbrick, D.J., Holub, B.J., Janzen, E.G., Takahashi, H. (1991) *MRI* 9:429.
213. Traber, F., Block, W., Layer, G., Braucker, G., Gieseke, J., Kretzer, S., Hasan, I., Schild, H.H. (1996) *J Magn Reson Imaging* 6:541.
214. Twentyman, P.R., Brown, J.M., Gray, J.W., Franko, A.J., Scoles, M.A., Kallman, R.F. (1980) *J Natl Cancer Inst* 64:595.
215. Van lom, K.J., Brown, J.J., Perman, W.H., Sandstrom, J.C., Lee, K.H.T. (1991) *MRI* 9:165.
216. Vogl, T.J.., Dresel, S.H.J., Spath, M., Grevers, G., Wilimzig, C., Schedel, Hk, Lissner, J. (1990) *Radiology* 177:667.
216a. Wagner-Manslan, C., Lukas, P., Herzog, M., Kau, R., Beckers, K. (1994) *European Radiology* 4:314.
217. Wahlund, La, Boethius, J., Kindstrand, E., Marions, O., Saaf, J., Wetterberg, L. (1989) *MRI* 7: 599.
218. Walker, P.M., Marie, P.Y., Merzeray, C., Bessieres, M., Escanye, J.M., Karcher, G., Danchin, N., Mattei, S., Villemet, J.P., Bertrand, A. (1993) *Magn Reson Med* 29:637.
219. Watabe, T., Azuma, T. (1989) *AJNR* 10:463.
220. Weisman, I.D., Bennett, L.H., Maxwell, L.R., Woods, M.W., Burk, D. (1972) *Science* 178:1288.
221. Weissleder, R., Stark, D.D., Elizondo, G., Hahn, P.F., Compton, C., Saini, S., Wittenberg, J., Ferrucci, J.T. (1988) *MRI* 6:675.
222. Weissleder, R., Stark, D.D., Compton, C.C., Wittenberg, J., Ferrucci, J.T. (1987) *AJR* 149:1161.
223. Wikstrom, M., Martinussen, H.J., Wikstrom, S., Ericsson, A., Nyman, R., Waldenstrom, A., Hemmingsson, A. (1990) *Acta Radiologica* 31:619.
224. Wilmes, L.J., Hoehn-Berlage, M., Els, T., Bockhorst, K., Eis, M., Bonnekoh, P., Hossmann, K.A. (1993) *J Magn Reson Imaging* 3:5.
225. Yoshida, K., Furuse, M., Kaneoke, Y., Saso, K., Inao, S., Mategi, Y., Ichihara, K., Izawa, A. (1989) *MRI* 7:9.
226. Zamaroczy, D., Schluesener, Hj, Jlesz, F.A., Sobd, R.A., Colucci, V.H., Weiner, H.L. (1991) *Invest Radiol* 26:317.
227. Zimmerman, J.R., Brittin, W.E. (1957) *J Phys Chem* 61: 1328.
228. Zipp, A., James, T.L., Kuntz, I.D., Shohet, S.B. (1976) *Biochim Biophys Acta* 428:291.

Received July 25, 2008;
accepted October 1, 2008.

Physiol. Chem. Phys. & Med. NMR (2008) *40*: 43–54

Variation of Substituents on Pirarubicin for Enhancing Response to Hepatocellular Carcinoma and Pattern Recognition Analysis to Determine Analogy to Parent Drug

Ronald L. Bartzatt

University of Nebraska
College of Arts & Sciences
Chemistry Department
Omaha, Nebraska 68182 USA
E-mail: rbartzatt@mail.unomaha.edu

Abstract: Hepatocellular carcinoma arises from hepatocytes, it is the most common primary malignant tumor of the liver and accounts for the majority of liver cancers. Pirarubicin is a compound analog to the antineoplastic anthracycline antibiotic doxorubicin. Thereby as an intercalator of DNA, pirarubicin has shown efficacy in reducing tumor activity of hepatocellular carcinoma. Utilizing in silico optimized similarity of structure search of data base and replacement by isosteres, a total of nine analogs to pirarubicin were generated. The molecular size of ring substituents (approximately a base pair) were preserved and isosteres chosen to preserve the weak electrostatic properties permitting DNA intercalation. Only a small range in molecular weight and volume was permitted in order to preserve intercalation activity. Standard deviations for polar surface area, number of heavy atoms, molecular weight, molecular volume, and number of oxygens and nitrogens, were only 3.98%, 1.76%, 16.5%, 2.51%, and 0 %, respectively, of the overall average for these properties. Variation of the target substituent resulted in insignificant changes in many properties; there was a striking variation in the lipophilic property Log P. Values of Log P ranged from 0.142 to 2.078 inclusive of pirarubicin and plays an important role in bioavailability. Hierarchical cluster analysis indicated that all analogs, except analog 6, were substantially similar to pirarubicin. A similar outcome was obtained from non-metric multidimensional scaling of descriptors. However detrended correspondence analysis distinguished both analogs 6 and 5 from the remaining analogs and pirarubicin. Nonhierarchical K-means clustering analysis determined greater differentiation among the analogs and pirarubicin. Analysis of similarity (ANOSIM) affirmed all compounds to be highly similar which shows structural optimization was achieved.

KEY WORDS: hepatocellular carcinoma, DNA intercalation, pirarubicin, intercalators

THE LIVER is the largest gland and organ in the human body with considerable ability to regenerate (1). Hepatocytes, which comprise 70% to 80% of the liver mass, are involved in protein synthesis, detoxification, transformation of carbohydrates, and excretion of exogenous substances (1). Hepatocellular carcinoma (hepatoma) is the most common primary malignant tumor of the liver (2) and one of the most common tumors worldwide accounting for up to 90% of all liver cancers. The majority of hepatocellular carcinoma are secondary to viral liver infections (hepatitis B and C) or cirrhosis (2). While surgery (including transplantation) is effective for small tumors, large or metastasized tumors receive radiation, chemotherapy, and ligation which are not considered curative.

Pirarubicin is an analog of the antineoplastic anthracycline antibiotic doxorubicin. The mode of action is intercalation of DNA (3) and is thought to interact with topoisomerase II to inhibit RNA and protein synthesis and DNA repair. Drugs acting as intercalators insert perpendicularly within DNA without the necessity of covalent bonds (4). Stability of the DNA-intercalation is maintained through hydrogen bonding, van der Waals, hydrophobic, and/or charge transfer forces (4). The large majority of these types of compounds have little or no biological activity and those that do have encountered problems with multidrug resistance (4). These factors motivate the continued search for additional compounds of this sort.

Pirarubicin has been shown to provide significant benefit in combinatorial treatment of salivary gland carcinoma (5), operable primary breast cancer (6), resectable oral and maxillary carcinoma (7), acute myeloid leukemia (8), and non-Hodgkin's lymphoma (9) and useful when unaccompanied in the clinical treatment of malignant pleural effusion (10). Previous studies have found that pirarubicin injection for cancer treatment produces doxorubicin as a major plasma metabolite, but with pirarubicinol and doxorubicinol also present (11). Extensive injections of pirarubicin results in accumulation of metabolites doxorubicin and doxorubicinol (11). Pirarubicin entry into blood cells has been determined to be a carrier-mediated process (12). Studies have shown that an increase of pirarubicin uptake results in improved antitumor activity that is superior to doxorubicin (13, 14). To effectuate the uptake of pirarubicin into the target cell clinicians have shown that a lipiodol-pirarubicin emulsion can increase cytotoxicity on hepatoma cancer cells (15). Hepatic arterial infusion of pirarubicin accompanying systemic chemotherapy was found to prevent extra-hepatic spread of tumor and prolong survival time (16). A substantially successful approach to increase pirarubicin uptake into target cancer cells incorporates pirarubicin into liposomes which stabilizes and greatly improves accumulation in the liver (17, 18), with reduced adverse effects (17), and increases in antitumor response (17, 18).

Problems for clinicians occur due to multidrug resistance to antitumor intercalators in general (4) and cross-resistance between pirarubicin (also other anthracyclines) and various other antitumor drugs (albeit pirarubicin shows lower cross-resistance than doxorubicin and epirubicin) (19). Therefore problems of multidrug resistance and apparent success of modifying the structure of pirarubicin such as the 3'-deamino- 3'-morpholino derivative that increased effectiveness (20) clearly supports the contention that exploring variations of the pirarubicin scaffold may yield designs that improve antitumor activity and length of survival. This work presents nine such variations of pirarubicin and comprehensive analysis of important pharmaceutical properties.

Methods

Molecular Modeling and Assembly of Constructs

Database search for molecular similarity was accomplished utilizing in silico database technology of Molsoft (Molsoft L.L.C., 3366 North Torrey Pines Court, La Jolla CA 92037). The numerical values of molecular properties/descriptors and 2-D molecular modeling was accomplished through ACD/ChemSketch Molecular Modeling v. 10.00 (Advanced Chemistry Development, 110 Yonge Street, Toronto Ontario, M5C 1T4 Canada). Other physicochemical properties: polar surface area, violations of Rule of 5, molecular volume, number of oxygens/nitrogens/amines/hydroxyls, were determined using Molinspiration (Molinspiration Chemiformatics, Nova ulica 61, SK-900 26 Slovensky Grob, Slovak Republic). Visualization of 3-dimensional form was accomplished utilizing SPARTAN (Wavefunction, 18401 Von Darman Avenue, Irvine CA 92612 USA).

Pattern Recognition and Elucidation

To identify underlying associations/patterns within the data matrix of numerical values for molecular properties (descriptors) various pattern recognition techniques were applied. Included in application were hierarchical cluster analysis, non-metric multidimensional scaling analysis, analysis of similarity (ANOSIM), and non-hierarchical K-means cluster analysis were performed by PAST v. 1.80 (copyright Oyvind Hammer, D.A.T. Harper 1999–2008).

Numerical Analysis of Multivariate Matrices

Statistical analysis of all numerical data was performed by Microsoft EXCEL (EXCEL 2003). Multiple regression using molecular property numerical values was accomplished by Smith's Statistical Package v. 2.75 (copyright G. Smith, Pomona College, Claremont CA). Correlation analysis for Pearson r was done for all descriptors and was accomplished by EXCEL (2003).

Results and Discussion

Ligands can interact with DNA through covalent bonding, electrostatic binding, and intercalation (21). Intercalating compounds are generally aromatic or heteroaromatic in structure and bind to DNA through insertion and stacking between the base pairs (22). The insertion causes the DNA helix to partially unwind itself at the site of intercalation, the degree of unwinding depends on the intercalating compounds (21, 23). The unwinding induces structural changes and inhibits transcription and blocks replication processes within the cell (21). The ligand displaces a magnesium and/or sodium ion that surround the DNA helix and forms a weak electrostatic bond with the outer surface of the DNA (21). Consequently the flat aromatic/heteroaromatic portion of the intercalator can slide into the hydrophobic area between the base pairs (whereas the outer environment of the DNA is considered hydrophilic) (21). These interactions can occur within the minor and major grooves of the DNA (23). Once in position the intercalate is held by hydrogen

bonds, van der Waals' forces, and charge-transfer bonds (23). It is believed that the intercalation process is actually energetically favorable because of the readiness of execution (22). The unwinding of the DNA to accommodate the intercalator also interferes with the action of DNA topoisomerases (22, 23). These effects leading to problems in replication and eventual cell death (22, 23).

Retention of hydrogen bonding sites then is necessary in any analog of pirarubicin to retain the electrostatic characteristics needed to dislodge magnesium or sodium ions and implement forces that retain the flat heteroaromatic portion between DNA bases. Hydrogen bonding being the summation of hydrogen bond donors (amine and hydroxyl groups) and hydrogen bond acceptors (oxygen and nitrogen atoms). The molecular structures of pirarubicin and nine analogs are presented in Figure 1 with the substituent which is varied indicated. Pirarubicin has within the indicated substituents two hydroxyl groups (–OH) and one oxygen (as carbonyl group), giving a total of two hydrogen bond donors, one acceptor (=O) with a total of three donor/acceptor sites. Note that in analogs 2 through 10 the varied substituents (enclosed in rectangle) have at least one hydrogen bond acceptor (oxygen of carbonyl group) and at least one hydrogen bond donor (whether as amine –NH or hydroxyl –OH). For all analogs there are at least three hydrogen bond donor/acceptors within the varied substituent as there are with the parent pirarubicin. Remembering that the flat heteroaromatic portion inserting between DNA bases remains unchanged, the overall electrostatic characteristic of the analogs remains the same as the parent pirarubicin. Clearly the variation of a substituent of pirarubicin can be accomplished in a manner that retains important physicochemical properties.

Presented in Table I are molecular properties (descriptors) determined for pirarubicin and nine analogs, that represent vital pharmaceutical traits as well as the physicochemical parameters for electrostatic forces necessary for assimilation between DNA bases. Note that the total number of oxygens and nitrogens (crucial for hydrogen donor/acceptor) remain constant at 13, with the number of amines and hydroxyls changing only 13% from the average number for all drugs. Standard deviations for polar surface area, number of heavy atoms, molecular weight, molecular volume, and number of oxygens and nitrogens, were only 3.98%, 1.76%, 16.5%, 2.51%, and 0 %, respectively, of the average for these properties. Variation of the target substituent resulted in insignificant changes in many properties. Number of rotatable bonds for this group of drugs has only a small range from 6 to 8. While the range of the polar surface area varies only from 187.328 A^2 (analog 5) to 215.908 A^2 (analogs 4 and 8), these values are sufficiently large to adversely affect bioavailability. These values of polar surface area have been shown to permit less than 10% of drug amount in the intestinal system to be absorbed (24). Problems in bioavailability are also indicated by the number of violations of the Rule of 5. All analogs (except analog 5 with 2 violations) and pirarubicin have three violations. The Rule of 5 was created to enhance the selection of potential drug candidates from high throughout screening and in silico elucidation, both mechanisms producing thousands of candidates. The Rule of 5 consists of the following parameters, which are important for a drug's pharmacokinetics, of which two or more violations suggests the drug will have problems in membrane permeation (25): 1) The drug should not have more than 5 hydrogen bond donors; 2) The drug should not have more than 10 hydrogen bond acceptors; 3) The formula weight should not be more than 500; and 4) The drug should not have a Log P of greater than 5. Problems with membrane permeation can influence the avenue of drug delivery. All compounds, including pirarubicin, are expected to have difficulties in absorption and

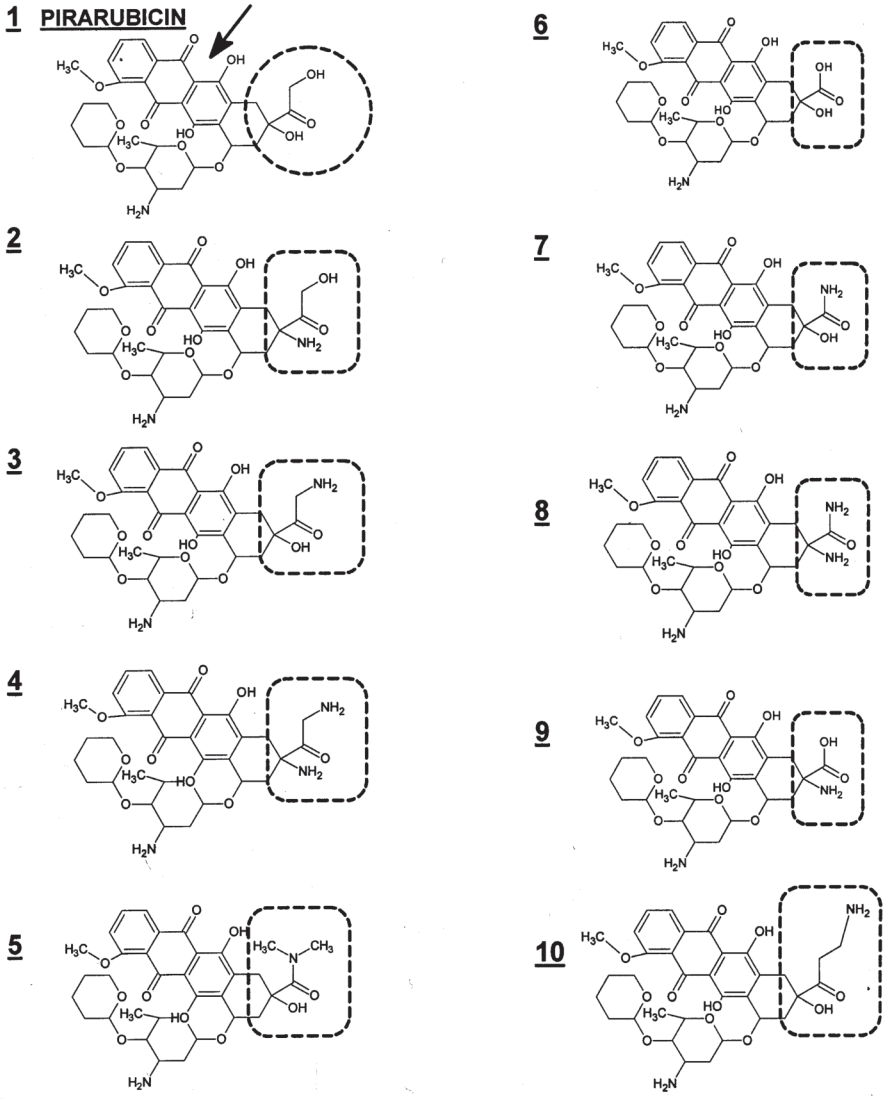

FIGURE 1. Molecular structure of the parent compound pirarubicin is shown with the substituent chosen for variation enclosed in circle and heteroaromatic moiety indicated by inset arrow. The nine analogs generated are presented in numerical order with the modified substituent indicated in rectangle (analogs).

membrane permeation. The number of heavy atoms (hydrogen atoms are excluded) deviates only 1.76% from the group average.

Numerical correlation, Pearson r, refers to the departure of two variables from independence (26). Utilizing the descriptors shown in Table I, it follows that there is substantial correlation from one drug to another, which is indicated by the calculated Pearson product-moment correlation coefficient among all drugs being greater than 0.9900. It is clearly observed that a very high correlation exists among these drugs (26). Although

TABLE I. Molecular Properties

Drug	Log P	Polar Surface Area (A^2)	Number of Atoms	Molecular Weight	Molecular Volume (A^3)	Number of Oxygens & Nitrogens	Number of Amines & Hydroxyls	Violations of Rule of Five	Number of Rotatable Bonds
Pirarubicin									
1	2.05	204.318	45	627.643	542.325	13	6	3	7
2	1.413	210.113	45	626.659	545.596	13	7	3	7
3	0.806	210.113	45	626.659	545.596	13	7	3	7
4	0.849	215.908	45	625.675	548.866	13	8	3	7
5	1.742	187.328	46	640.686	563.411	13	5	2	6
6	2.078	214.318	44	613.616	525.523	13	6	3	6
7	1.564	210.113	44	612.632	528.794	13	7	3	6
8	1.607	215.908	44	611.648	532.065	13	8	3	6
9	0.142	210.113	44	612.632	528.794	13	7	3	6
10	1.077	210.113	46	640.686	562.398	13	7	3	8

A = Angstrom

correlation does not prove causation, clearly analogs 2 to 10 are very closely related to the parent pirarubicin.

Analysis of similarity (ANOSIM) implements a statistical test to determine whether there exists a significant difference between two or more groups of data (27). In this analysis a large positive R of up to 1.000 signifies substantial dissimilarity between groups, whereas a positive value near zero indicates numerical similarity. Analysis of the data matrix shown in Table I produced an ANOSIM value of 0.2381, thereby indicating considerable similarity among the drug molecular properties inclusive of parent pirarubicin and nine analogs. This confirms evaluation by Pearson r and supports the contention that analogs of pirarubicin are highly similar to the parent.

Pattern recognition analysis presents powerful tools for visualizing and understanding complex information from databases, molecular modeling, data mining, etc, for both biological and physicochemical sources (28). Prior studies have shown that unsupervised learning techniques are particularly well suited for analysis of large data sets produced from computed molecular properties (29). In this work pattern recognition analysis will be applied to identify and elucidate underlying associations of molecular properties presented in Table I for pirarubicin and nine analogs. Hierarchical cluster analysis (HCA) is used extensively in biology, psychiatry, and physical sciences (30, 31). HCA results can be represented in a vertical or horizontal dendrogram in which subjects are classified into groups having the highest similarity (30, 31). A vertical dendrogram is presented in Figure 2 showing outcome of HCA applied to Table I data matrix. Strikingly clear is that analog 6 is distinct from all other drugs and placed into a separate cluster to itself. The

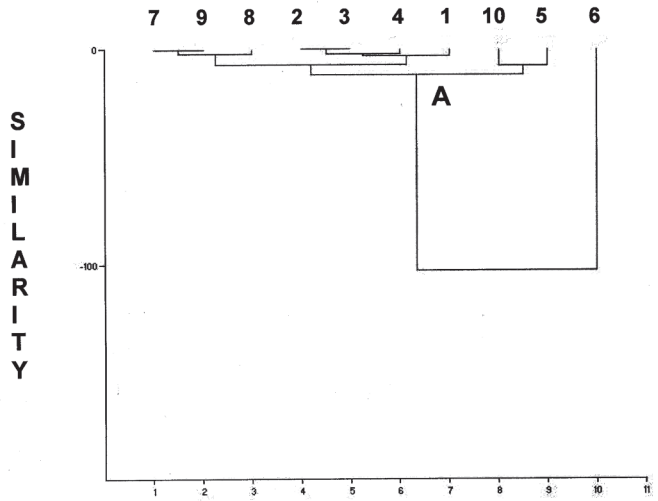

FIGURE 2. Hierarchical cluster analysis outcome produces clusters that gives placement of compounds associated by highest similarity. Only analog 6 is considered unique from the parent pirarubicin and other analogs. Super node (A) is resolved into subclusters that places pirarubicin (1) into a cluster (ie., highest similarity) that includes analogs 2, 3, and 4. In separate subclusters are analogs 7, 9, 8, and a two-member cluster having analog 10 and 5. This analysis performed utilizing standard Euclidean distance and paired-group clustering.

remaining drugs are joined at Node A, from which they are grouped into three subclusters. Analogs 7, 8, and 9 are clustered together and most similar. Analogs 2, 3, 4, and pirarubicin (1) are clustered and therefore considered most similar. The remaining analogs 10 and 5 are paired into subcluster. Joining at Node A visualizes the similarity by properties for all, save for analog 6, and supports ANOSIM and Pearson r analysis. HCA is sufficiently sensitive to increasingly resolve these drugs into subclusters beyond Node A. This outcome permits elucidation of interrelationships that may enhance clinical application. With HCA resolution then analogs 2, 3, and 4 would be considered to have the highest likeness and uniformity to pirarubicin, with potentially the likeness in drug activity.

Non-hierarchical cluster analysis, K-means cluster analysis, assigns subjects into the number of clusters designated by the investigator (32). K-means is an iterative analysis where subjects are placed into a cluster having the greatest proximity to a cluster mean. Hence the outcome is analogous to HCA where subjects are grouped so that highest similarity is identified. Utilizing the data matrix in Table I the initial results places these 10 drugs into three clusters: Cluster 1) Pirarubicin (1), 2, 3, 4, 7, 8, and 9; Cluster 2) Analog 5 and 10; Cluster 3) Analog 6. Analogously to HCA results, K-means determines analog 2, 3, and 4 to be most similar to pirarubicin (1), and analog 6 to be distinct from all others. With increased resolution into four clusters the results appear as follows: Cluster 1) Analog 6; Cluster 2) Pirarubicin (1), 2, 3, 4, 7, 8, and 9; Cluster 3) Analog 5; Cluster 4) Analog 10. Again, analogously to HCA results, K-means determines analog 2, 3, and 4 to be most similar to pirarubicin (1). Again, analog 6 is determined to be distinct from all other drugs.

Correspondence analysis is an exploratory technique and not a confirmatory method of numerical analysis (33, 34). Correspondence analysis may be applied to many discrete variables having many categories (ie., very large data tables) (33, 34). It is a nonparametric technique that makes no distributional assumptions, which is unlike factor analysis, and may be used with any level of data (34). Also referred to as correspondence mapping the outcome can be viewed as a correspondence map having two dimensions. Detrended correspondence analysis (DCA) contends with arch effect and compression of gradient ends which are two problems of ordinary correspondence analysis (33). Detrending removes the arch effect and end compression so interpretation of distances between points of a 2-way representation is accurate and expedient. Results of DCA applied to Table I are presented in Figure 3. Note that distances between points also indicates underlying associations and while plotted Axis 1 versus Axis 2 it is readily recognized that Analog 6 and 5 are distinguished from all remaining drugs along both axis. Placement along Axis 1 (primary) for drugs 1 (pirarubicin), 2, 3, 4, 7, 8, 9, and 10 coincides, suggesting likeness, with an essentially linear relationship along Axis 2 (secondary), suggesting consistency. Altogether the appearance of the 2-way DCA plot supports the contention of high similarity among the analogs with pirarubicin, with consistency, but not congruity in molecular properties (ie., the descriptors of Table I used for inter-drug comparison).

Preserving ranked differences within a data matrix while computing distance measurement is the basis of non-metric multidimensional scaling (NMDS) (35). The algorithm can then place the subjects (drugs in this study) in a two or three dimensional coordinate system with preserved ranks, such as shown in Figure 4 for all drugs. Clearly analog 6 is substantially distinct from all remaining drugs along coordinates 1 and 2. Essentially pirarubicin (1), 2, 3, 4, 5, 7, 8, 9, and 10 are grouped together, albeit analog 5 is somewhat offset from the remainder. Again the appearance supports the contention that the analog

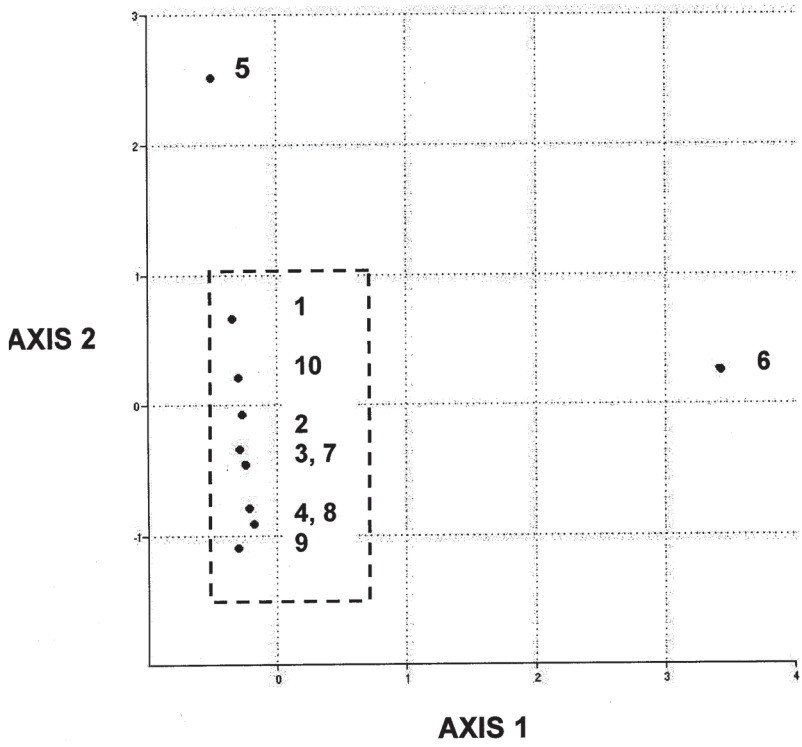

FIGURE 3. Detrended correspondence analysis clearly demonstrates that pirarubicin (1) is closely associated by molecular properties to analogs 10, 2, 3, 7, 4, 8, and 9 (see inset rectangle). The 2-way plot distinguishes analog 6 and 5 for all other compounds, which by both Axis 1 and Axis 2 shows a significant separation.

compounds modeled after pirarubicin are recognized as highly similar to the parent, and consequently similar in potential bio-activity. However the variation of substituents indicated in Figure 1 still produces a broad range in lipophilicity measured as Log P. Values of Log P run from 0.142 of analog 9 to as high as 2.078 of analog 6. Values of Log P play a significant role in bioavailability and consequently drug-likeness in criteria such as the Rule of 5. It is desirable that any variation of the substituents of pirarubicin avoids significant deviation in physicochemical properties vital for the mechanism of DNA intercalation. Hence the heteroaromatic portion is sustained as well as overall size, formula weight, and number of heavy atoms. Hydrogen bond donors (amines and hydroxyls) do not deviate significantly, and hydrogen bond acceptors (oxygens and nitrogens) remain constant. The standard deviation in Log P values is 45.89% of the population mean (range of 1.936), a value indicating considerable incongruity with the possibility of noticeable contribution to changes in bioavailability. Conceivably the changes in bioavailability may act efficacious in clinical application.

Given that consistency in properties is established through analysis by high resolution pattern recognition methods, then multiple regression analysis can be performed with appropriate descriptors to produce a mathematical depiction that can predict drugs of

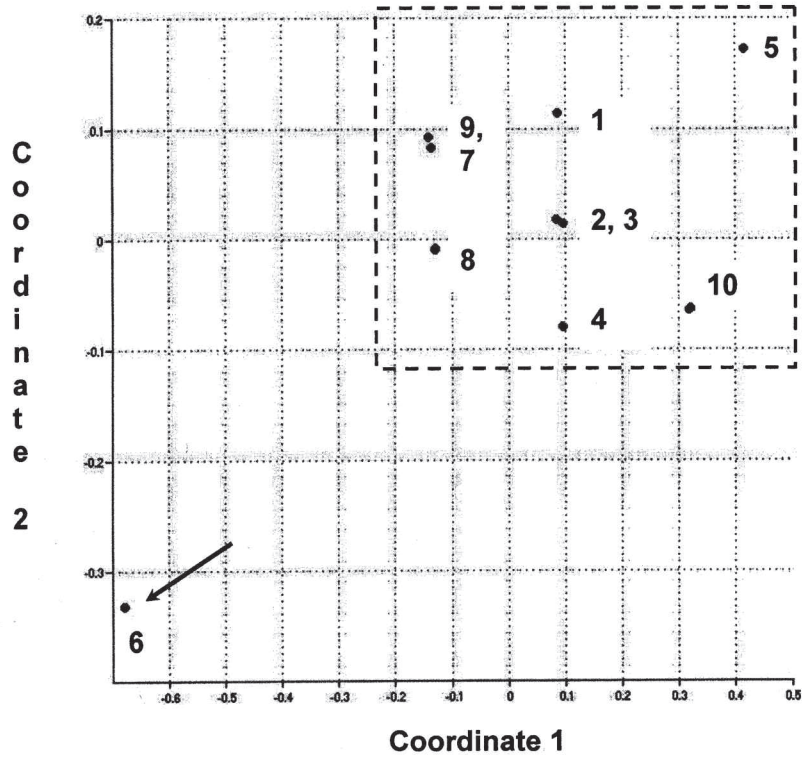

FIGURE 4. Non-metric multidimensional scaling presents results within a 2-way plot of the coordinate assignment and association contrived as similarity. Clearly the parent pirarubicin (1) is highly similar to analogs 2, 3, 4, 5, 7, 8, 9, and 10 enclosed within the inset rectangle. Only analog 6 (inset arrow) is determined to be significantly distinct from all other compounds.

similar nature. Multiple regression for prediction of formula weight was accomplished utilizing molecular volume (MV), number of heavy atoms (nAtoms), and number of -NH_n and –OH (nNHOH) as independent variables (formula weight (FW) as the dependent variable). The equation appears as follows:

FW = –58.4669 – 0.2605[MV] + 18.4042[nAtoms] – 0.1319[nNHOH].

The percent of the variance explained by the model (R^2) is determined to be 100%.

Conclusion

Utilizing pirarubicin as parent compound, nine structural analogs were modeled by applying in silico database search and isosteres replacement. Components vital to the bioactivity of these analogs, namely as DNA intercalators, such as the heteroaromatic moiety are preserved. Because of the electrostatic and hydrogen donor/acceptor requirements for successful incorporation of the drug between DNA bases, other properties of the struc-

tures must be consistent. Variation of target substituents is accomplished, however the overall hydrogen bond donor and acceptor summation remains consistent. Replacement of the hydroxyl (–OH) groups of pirarubicin is accomplished by insertion of $–NH_n$ groups, movement of the –OH groups, and maintaining the carbonyl group (C=O). The total number of hydrogen bond acceptors/donors within the varied substituents remains consistent.

Powerful and sensitive pattern recognition techniques were utilized to establish the similarity of the nine analogs to the parent pirarubicin. These included hierarchical cluster analysis, K-means cluster analysis, detrended correspondence analysis, and non-metric multidimensional scaling. Analog 6 consistently appeared to be distinct from all other drugs (by HCA, NMDS, and DCA). Analog 5 appeared distinct from all other drugs when examined by detrended correspondence analysis. However, pirarubicin is strikingly similar to analogs 2, 3, 4, 7, 8, 9, and 10, through these identical pattern recognition algorithms. In addition, Pearson r correlation determination showed high interdrug association of greater than 0.9900 and ANOSIM outcome showed high similarity at 0.2381. Multiple regression analysis utilized molecular volume, number of heavy atoms, and quantity of $–NH_n$ and –OH, to determine an equation for predicting formula weight of similar constructs.

This work demonstrates the efficacy of applying pattern recognition methods to discern underlying associations among classes of drugs and provide an approach of ascertaining the effectiveness of analog derivation of parent structure. Pattern recognition permitted the evaluation of the extent of similarity of analogs to the parent compound. Alteration of substituents on pirarubicin did produce additional anticancer drugs with intercalation potential yet retaining vital properties of polar surface area, molecular volume, and hydrogen bond donor/acceptors. Only a wide variance in the lipophilicity Log P descriptor was observed, however this feature provides the clinician the potential of applying these novel drug analogs beneficially according advantages in permeation and bioavailability. Clearly pattern recognition analysis and substituent derivatization have substantial efficacy in the design of novel anticancer drugs for the treatment of challenging hepatocellular carcinoma.

Computer and software support was provided by the Department of Chemistry, College of Arts & Sciences, University of Nebraska, NE 68182 USA.

References

1. Maton, A., Hopkins, J., McLaughlin, C., Johnson, S., Quon, M., Warner, D., Warner, M., Lahart, D., Wright, J. (1993) *Human Biology and Health*, Englewood Cliffs: Prentice Hall.
2. Dumar, V., Fausto, N., Abbas, A. (2003) *Pathologic Basis of Disease,* 7th edn. New York: Saunders.
3. Yang, P., Xi, X., Yang, M. (2007) *Ziran Kexueban* 30(2): 220–223.
4. Martinez, R., Chacon-Garcia, L. (2005) Current Med. Chem. 12: 127–151.
5. Hideaki, K., Mamoru, T. (2006) *Acta Oto-Laryngologica* 126(12): 1309–1314.
6. Li, J., Ben-Yao, L., Ou, Y., Wang, T. (2004) *Chinese Cancer Res.* 16(3): 197–202.
7. Iguchi, H., Kusuki, M., Nakamura, A., Nishiura, H., Kanazawa, A., Takayama, M., Sunami, K., Yamane, H. (2004) *Acta Oto-Laryngologica* 554: 55–61.
8. Kudo, K., Kojima, S., Tabuchi, K., Yabe, H., Tawa, A., Imaizumi, M., *et al*. (2007) J. Clin. Oncol. 25(34): 5442–5447.

9. Jiitsu, N., Umeda, M. (1998) Leukemia 12(9): 1457–1460.
10. Gotoh, T., Tanaka, Y., Fujita, Y., Hiramori, N., Fuji, T., Arimoto, T., Iwasaki, Y., Fukabori, T., Nakamura, T., Ono, N., Nakagawa, M. (1996) Japanese J. Clin. Oncol. 26: 328–334.
11. Robert, J., David, M., Huet, S., Chauvergne, J. (1988) *Eur. J. Cancer Clin. Oncol*. 24(8): 1289–1294.
12. Nagasawa, K., Kitada, N., Tsuji, C., Ogawa, M., Yokoyama, T., Ohnishi, N., Iwakawa, S., Okumura, K. (1992) *Chem & Pharmaceu. Bull.* 40(10): 2866–2869.
13. Sugiyama, T., Sadzuka, Y., Miyagishima, A., Nozawa, Y. (1998) *Drug Delivery System* 13(1): 35–40.
14. Sugiyama, T., Sadzuka, Y., Nagasawa, K., Ohnishi, N., Yokoyama, T., Sonabe, T. (1999) Japanese J. Cancer Res. 90(7): 775–780.
15. Favoulet, P., Cercueil, J., Faura, P., Osmsk, L., Isambert, N., Beltramo, J., Cagnet, F., Krause, D., Bedenne, L., Chauffert, B. (2001) *Anticancer Drugs* 12(10): 801–806.
16. Fallik, D., Ychou, M., Jacob, J., Colin, P., Seitz, J., Baulieux, J., *et al.* (2003) Ann. Oncol. 14(6): 856–863.
17. Kawano, K. (2003) *Hoshi Yakka Daigaku Kiyo* 45: 23–29.
18. Kawano, K., Takayama, K., Nagai, T., Maitani, Y. (2003) *Interna J. Pharmaceut.* 252(1–2): 73–79.
19. Dudov, A., Ilarionova, M., Horvath, L., Todorov, D. (2002) *Biotechnology & Biotechnological Equipment* 16(2): 164–167.
20. Keiichi, A., Daishiro, I., Nosaka, C., Komuro, K., Kondo, S., Takeuchi, T. (1990) *J. Antibiotics* 43(11): 1464–1470.
21. Richards, A., Rodgers, A. (2007) *Chem. Soc. Rev*. 36: 471–483.
22. Silverman, R. (1992) The Organic Chemistry of Drug Design and Drug Action, New York: Academic Press.
23. Thomas, G. (2000) Medicinal Chemistry, New York: John Wiley & Sons.
24. Ertl, P., Rohde, B., Selzer, P. (2000) *J. Med. Chem*. 43; 3714–3717.
25. Lipinski, C., Lombardo, F., Dominy, B., Feeney, P. (2001) *Adv. Drug Del. Rev*. 46: 3–26.
26. Cohen, J. (1988) *Statistical Power Analysis for the Behavioral Sciences*, 2nd edn. Hillsdale: Lawrence Erlbaum Associates.
27. Clarke, K. (1993) *Australian J. Ecol.* 18: 117–143.
28. Livingston, D. (1991) *Methods Enzymol*. 203: 613–638.
29. Hudson, B., Livingston, D., Rahr, E. (1989) *J. Comput. Aided Mol. Des.* 3(1):55–65.
30. Anderberg, R. (1973) *Cluster Analysis for Applications*, San Diego: Academic Press.
31. Romesburg, C. (1984) *Cluster Analysis for Researchers*, New York: Life Time Learning.
32. Bow, S. (1984) P*attern Recognition,* New York: Marcel Dekker.
33. Greenacre, M. (1984) *Theory and Applications of Correspondence Analysis*, New York: Academic Press.
34. Weller, S. Romney, A. (1990) *Metric Scaling: Correspondence Analysis*. Thousand Oaks: Sage Publications.
35. Davis, J. (1986) *Statistics and Data Analysis in Geology*, New York: John Wiley & Sons.

Received September 8, 2008;
accepted January 12, 2009.

Physiol. Chem. Phys. & Med. NMR (2008) *40*: 55–65

Four Hydrazide Compounds that Inhibit the Growth of Mycobacterium Tuberculosis

Ronald Bartzatt[1], Suat L.G. Cirillo[2], Jeffrey D. Cirillo[2]

[1]*University of Nebraska, College of Arts & Sciences, Chemistry Department, Omaha, Nebraska 68182 U.S.A., E-mail: rbartzatt@mail.unomaha.edu*
[2]*Texas A & M Health Science Center, Dept. of Microbial and Molecular Pathogenesis, College Station, Texas 77843 U.S.A.*

Abstract: Over one-third of the world's population has been exposed to Mycobacterium tuberculosis (TB). New drug designs are necessitated by the appearance of multi-drug resistant tuberculosis (MDR-TB) and extensively drug-resistant tuberculosis (XDR-TB). This work presents four hydrazide compounds that inhibit Mycobacterium tuberculosis growth at potency comparable to isoniazid. The hydrazide drugs A, B, C, and D were synthesized utilizing microwave excitation methodologies. Hydrazide agents are produced from parent carboxyl compounds. All reactions were accomplished in dry conditions. Using suitable molecular scaffolds the final hydrazides possessed the desired properties in Log P, polar surface area, molecular weight, etc. All four hydrazide compounds induced at least 60% inhibition of TB at concentrations at less than 31.5 microgram/mL. Measured as relative survival, all four hydrazide compounds induced greater than 95% death of TB bacteria at concentrations less than 31.5 microgram/mL. Drugs A, B, C, D exhibited zero violations of the Rule of 5, indicating favorable bioavailability. Although isoniazid, A, B, C, and D were determined to have a polar surface area less than 70 Angstroms^2, the values of Log P (a measurement of lipophilicity) showed a broad range of –1.463 (drug C) to 4.46 (drug A). The numerical values of polar surface area suggests that all drugs would have greater than 50% intestinal absorption. For all drugs the number of amine (-NH) and hydroxyl (-OH) groups remains constant at three, with number of oxygens and nitrogens varying only three to four. ANOSIM (analysis of similarity) indicated that isoniazid, A, B, C, and D are highly similar. Correlation of molecular properties for all five drugs is greater than r = 0.9500. Drugs A, B, C, and D are members of two homologous series of anti-tuberculosis agents. All hydrazides effectively inhibited TB at 31.5 micrograms/mL and lower concentrations.

KEY WORDS: Mycobacterium tuberculosis, hydrazides, isoniazid, TB, bacteria

THE PRIMARY cause of Mycobacterium tuberculosis (TB) is an aerobic bacterium which divides at an extremely slow rate every 16 to 20 hours (1). While latent TB infection is most common, over one-third of the world's population has been exposed to TB

bacterium (with death and new cases occurring primarily in developing nations) (2). The emergence of multi-drug resistant TB (MDR-TB) resistant to isoniazid and rifampicin (of first line drugs ethambutol, isoniazid, pyrazinamide, rifampicin, streptomycin) and extensively drug resistant TB (XDR-TB) resistant to second line drugs (aminoglycosides, polypeptides, fluoroquinolones, thioamides, cycloserine, p-aminosalicylic acid) have contributed to the spread of the disease (3). TB replicate within the alveolar macrophages of the lung forming a primary site referred to as the Ghon focus (4), however all parts of the body can be affected by the disease. A latent infection of TB is usually treated with a single antibiotic, while an active infection is treated with combinations of several antibiotics (5).

The mycobacterial cell wall is extraordinarily thick and consists mainly of long-chain fatty acids and polysaccharide arabinogalactan (6,7). The cell wall is responsible for the hydrophobicity of TB and helps the bacteria to resist oxidative damage within the macrophages. The thick wall of high lipid content contributes to the difficulty for drug penetration, but these bacteria are sensitive to heat and ultraviolight light.

Isoniazid itself is a prodrug that must be activated by catalase-peroxidase enzyme KatG to form an isonicotinic acyl anion (or radical). These forms then react with NADH anion (or radical) to an isonicotinic acyl-NADH complex (8). The complex binds tightly to ketoenoylreductase (InhA) and will prevent access to the natural enoyl-AcpM substrate (8). This process inhibits the synthesis of mycolic acid in the mycobacterial cell wall (8). Previous studies have shown that isoniazid transport to TB proceeds by passive diffusion mechanism and KatG is not involved in the transport (9).

To contend with the appearance of MDR-TB and XDR-TB investigators have pursued novel carrier moieties for isonicotinic acid, such as trans-cinnamic acid derivatives (10) and activating peroxidases (11). Novel drug designs are pursued due to worldwide reports of MDR-TB resistance to isoniazid and rifampicin, as well as XDR-TB resistance to fluoroquinolones and aminoglycosides (12). Treatment for TB infections within health facilities of Turkey often encounter the MDR-TB form that requires an extensively monitored and administered combination regimen of three drugs based on susceptibility tests (13). Other studies conducted in Turkey revealed that diabetes mellitus and sexual-intercourse were risk factors for the development of drug resistance(14). A large number of MDR-TB and XDR-TB cases have been recently reported (2007) in Europe (15), with MDR-TB emerging in Nigeria (16). Within the United States reports from an area hospital indicate that MDR-TB type infections are not successfully responding to available treatment, with only half of the patients ultimately having the disease subdued after carefully selected regimens (17).

These alarming trends clearly indicate the continued exploration of treatment methods and new/modified drug designs. Presented are four hydrazide agents exhibiting TB inhibition at a level that is comparable to isoniazid. In addition, these agents constitute members of two homologous series of anti-tuberculosis drugs.

Materials and Methods

Reagents and Instrumentation

All solvents and reagents were analytical grade and obtained from Aldrich Company (Milwaukee, WI, USA). Fourier transform infrared spectroscopy was accomplished using

a Mattson Galaxy FTIR, with analytes dissolved in dimethyl sulfoxide (DMSO) that was previously dried over molecular sieves. Tissue culture 7H9 broth and 7H9 (M-ADC) agar were utilized (Difco, Detroit, MI, USA).

Molecular Modeling and Numerical Analysis

Modeling and property determinations were accomplished by ChemSketch v. 5 (ACD, 90 Adelaide Street West, Toronto, Ontario Canada). Some properties were determined by EPISUITE v 1.40 (US Environmental Protection Agency, Washington D.C., USA). ANOSIM (analysis of similarity) and multivariate analysis were performed by PAST v. 1.28 (Oyvind Hammer, D.A.T. Harper copyright 1999–2004). Correlation analysis was performed by Microsoft Excel 2003 (copyright 1985 to 2003).

Culture of Mycobacteria

Mycobacterium tuberculosis strain Erdman (ATCC35801) cultures were grown in Difco 7H9 media supplemented with 0.5% glycerol, 10% albumin-dextrose complex (ADC), and 0.25% Tween 80 (M-ADC-TW) for 10 days at 37° C prior to use in experiments. Colony forming units were determined for all cultures and after treatment with antimicrobials by plating dilutions on Difco 7H9 agar and growth until colonies formed at 37° C. All drugs were tested within the same length of time period.

Synthesis of Compounds

Prior to use the hydrazine (NH_2NH_2) must be distilled out from the stock mixture over CaO and NaOH. The anhydrous hydrazine (NH_2NH_2) is collected at 113° C. Microwave Irradiation Synthesis of Compounds A, B, C, and D: Place 150 mg of compound into pyrex test tube with 50 µL of $SOCl_2$. Microwave 3 to 5 minutes, then cool. Add about 20 mg of Na_2CO_3 to the mixture and mix. Add 50 µL of anhydrous NH_2NH_2 and microwave up to 1 minute. The NaCl formed can be removed by dissolving the preparation in minimal water and extracting with ethyl acetate or acetonitrile, which is pooled, dried over anhydrous magnesium sulfate then evaporated to obtain the final product residue. The presence of the hydrazine group was confirmed on 1 through 5 by FTIR, showing peaks at 944 cm^{-1} for hydrazine and 1000 cm^{-1} to 1200 cm^{-1} for C-N stretch (3000 cm^{-1} to 3500 cm^{-1} N-H stretch).

Results and Discussion

The leading causes of death from a single infectious agent are comprised of TB, malaria, and HIV (18). However, TB remains the important infectious disease causing morbidity and death (18). The most common form is pulmonary TB that is highly contagious and life threatening (18). The development of new drugs for the clinical treatment of TB is a slow and expensive process which is inhibited by the lack of suitable animal models and difficulties implementing clinical studies (18). Drugs A, B, C, and D are hydrazide compounds that are members of two homologous series of agents and inhibit TB comparably to isoniazid-a first line TB treatment drug.

Previous studies have shown the efficacy of microwave excitation to synthesize hydrazide agents that inhibit the growth of Mycobacterium tuberculosis (19,20). A homologous

series is a group of compounds that differ only by a constant unit which is usually a -CH_2- group (21,22). In general, the lengthening of a saturated carbon chain from one to five, or to nine carbons, increases the pharmacological effects of the agent (21,22). However, the increase of chain length past nine carbons produces a decrease in potency (21). It is believed that this phenomena is affected largely due to the steady increase of lipophilicity and solubility into cell membranes but that the decrease in water solubility becomes problematic at higher chain lengths (21). Other shapes in response curves have been reported but the bell shaped curve is most common (22).

Previous studies also have shown that two identical twin drugs ethanedihydrazide (22) and hexanedihydrazide (19) can significantly inhibit the growth of TB bacteria. These two agents also comprise two members of a homologous series that are characterized by the presence of a non-branched aliphatic chain of carbon atoms between hydrazide functional groups. Previous work has demonstrated the efficacy of covalently bonding a hydrazide functional group onto an aliphatic non-branched chain of 11 carbons forming dodecanohydrazide [20], which was able to induce greater than 50% reduction of TB at concentrations of less than 50 micrograms/milliliter. The latter compound suggested then that a homologous series could be formed by extending the aliphatic carbon chain covalently bonded to the hydrazide functional group.

The molecular structures for drugs A, B, C, and D are presented in Figure 1 for comparison with isoniazid. Note that dodecanohydrazide is a member homolog with drug A

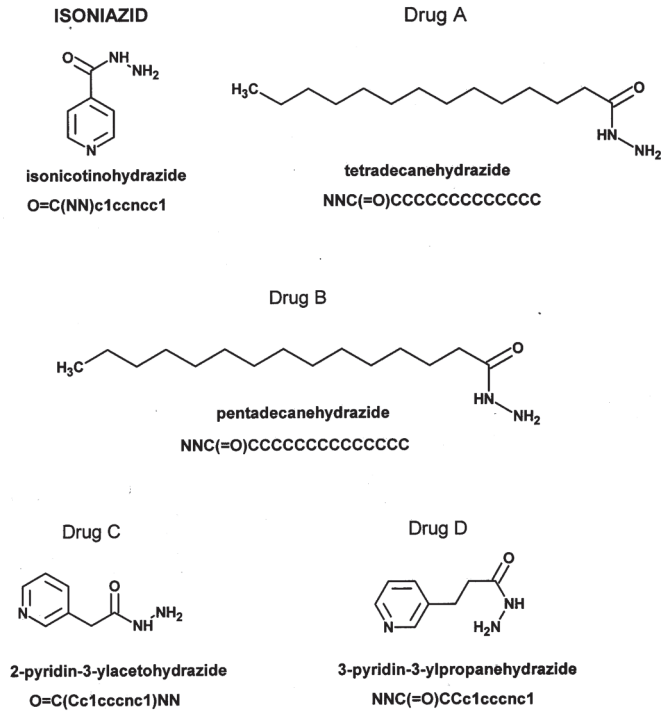

FIGURE 1. The molecular structures of drugs A, B, C, and D are shown for comparison to isoniazid. Note that all compounds are hydrazides with isoniazid, drug C, and drug D having a single aromatic ring. Drugs A and B have an aliphatic hydrocarbon chain.

(tetradecanehydrazide) and drug B (pentadecanehydrazide), with all three having a long non-branched chain of carbon atoms. Another homologous series is defined by drug C (2-pyridin-3-ylacetohydrazide) and drug D (3-pyridin-3-ylpropanehydrazide), where the hydrazide functional group is separated from an aromatic ring by one (drug C) or two (drug D) aliphatic carbon atoms. Therefore, three homologous series of anti-TB agents have been synthesized by microwave excitation and shown to have significant growth inhibition directed at Mycobacterium tuberculosis. Note that similarly to isoniazid all drugs A, B, C, and D have a single hydrazide functional group present. The SMILES (Simplified Molecular Input Line Entry Specification) designation for all compounds are presented in Figure 1. Effects of movement of the nitrogen atom around the aromatic ring from isoniazid (para to hydrazide group) to the meta position within drug C and D induce no significant change in Log P. However, the addition of a single carbon atom to an aliphatic chain portion of a homolog induces a significant increase in Log P. For example, an eleven carbon chain substituent would undergo about a 26% increase in Log P value (higher lipophilicity) by adding three carbons (total of 14 carbons). Even the addition of only one carbon atom from 14 to 15 will bring about a 7% increase in Log P and increase in lipid solubility. The hydrazide group (-C(O)NHNH$_2$) is clearly hydrophilic while comparatively the aromatic ring and aliphatic carbon chain are lipophilic.

The general synthesis methodology is presented in Figure 2 showing the major steps of the microwave excitation approach of activating the carbonyl carbon (-C(O)-) of the carboxyl group (-C(O)OH) and followed by completion of the hydrazide functional group. Initially the carboxyl group of the parent structure is activated by reaction with thionyl chloride under dry conditions and microwave excitation. By-products HCl and SO_2 are released then as gases and allowed to escape the reaction chamber. This activated carbonyl carbon is highly reactive, should not be stored, and must be kept in dry conditions. Hydrazine (NH_2NH_2) is prepared previously by distillation and introduced into the reaction mixture quickly. The microwave excitation should be done in short pulses with careful examination to avoid degradation due to excessive heating. The presence of Na_2CO_3

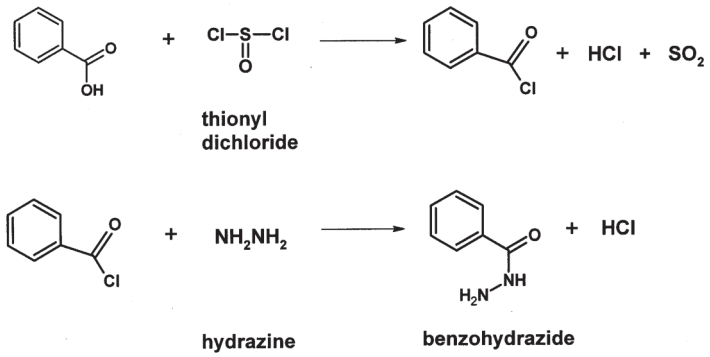

FIGURE 2. The general synthesis methodology for obtaining a small hydrazide compound is presented here. Initially the parent compound is treated with thionyl chloride to activate the carbonyl carbon for reaction with hydrazine. The purified hydrazine is then introduced in a non-aqueous environment which produces the final hydrazide compound. These steps are performed with microwave excitation and non-aqueous conditions.

neutralizes the HCl which is formed as a by-product, and the hydrazide group is produced. The products are solids and soluble in aqueous solution. The hydrazide compounds should be stored at –20 °C and kept dry until use.

Molecular properties of all five hydrazides are presented in Table I for comparison to isoniazid. Analysis of similarity (ANOSIM) determines what extent of numerical sameness exists in a multivariate data matrix (23). ANOSIM determined that the properties of Table I are highly similar, producing R of 0.08333 (where an R equal to 1.000 shows properties that are highly dissimilar). Therefore, among these five small molecule hydrazides there exists substantial continuity of molecular structure. Isoniazid has been shown to be highly effective in deterring TB proliferation and the further design of anti-TB drugs modeling isoniazid is shown here to have great efficacy. Properties known to describe water solubility features include Log P (lipophilicity), polar surface area (PSA), number of oxygens and nitrogens nON (hydrogen bond acceptors), and number of amines and hydroxyls nNHOH (hydrogen bond donors). Considering that PSA has an average value of 62.86 A^2 with a standard deviation of 7.06 A^2, a value only 11.2% of the average, the range of this descriptor is small and by PSA the structures are consistent. The values of PSA (< 70 A^2) suggest that these hydrazides will have a high probability of good oral availability (24), with an intestinal absorption of greater than 60% (25,26,27). By utilizing the following equation it is possible to estimate the extent of brain penetration (ie., penetration of the blood brain barrier-BBB) as Log BB (where BB = Cbrain/Cblood) for these hydrazides (25,26): Log BB = –0.021(PSA) – 0.003(molecular volume) + 1.643. Results obtained produced Log BB values of isoniazid, A, B, C, and D to be –0.153, –0.335, –0.385, –0.204, and –0.253, respectively. Accordingly the values of BB for isoniazid, A, B, C, and D are 0.703, 0.462, 0.412, 0.625, and 0.557, respectively. This outcome suggests that a substantial number of these hydrazides will cross the BBB and penetrate into the central nervous system from blood vessels. Other studies have shown that a drug has a high probability of entering the central nervous system if the sums of the oxygens and nitrogens is less than five (29), a charactistic shared by all five hydrazides. Passage through the BBB is not a requirement for beneficial treatment of tuberculosis.

The average in molecular weight is 190.469 ± 54.9 with a standard deviation that is 28.8% of the average. Likewise, the average of the molecular volume is 196.375 ± 79.2 A^3 with a standard deviation that is 40.3% of the average. The utilization of an aliphatic carbon chain in place of or in addition to the aromatic ring found in isoniazid results in considerable alteration of molecular weight and molecular volume of drugs A, B, C, and D, compared to isoniazid. The number of amine and hydroxyl groups remains constant at 3 for all hydrazides, with the total number of oxygens and nitrogens varying only between 3 and 4. There is very high correlation among the numerical values for all descriptors (see Table I) of isoniazid, A, B, C, and D, found to result in R values greater than 0.9600. Likewise, the correlation R values comparing each drug produced very high correlation and values greater than 0.9700. Very high correlation among descriptors purports the molecular relatedness of these five hydrazides.

The Rule of 5 are criteria to evaluate druglikeness of a known structure or in other words determine if a chemical compound with a certain phamacological or biological activity would also make a likely orally active drug (30). The required parameters are as follows: 1) There are not more than 5 hydrogen bond donors; 2) No more than 10 hydrogen

TABLE I. Molecular Properties of Isoniazid and Drugs A, B, C, D

Drug	Log P	Polar Surface Area (Angstroms^2)	Number of Atoms	Molecular Weight	Number of oxygens & nitrogens	Number of -NH & -OH	Violations of Rule of Five	Number of Rotatable Bonds	Molecular Volume (Angstroms^3)
isoniazid	–0.969	68.013	10	137.142	4	3	0	1	122.562
A	4.46	55.121	17	242.407	3	3	0	12	273.492
B	4.965	55.121	18	256.434	3	3	0	13	290.294
C	–1.463	68.013	11	151.169	4	3	0	2	139.363
D	–0.945	68.013	12	165.196	4	3	0	3	156.165

bond acceptors; 3) A molecular weight less than 500; and 4) Log P value less than 5. The violations of Rule of 5 for all hydrazide drugs are zero (see Table I) and consequently these hydrazides are expected to be orally active and assimilable through the intestinal tract. This characteristic and others support the strong clinical potential of drugs A, B, C, and D. The capacity of a drug to be administered orally enhances patient compliance and facilitates clinical application.

Not all people who become infected with TB develop the active disease. Many individuals having healthy immune systems can fight the bacteria, have no symptoms, and cannot spread TB in this latent (inactive) condition. However, the active infection produces symptoms and these individuals can spread TB by coughing or sneezing. Treatment of active infections is vital for restraining proliferation of the bacteria throughout a community. The hydrazide compounds A, B, C, and D have been determined to effectively inhibit the growth of TB and accomplish this at a level comparable to isoniazid. All five hydrazide drugs were placed into tissue culture similarly and evaluated for TB growth inhibition. Similarly to isoniazid, drugs A, B, C, and D were able to reduce growth of TB at low concentrations. In terms of relative survival of bacteria, drugs A, B, C, D, and isoniazid induced essentially zero percent survival (ie., no surviving bacteria) at concentrations of approximately 31.5 micrograms/milliliter and greater. This clearly demonstrates the potential clinical efficacy of these microwave synthesized homologous hydrazides.

The inhibitory action of these hydrazides was also measured based on relative optical density of TB bacteria. The results for drugs A and B compared to isoniazid are shown in Figure 3. Greater than 70% inhibition of TB bacteria is achieved by isoniazid, A, and B at concentrations below 62.5 micrograms/mL. Similarly to isoniazid, the hydrazides A and B are highly effective at a concentration as low as 31.5 micrograms/milliliter.

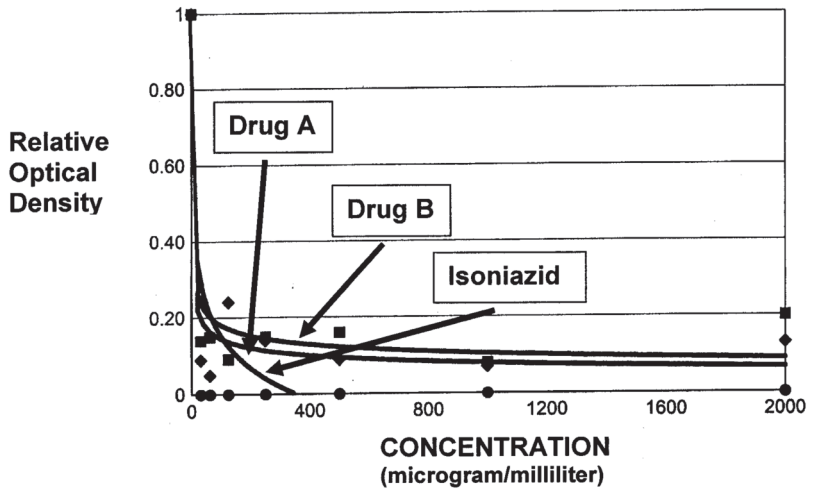

FIGURE 3. The relative inhibition of Mycobacterium tuberculosis by drugs A and B are compared to isoniazid using measured optical density of treated cultures. Essentially isoniazid, drug A, and drug B reach greater than 80% growth inhibition at less than 60 microgram/mL of compound. The comparable growth inhibition of bacteria by drugs A and B shows the relevancy of constructing drug structures having favorable size, Log P, and polar surface area.

Similarly measurements of drugs C and D in tissue culture produced results comparable to the first-line drug isoniazid. The results for drugs C and D compared to isoniazid are shown in Figure 4. Greater than 70% inhibition of TB bacteria is achieved by isoniazid, C, and D at concentrations at and below 62.5 micrograms/milliliter. Similarly to isoniazid, the hydrazides C and D are highly effective at a concentration as low as 31.5 micrograms/milliliter. At all concentrations of drug, growth of the TB bacteria is substantially inhibited and reduced. These results demonstrate the potent action of hydrazide antibiotics in substantially inhibiting the growth of TB bacteria. Clearly hydrazide constructs have an important function in the clinical treatment of TB infections. The further design of hydrazide constructs having optimized molecular properties suitable for clinical treatment of TB infections is justified.

Conclusion

Isoniazid is a hydrazide compound that is a first-line treatment drug for infections of Mycobacterium tuberculosis. Using microwave excitation four hydrazide drugs were synthesized that also carry the hydrazide functional group and varying number of aliphatic carbon atoms (ie. $–CH_2–$) that define them as members of a homologous series of compounds. Determination of descriptors such as Log P, polar surface area, molecular weight, and number of hydrogen bond donors/acceptors revealed important facets of this group of compounds. The correlation R of molecular properties for this group of drugs was extremely high as was correlation between the drugs themselves. In addition, ANOSIM analysis showed these hydrazides to be highly similar. Zero violations of the Rule of 5 indicate drugs A, B, C, and D would have favorable bioavailability, substantial intestinal

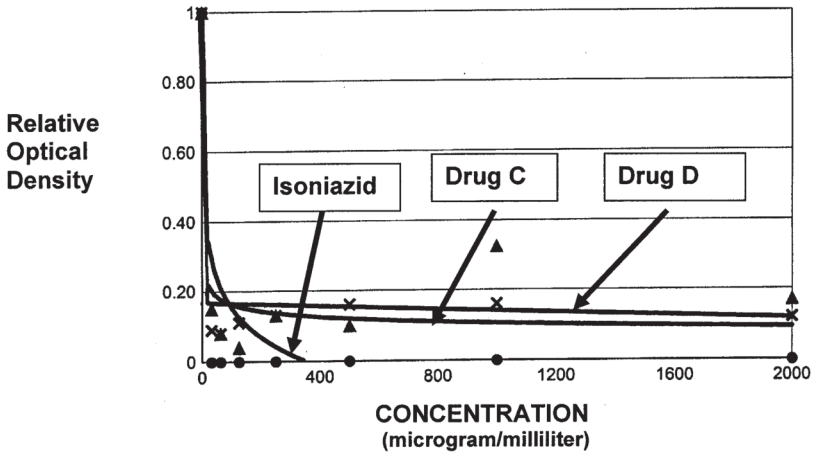

FIGURE 4. The relative inhibition of Mycobacterium tuberculosis by drugs C and D are compared to isoniazid using measured optical density of treated cultures. Essentially, isoniazid, drug C, and drug D reach greater than 80% growth inhibition at less than 60 microgram/mL of compound. These results support the strong clinical potential for drugs A, B, C, and D.

absorbance, and conformity to parameters suggesting active orally administered pharmaceuticals. Calculation of Log BB indicated that a substantial fraction of these hydrazides that are in the bloodstream would cross through the BBB and enter the central nervous system. A wide range in Log P values reflects the diversity in molecular scaffolding that is useful for hydrazide type pharmaceuticals. Relative survival of TB bacteria is essentially zero for isoniazid, A, B, C, and D at concentrations as low as 31.5 micrograms/mL. Measurements of relative optical density likewise showed isoniazid, A, B, C, and D to be highly effective in inhibiting the growth of TB bacteria at very low concentrations. Drugs A, B, C, and D achieved greater than 70% inhibition at concentrations as low as 31.5 micrograms/mL based on relative optical density. The efficacy of utilizing microwave excitation for hydrazide synthesis is shown.

This work was funded by the College of Arts & Sciences, University of Nebraska, Chemistry Department, Durham Science Center, 6001 Dodge Street, Omaha NE 68182.

References

1. Cox, R. (2004) Quantitative relationships for specific growth rates and macromolecular compositions of Mycobacterium tuberculosis, Streptomyces coelicolor A3(2) and Escherichia coli B/r: an integrative theoretical approach. *Microbiology* 150(pt 5): 1413–1426.
2. Raviglione, M.C. and O'Brien, R.J. (2004) Tuberculosis, *Harrison's Principles of Internal Medicine*, McGraw-Hill Professional, New York,.
3. Centers for Disease Control and Prevention. (2006) Emergence of Mycobacterium tuberculosis with extensive resistance to second-line drugs—worldwide, 2000–2004. *MMWR Morb. Mortal. Wkly. Rep.* 55(11):301–305.
4. Houben, E., Nguyen, L. and Peters, J. (2006) Interaction of pathogenic mycobacteria with the host immune system. Curr. Opin. Microbiol. 9(1):76–85.
5. O'Brien, R. (1994) Drug-resistant tuberculosis: etiology, management and prevention. *Semin. Respir. Infect*. 9(2):104–112.
6. Hong, X. and Hopfinger, A.J. (2004) Construction, molecular modeling, and simulation of Mycobacterium tuberculosis cell walls. *Biomacromolecules* 5(3):1052–1065.
7. Davis, B., Dulbecco, R., Eisen, H. and Ginsberg, H. (1990) *Microbiology*, JB Lippincott, London,.
8. Timmins, G.S. and Deretic., V. (2006) Mechanisms of action of isoniazid. *Mol. Microbiol.* 62(5):1220–1227.
9. Bardou, F., Raynaud, C., Ramos, C., Laneelle, M.A., and Laneelle, G. (1998) Mechanism of isoniazid uptake in Mycobacterium tuberculosis. *Microbiology* 144:2539–2544.
10. Carvalho, S.A., da Silva, E.F., de Souza, M.V., Lourenco, M.C. and Vicente, F. (2008) Synthesis and antimycobacterial evaluation of new trans-cinnamic acid hydrazide derivatives. *Biorg. Med. Chem. Lett*. 18(2):538–541.
11. Metcalfe, C.L., Macdonald, I.K., Murphy, E.J., Brown, K.A., Raven, E.L. and Moody, P.C. (2008) The tuberculosis prodrug isoniazid bound to activating peroxidases. *J. Biol. Chem*. 283(10):6193–6200.
12. Greinert, U., Hillemann, D., Lange, C. and Richter, E. (2007) Antibiotic drug-resistant tuberculosis. *Med. Klin.* (Munich). 102(12):957–966.
13. Tahaogiu, K., Torun, T., Sevim, T., Atac, G., Kir, A., Karasulu, L., Ozmen, I. and Kapakii, N. (2001) The treatment of multidrug-resistant tuberculosis in Turkey. *N. Engl. J. Med.* 345(3):170–174.
14. Gonlugur, T.E., Goniugur, U. and Hasbek, M. (2007) Antitubeculosis drug resistance in a Turkish state hospital with national data. *Acta Microbiol. Immunol. Hung*. 54(9):421–451.

15. Macedo, R., Perdigao, J., Brum, I. and Portugal, I. (2007) Multidrug resistant tuberculosis in Lisbon. *Rev. Port. Pneumol.* 13(6):20–21.
16. Kehinde, A.O., Obaseki, F.A., Ishoia, O.C. and Ibrahim, K.D. (2007) Multidrug resistance to Mycobacterium tuberculosis in a tertiary hospital. *J. Natl. Med. Assoc*. 99(10):1185–1189.
17. Gobie, M., Iseman, M.D., Madsen, L.A., Waite, D., Ackerson, L. and Horsburgh, C.R. Jr. (1993) Treatment of 171 patients with pulmonary tuberculosis resistant to isoniazid and rifampin. *N. Engl. J. Med*. 328(8):527–532.
18. Tomioka, H. and Namba, K. (2006) Development of antituberculosis drugs: current states and future prospects. *Kekkaku* 12:753–754.
19. Bartzatt, R., Cirillo, S.L.G. and Cirillo, J.D. (2007) Design and in vitro evaluation of five inhibitors of Mycobacterium Tuberculosis. *Letters in Drug Design & Discovery* 4(2):137–143.
20. Bartzatt, R., Cirillo, S.L.G. and Cirillo, J.D. (2008) Determination of molecular properties effectuating the growth inhibition of Mycobacterium tuberculosis by various small molecule hydrazides. *Letters in Drug Design & Discovery* 5(3):162–168.
21. Silverman, R.B. (1992) *The Organic Chemistry of Drug Design and Drug Action*, Academic Press, San Diego,.
22. Wermuth, C.G. (1996) *The Practice of Medicinal Chemistry*, Academic Press, San Diego,.
23. Clarke, K.R. (1993) Non-parametric multivariate analysis of changes in community structure. *Australian J. Ecology* 18:117–143.
24. Veber, D.F., Johnson, S., Cheng, H.Y., Smith, B., Ward, K. and Kopple, K. (2002) Molecular properties that influence the oral bioavailability of drug candidates. *J. Med. Chem*. 45(12):2615–2623.
25. Clark, D.E. (1999) Rapid calculation of polar molecular surface area and its application to the prediction of transport phenomena. 1. Prediction of blood-brain penetration. *J. Pharm. Sci.* 88:815–821.
26. Palm, K., Stenberg, P., Luthman, K. and Artursson, P. (1997) Polar molecular surface properties predict the intestinal absorption of drugs in humans. *Pharm. Res*. 14: 568–571.
27. Clark, D.E. (1999) Rapid calculation of polar molecular surface area and its application to the prediction of transport phenomena. 1. Prediction of intestinal absorption. *J. Pharm. Sci*. 88:807–814.
28. Kelder, J., Grootenhuis, P., Bayada, D., Delbressine, L., Ploemen, J. (1999) Polar molecular surface as a dominating determinant for oral absorption and brain penetration of drugs. *Pharm. Res.* 16:1514–1519.
29. Osterberg, T., Norinder, U. (2000) Prediction of polar surface area and drug transport processes using simple parameters and PLS statistics. *J. Chem. Inf. Comput. Sci*. 40:1408–1411.
30. Linpinski, C.A., Lombardo, F., Dominy, B., Feeney, P. (2001) Experimental and computational approaches to estimate solubility and permeability in drug discovery and development settings. *Adv. Drug Del. Rev.* 46:3–26.

Received December 23, 2008;
accepted July 13, 2009.

Physiol. Chem. Phys. & Med. NMR (2008) *40*: 67–88

Proton HR-MAS NMR Spectroscopic Characterization of Metabolites in Various Human Organ Tissues: Pancreas, Brain and Liver from Trauma Cases

Divya Misra[1], Vivek Gupta[2], Abhinav A. Sonkar[2*]
Usha Bajpai[1] and Raja Roy[3*]

[1] *Department of Physics, University of Lucknow, Lucknow — 226001, India;*
[2]*Department of General Surgery, Chhatrapati Shahuji Maharaj Medical University, Lucknow-226001, India;*
[3]*Centre of Biomedical Magnetic Resonance, Sanjay Gandhi Post Graduate Institute of Medical Sciences, Rae Bareli Road, Lucknow-226014, India*
**Corresponding Authors: E-mail: vandana_abhinav@rdiffmail.com, E-mail: rajaroy28@gmail.com*

Abstract: High-Resolution Magic Angle Spinning (HR-MAS) NMR has been employed to characterize various metabolites of human pancreas, liver and brain tissues from trauma cases. The potential usefulness of NMR in identifying the metabolites in human tissues has been explored using a combination of one- and two-dimensional experiments. The complete resonance assignments of pancreas tissue have been carried out for the first time. Two new metabolites, α-hydroxyisovalarate and α-hydroxybutarate were identified in all the tissue specimens. The metabolites information of these human tissues can further be utilized in correlating several diseases associated with pathological manifestations as well in distinguishing traumatic tissues along with control tissues of pancreas, liver and brain.

KEY WORDS: trauma; HR-MAS NMR; lipids; pancreas; liver; brain; tissue specimen; α-hydroxyisovalarate; α-hydroxybutarate

HIGH-RESOLUTION ^{1}H nuclear magnetic resonance (NMR) spectroscopy has proved to be one of the most powerful technologies for biofluids and essentially the only one capable of studying the biochemical profile of intact tissues (1–4) without the need for pre-selection of measurement-parameters or selection of separation- and/or derivatization procedures. Besides various laboratory methods available for identification of metabolites, their characterization has been a topic of interest. In addition to the current procedures, the utility of other bio-analytical technique such as mass spectrometry in understanding

the biochemistry of metabolites in human tissues has been explored in recent times (5). NMR spectral analysis of tissues has largely relied upon tissue extraction methods (6). However, different invasive extraction processes are required for characterisation of small metabolites and lipids, which may be time consuming. During the last few years, the development of high-resolution ^{1}H magic angle spinning (HR-MAS) NMR spectroscopy has allowed the ability to analyze intact tissues as small as 8–10 mg. Rapid spinning of the sample (typically around 4–6 kHz) at an angle of 54.7º relative to the applied magnetic field serves to reduce severe line-broadening effects seen in such heterogeneous samples under HR-MAS (7–11). The angular factor ($3\cos^2\theta - 1$) is averaged out to zero and it is possible to obtain very high-quality NMR spectra of whole tissue samples with no sample pre-treatment. Such experiments have also indicated that diseased- or toxin-affected tissues may have substantially different metabolic profiles compared to those taken from healthy organs.

Several reports exist in literature regarding the metabolic identification of human tissue specimens (12–15), and more recently, metabolic profiling has also been applied to study tissue samples affected with breast cancer (16). The HR-MAS NMR spectra show resolution comparable to that of extracts (solution-state NMR), and application of two-dimensional techniques have further led to identification of a majority of the structural constituents. While ^{1}H and ^{13}C NMR spectroscopic techniques have become methods-of-choice to obtain full-length structural information regarding the metabolites present in tissues, these can be mapped and quantitated from a single experiment (17). Using this technology, it is also possible to bridge the gap between tissue NMR analyses and histopathology, and both could be performed for the same tissue specimen in order to gain real insights into the mechanisms of pathology at molecular level.

This work presents the application of HR-MAS ^{1}H NMR spectroscopy to characterize the metabolites of human traumatic tissue samples. The potential usefulness of 2D NMR experiments such as COSY (Correlated Spectroscopy) and ^{1}H-^{13}C HSQC (Heteronuclear Single Quantum Coherence) has been explored to full extent to identify the metabolites. An attempt has been made to identify new metabolites in these tissue systems, if any, which may be useful in understanding possible disease states in such tissues and its analysis may also aid to distinguish diseased tissues from traumatic ones.

Materials and Methods

Human brain tissues (n = 6), liver (n = 6) and pancreas (n = 6) were obtained from accident-associated trauma patients in the age group of 22–28 years (all males free from any disease state) undergoing emergency surgical procedures. Devitalized tissues and their margins, removed as part of the surgical procedure, were also taken for NMR analysis. Only non-decomposed tissues that were macroscopically free from disease were chosen. Prior approval was taken from the ethics committee of the trauma center at King George's Medical University, (now Chattrapati Shahuji Maharaj Medical University) Lucknow. The selected tissues were stored in high-quality plastic vials and were snap-frozen in liquid nitrogen until the time of spectroscopic analysis. HR-MAS NMR of the intact tissue from each specimen were taken (30–35 mg wet weight). Each sample was introduced in a 4 mm ZrO_2 rotor fitted with 50 µl cylindrical insert. The rotor was transferred into the NMR probe. All NMR measurements were carried out at 25.0 °C.

The HR-MAS spectra were recorded on a Bruker Avance 400 spectrometer operating at a frequency of 400.3 MHz, equipped with a 4 mm $^{1}H/^{13}C$ dual HR-MAS probe with magic angle gradient. For all NMR experiments, the samples were spun at 4.0 kHz in order to keep the rotation side bands out of the acquisition window. One-dimensional proton NMR spectra with water presaturation were acquired using one-dimensional NOESY pulse sequence with a mixing time τ_m of 100 ms. Total relaxation delays of 3.99 s were used with 8250.8 Hz spectral width, 128 transients with a total recording time of 9 minutes. The one-dimensional CPMG pulse sequence with water presaturation using echo time of 200 ms was used in order to remove short T_2 components arising from large molecules like lipids. The one-dimensional spin echo experiment with water presaturation was also recorded using an echo time of 160 ms, which simultaneously suppresses the short T_2 components along with multiplicity information obtained for small molecules.

Two-dimensional COSY using water presaturation was carried out on each set of tissue samples. A spectral width of 4807.69 Hz and 2.2 s relaxation delay was used and 128 transients were averaged for each of the 256 t_1 increments corresponding to a total acquisition time of 7 hrs. The data were zero filled to 512 w and weighted with sine-bell window function, prior to double Fourier transformation. Two-dimensional, $^{1}H/^{13}C$ gradient HSQC with adiabatic pulses was performed on each set of the tissue specimens using water pre-saturation; 1.6 s of total relaxation delay was used and 128 transients were averaged for each 128 t_1 increments corresponding to a total acquisition time of 8.0 hours. The data were zero filled to a 1024 w matrix and weighted with 90° shifted square sine-bell function prior to double Fourier transformation.

Results and Discussion

The complete assignments of the various metabolites were carried out by a combination of one dimensional NOESY (Nuclear Overhauser Effect Spectroscopy), CPMG (Carr-Purcell, Meiboom Gill) and two-dimensional COSY and HSQC spectra. Prior to resonance assignments all the spectra were referenced with respect to the methyl group (CH_3) of lactate at 1.33 ppm in the ^{1}H NMR and its corresponding ^{13}C chemical shift at 22.6 ppm in the HSQC spectra. Resonances due to lipid moieties were effectively filtered by the use of CPMG experiments in all the three set of tissue samples. The one-dimensional proton NMR spectrum of all the three tissue specimens show a large number of signals and a high degree of overlap especially in the range of 3.0 ppm to 4.0 ppm and were significant with their own distinctive pattern as shown in Figure 1a–c respectively. Whereas the CPMG spectra provided detailed resonances of the small metabolites showing finger prints of pancreas, liver and brain tissue's metabolic profile (Figure 2a–c and their expansions). The assignments are based on the comparison of chemical shifts and spin multiplicities with data reported in literature (18–19).

Proton resonances between 0.68 ppm and 6.0 ppm in the spectra of all three tissue samples can be divided into three broad regions. From 0.65–2.9 ppm the presence of $(CH_2)n$-protons of lipid chain, sterol methyl and methylene proton resonances; phospholipid head group and glycerol back-bone proton and glucose resonances between 3.05 ppm and 5.25 ppm; vinyl proton signals between 5.30 ppm and 5.95 ppm. The two-dimensional COSY spectrum allowed us to assign signals to particular metabolites through the examination of the existing cross peak correlations. The detailed spectral assignments of each tissue specimens are as follows:

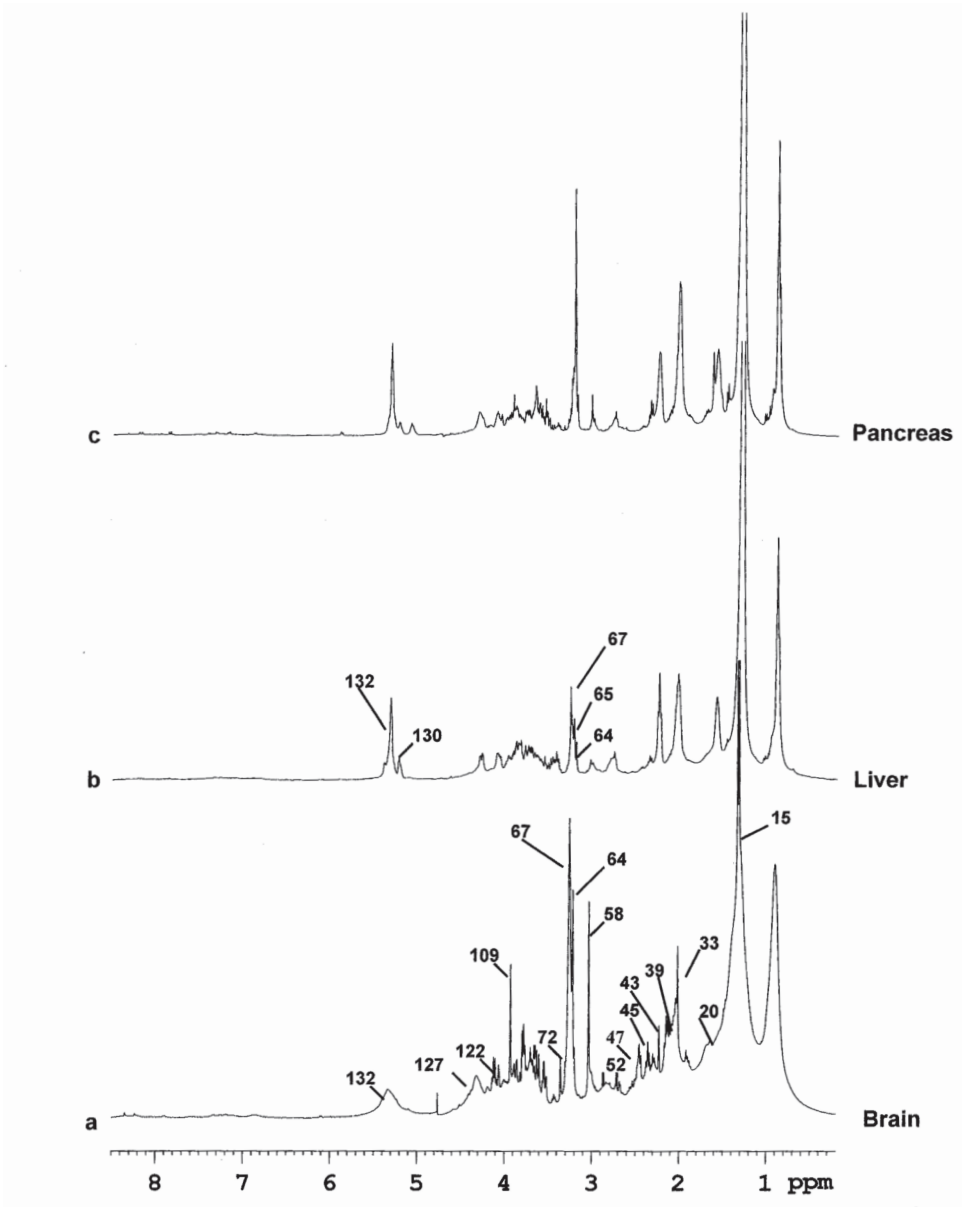

FIGURE 1a–c. The typical ^{1}H HR MAS one-dimensional NMR spectra (0.2–8.5 ppm) with water presaturation using NOESY pulse sequence of the (a) brain (b) liver and (c) pancreas tissues obtained from traumatic patients highlighting the assignments of the metabolites as given in Table I, see page 78.

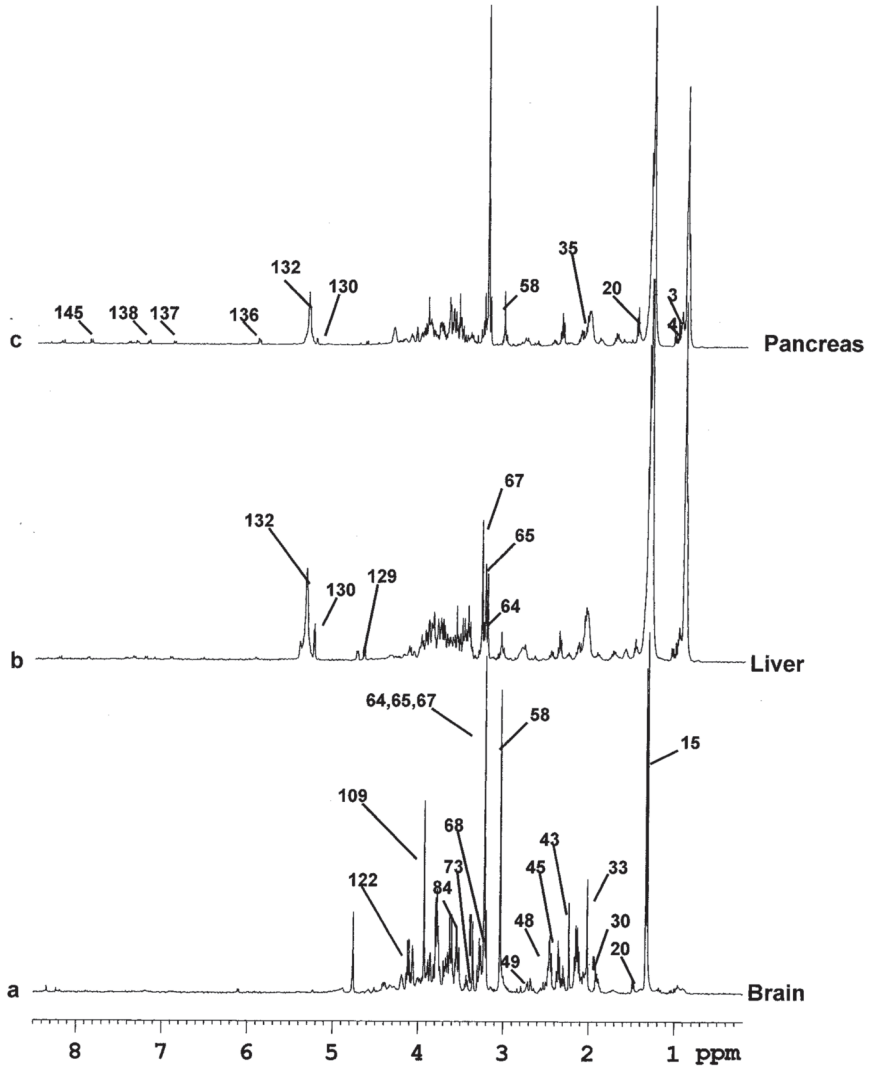

FIGURE 2a–c. The typical ^{1}H HR MAS one-dimensional CPMG NMR spectra (0.2–8.5 ppm) of the (a) brain (b) liver and (c) pancreas tissues along with their respective expansions (0.2–5.8 and 6.0–8.5ppm) obtained from traumatic patients highlighting the assignments of the small molecule metabolites as given in Table I, see page 78.

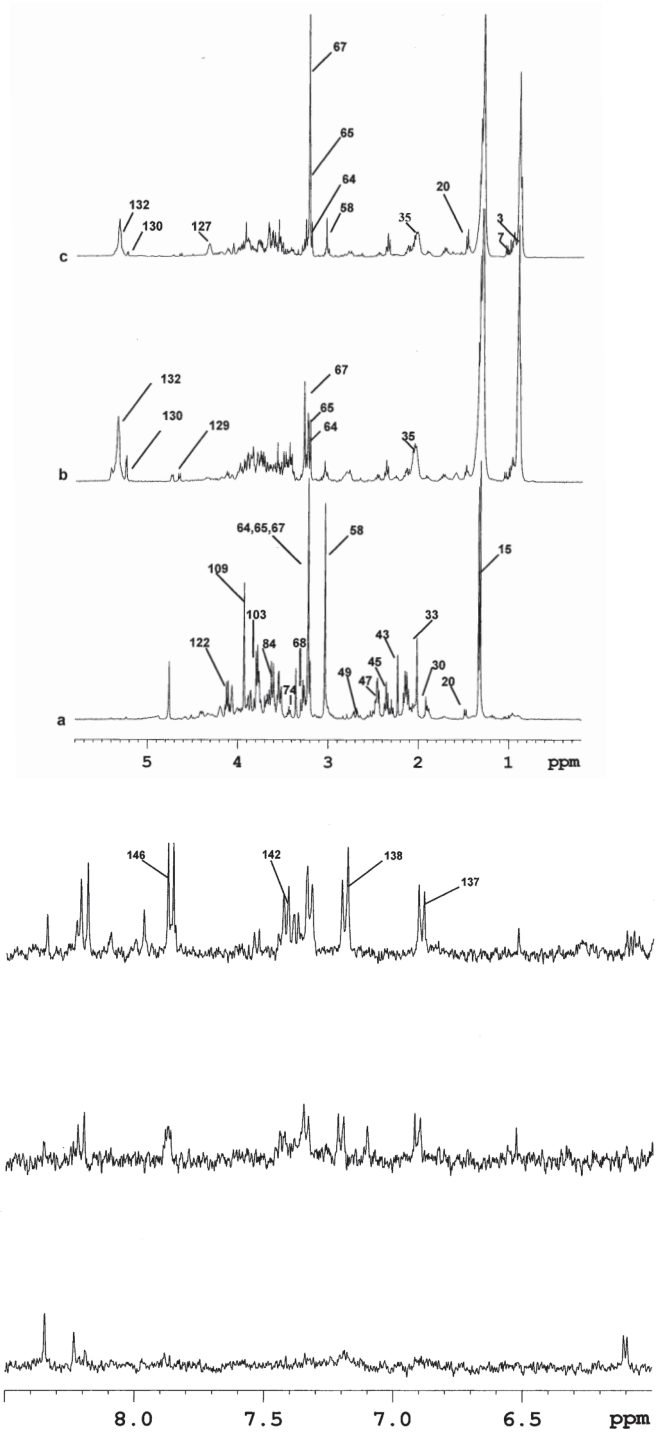

FIGURE 2a–c (EXPANSION).

Human Pancreas

By direct inspection of one-dimensional ^{1}H NMR spectra, and by comparison with literature data the following peaks were readily assigned: doublets at 1.33 ppm and 1.47 ppm for lactate and alanine, singlets at 2.29, 3.03, 3.19, 3.20, 3.24 and at 3.56 ppm for acetoacetate, creatine, choline, phosphocholine, glycerophosphocholine and the simplest amino acid glycine. Quartet of lactate due to CH group at 4.11 ppm, doublet of triplet of glutamate at 2.34 ppm and multiplet of glutamine at 2.14 ppm, doublets of α- and β-glucose at 5.23 ppm and 4.64ppm were clearly observed in the CPMG spectrum (Figure 2a–c and its expansions). Similarly, resonance assignments of myo-inositol at 4.04 ppm and doublet of uridine at 5.89 ppm, and of tyrosine at 6.81 and 7.17 ppm, multiplets of phenylalanine at 7.42 ppm and of fatty acids at 0.90, 1.58, 2.01, 2.81, and at 5.32 ppm were carried out.

The ^{1}H and ^{13}C NMR assignments of fatty acid chains indicated that the lipids consisted of mono-saturated and poly-unsaturated fatty acids. The overlapped signal of the terminal methyl protons of the fatty acid chains could be assigned based on the HSQC correlations. The $-(CH_2)_n-$ protons of fatty acids were found to occur as a highly intense and broad signal at 1.28 ppm–1.38 ppm. The allylic methylenes of type $-CH_2–CH=CH-$ were assigned at 2.04 ppm in the ^{1}H NMR spectra and at 27.3 ppm in the ^{13}C NMR spectra. The highly intense proton multiplet signal at 5.30 ppm had the collective contributions from vinyl (-CH=CH-) protons in the fatty acid chains and from sterols. Further, a broad multiplet signal at 2.76 ppm reinforced the presence of D^n methylenes $(-CH=CH-(CH_2–CH=CH)_n-; n \leq 1)$ in the fatty acid chain. The olefinic -CH's (at 5.32 ppm) gave the corresponding ^{13}C correlations between 130–132 ppm.

The presence of metabolites in one-dimensional ^{1}H spectra, specially the ones which were overlapped with resonances of other metabolites, was further confirmed by the cross-peak mapping of two-dimensional COSY spectrum as shown in Figure 3a, 3b. Since each metabolite has a distinct cross peak correlation in the COSY spectrum, it has therefore helped us in confirming the presence of threonine, phenyalanine, glycerol, proline, ethanolamine, tyrosine, taurine, myo-inositol, aspargine, aspartate, choline/glycerophosphocholine/phosphocholine, ethanolamine, lysine, serine, α-β glucose, lysine and uridine. The characterization of the α-hydroxyvalerate was carried out based on the distinctive cross-peak correlation pattern in the COSY spectrum. The methyl protons at 0.97 ppm showed strong cross peaks with the CH proton at 2.02 ppm only. Similarly, identification of α-hydroxybutarate was carried out by the observance of distinctive cross peak due to CH_3 and β-CH_2 groups at 0.90 and 2.24 ppm in the COSY spectrum (22). The presence of uridine was also characterized in the pancreas tissue specimen because of the presence of distinct cross peak between C1H and C5H protons at 5.89–7.88ppm of the uridine moiety. The COSY spectrum also showed strong cross peaks of macromolecules of lipids and triglycerides.

Further confirmation of the metabolites was carried out with the help of ^{1}H-^{13}C HSQC spectra Figure 4a–b. The HSQC spectra made possible a more reliable assignment of signals by comparison of ^{1}H and ^{13}C data with those of literature values. The HSQC spectra helped in the identification of proline, serine and glycerol. To aid spectral interpretation, the information provided by one-dimensional and two-dimensional COSY and HSQC spectra were combined and resonances of various metabolites were assigned. A complete list of identified metabolites along with their ^{1}H and ^{13}C chemical shift is given in Table I.

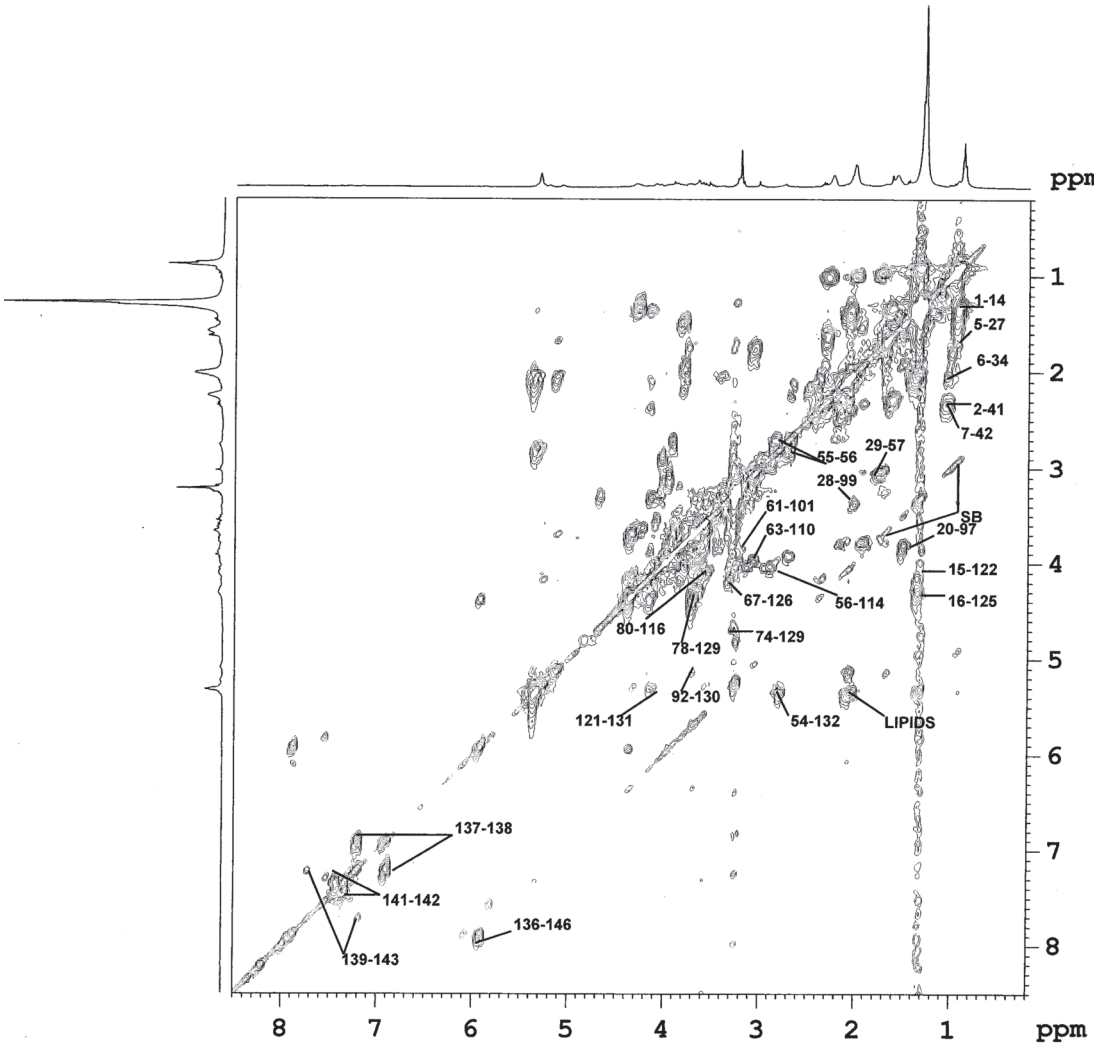

FIGURE 3a. The COSY spectrum of the pancreas tissue with labeled assignments of the metabolites as given in Table I, see page 78.

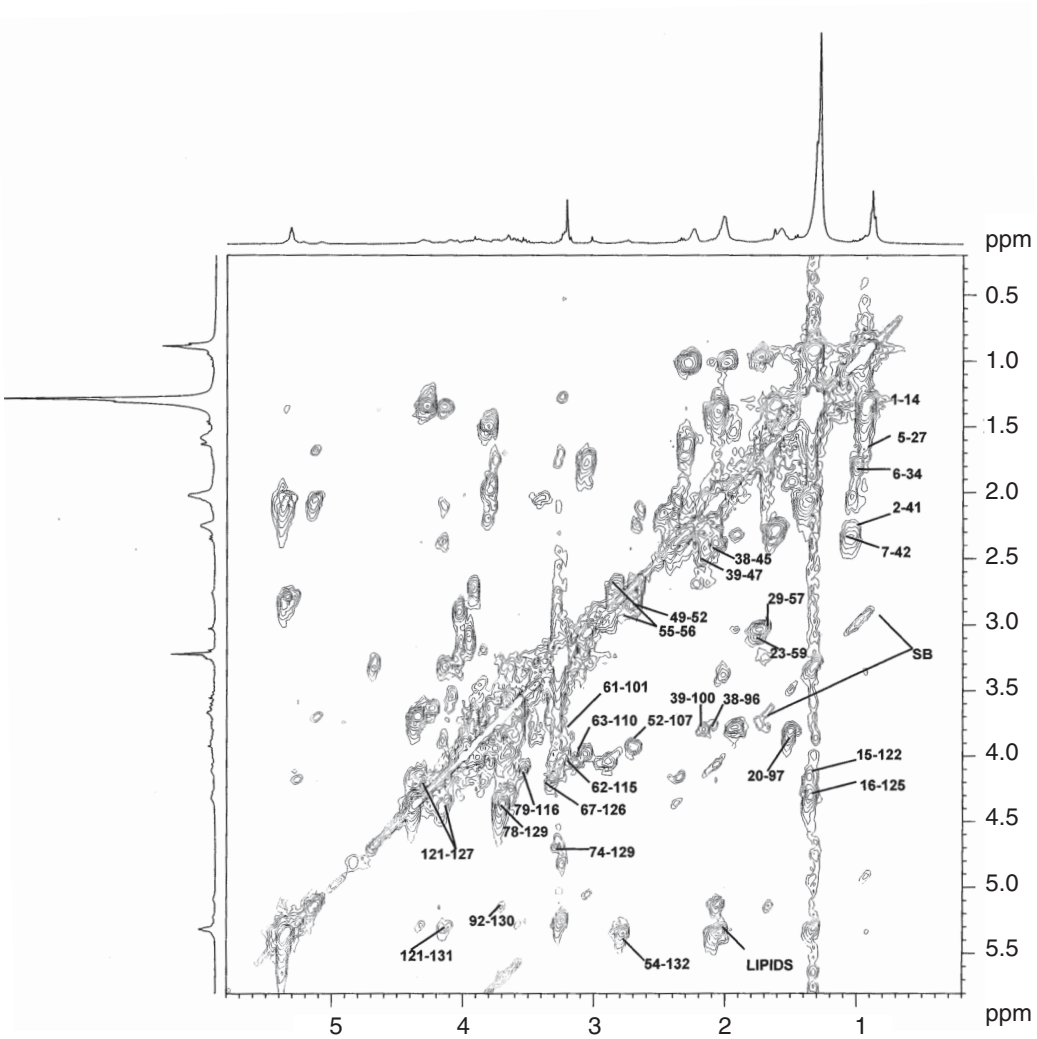

FIGURE 3b. Expansions of the COSY spectrum (0.2-5.8 ppm). The detailed labeled assignments are given in Table I, see page 78.

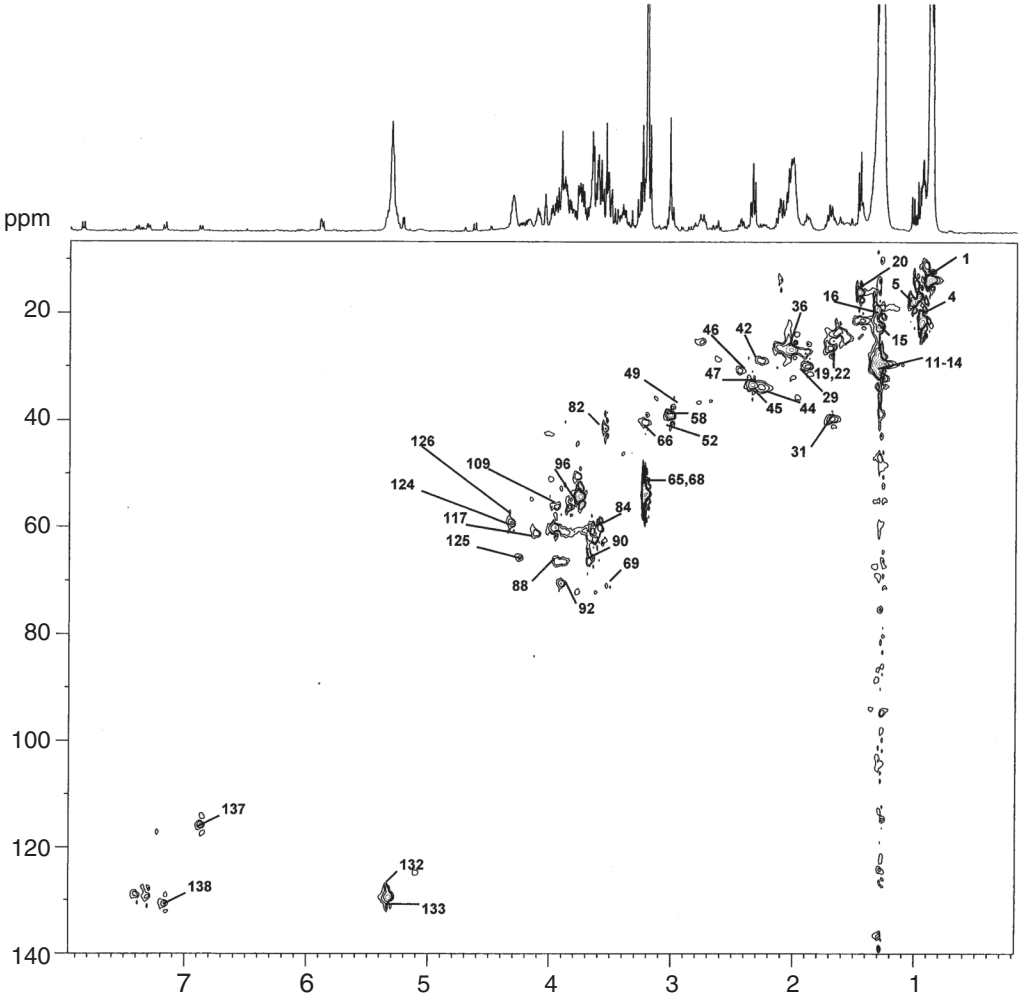

FIGURE 4a. The ^{1}H-^{13}C HSQC spectrum of the of the pancreas tissue specimen, highlighting the resonance assignments in the F1 dimension (^{13}C) and in the F2 dimension (^{1}H). The labeled assignments are as given in Table I, see page 78.

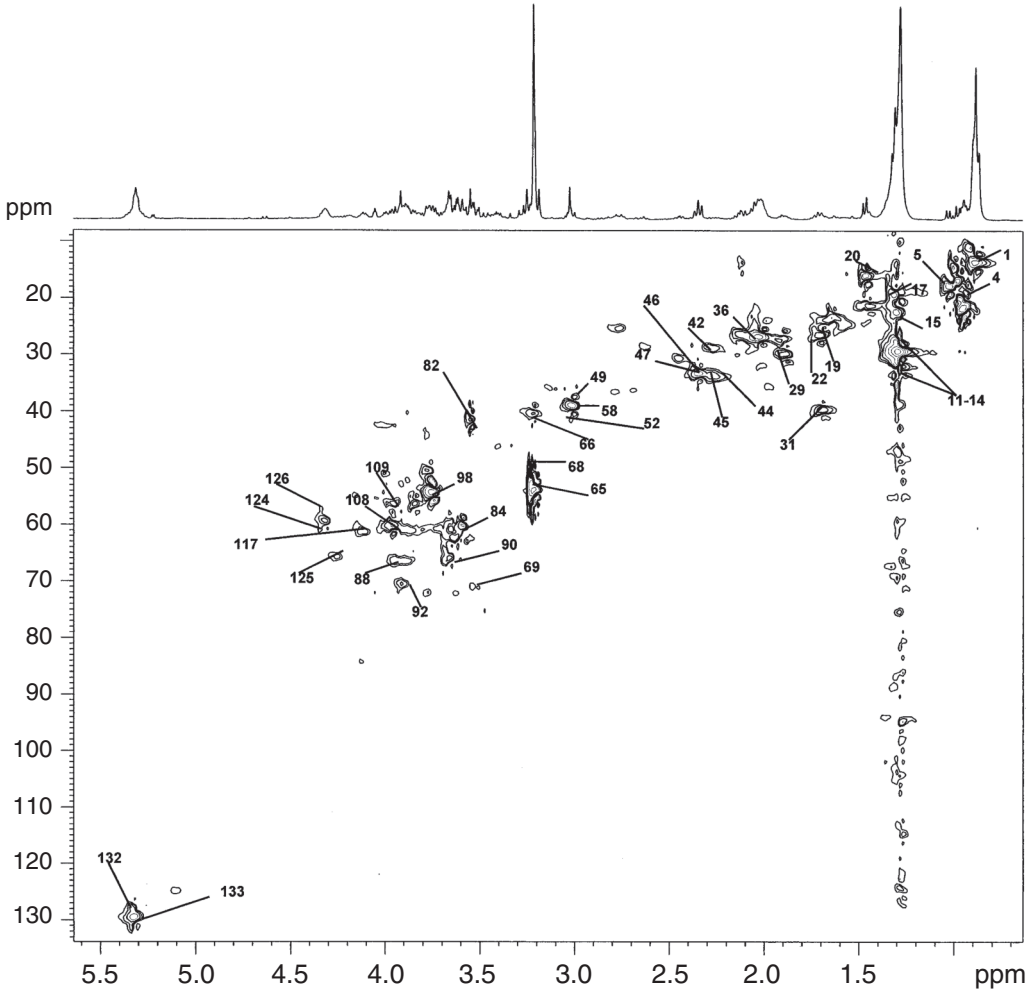

FIGURE 4b. Expansion of the ^{1}H-^{13}C HSQC spectrum of the pancreas tissue specimen, highlighting the resonance assignments between 9.0–133.0 ppm in the F1 dimension (^{13}C) and 0.55–5.22 ppm in the F2 dimension (^{1}H). The labeled assignments are as given in Table I, see page 78.

TABLE I. Resonance assignments of most significant metabolites in HR-MAS spectra of human brain, liver and pancreas tissue specimens trauma cases.

S.No	Metabolite	Group	^{1}H Shift	^{13}C Shift	Human Brain	Human Liver	Human Pancreas	Multiplicities
1	Fatty Acids	CH_3	0.90	19.7	P	P	P	t
2	a-Hydroxybutyrate	CH_3	0.90		P	P	P	
3	Isoleucine	δCH_3	0.94	13.8	*	P	P	t
4	Leucine	δCH_3	0.95	23.5	P	P	P	d
5	Leucine	δCH_3	0.96	24.7	P	P	P	d
6	α-Hydroxyisovalerate	CH_3	0.97		P	P	P	d
7	Valine	γCH_3	0.98	19.2	P	P	P	d
8	Isoleucine	γCH_3	1.01	17.4	P	P	P	d
9	Valine	γCH_3	1.04	20.6	P	P	P	d
10	Isoleucine	γCH_2u	1.24	27.2	P	P	P	m
11	Fatty acids(a)	$(2)CH_2$	1.28	34.6	P	P	P	m
12	Fatty acids(a)(b)	$(n)CH_2$	1.29	32.5	P	P	P	
13	Fatty acids(a)	$(1)CH_2$	1.29	25.5	P	P	P	
14	Fatty acids(c)	$(n)CH_2$	1.31	31.8	P	P	P	
15	Lactate	CH_3	1.33	22.6	P	P	P	d
16	Threonine	γCH_3	1.34	21.9	P	P	P	d
17	Fatty acids(b)	$(1)CH_2$	1.37	32.3	P	P	P	m
18	Isoleucine	γCH_2d	1.46	27.1	P	P	P	m
19	Lysine	γCH_2	1.46	24.1	P	P	P	d
20	Alanine	βCH_3	1.47	18.9	P	P	P	d
21	Fatty acids(c)	$(2)CH_2$	1.58	27.6	*	P	P	m
22	Arginine	γCH_2	1.67	26.5	P	P	P	m
23	Lysine	δCH_2	1.68	29.1	P	P	P	m
24	α-Hydroxybutyrate	γCH	1.69	-	P	P	P	
25	Arginine	βCH_2	1.71	29.1	*	P	*	m
26	Leucine	βCH_2	1.71	42.4	P	P	P	m
27	Leucine	γCH	1.71	27.1	*	P	P	m
28	Lysine	βCH_2	1.90	32.5	P	P	P	m
29	GABA	$3CH_2$	1.90	26.3	P	A	P	m
30	Acetate	CH_3	1.91	25.6	P	P	P	s
31	Isoleucine	βCH	1.98	38.5	P	P	P	m
32	Proline	γCH_2	2.01	26.5	P	P	P	m
33	NAA	CH_3	2.02	24.6	P	A	A	s
34	α-Hydroxyisovalerate	βCH	2.02	-	P	P	P	m
35	Fatty Acids (b)	$(2)CH_2$	2.04	27.3	P	P	P	m
36	Glutamate	βCH_2u	2.04	29.6	P	P	P	m
37	Proline	βCH_2u	2.06	31.6	P	P	P	m
38	Glutamate	βCH_2d	2.12	29.5	P	P	P	dt
39	Glutamine	βCH_2	2.14	28.8	P	P	P	m
40	Fatty Acids(c)	$(1)CH_2$	2.24	36.2	*	P	P	m
41	α-Hydroxybutyrate	βCH_2	2.24	-	P	P	P	
42	Valine	βCH	2.28	31.7	P	P	P	m
43	Acetoacetate	CH_3	2.29		P	P	P	s
44	GABA	$4CH_2$	2.29	37.1	P	A	P	t
45	Glutamate	γCH_2	2.34	36.1	P	P	P	dt
46	Proline	βCH_2d	2.35	31.1	P	P	P	m
47	Glutamine	γCH_2	2.44	33.5	P	P	P	m

TABLE I. (continued)

S.No	Metabolite	Group	^{1}H Shift	^{13}C Shift	Human Brain	Human Liver	Human Pancreas	Multiplicities
48	NAA	βCH_2u	2.49	40.4	P	A	A	dd
49	Aspartic Acid	βCH_2u	2.65	39.2	P	P	P	dd
50	Citrate	1/2 CH_2	2.67	*	P	P	A	d
51	NAA	βCH_2d	2.68	40.4	P	A	A	dd
52	Aspartic Acid	βCH_2d	2.80	39.2	P	P	P	dd
53	Citrate	1/2 CH_2	2.81		P	P	A	d
54	Fatty Acids(b)	CH_2	2.81	28.1	P	P	P	m
55	Aspargine	β CH_2u	2.86	37.2	P	P	P	dd
56	Aspargine	β CH_2d	2.96	37.2	P*	P	P	dd
57	GABA	$2CH_2$	3.01	41.9	P	A	P	t
58	Creatine	$N(CH_3)$	3.03	39.1	P	P	P	s
59	Lysine	CH_2	3.05	41.6	P	P	P	t
60	Tyrosine	β CH_2u	3.05	38.2	P	P	P	dd
61	Ethanolamine	CH_2-NH_3	3.12	44.1	P	P	P	t
62	Phenylalanine	βCH_2u	3.12	39.1	P	P	P	dd
63	Tyrosine	βCH_2d	3.19	38.1	P	P	P	dd
64	Choline	$N^+(CH_3)_3$	3.19	56.6	P	P	P	s
65	PCho	$N^+(CH_3)_3$	3.20	56.6	P	P	P	s
66	Arginine	γCH_2	3.23	43.2	P	P	P	t
67	GPCho	CH_2-NH_3	3.24	56.7	P	P	P	s
68	Taurine	CH_2-NH_3	3.25	50.1	P	P	P	t
69	Myo-Inositol	C5H	3.25	76.5	P	P	P	t
70	Phenylalanine	βCH_2d	3.30	39.1	P*	P	P	dd
71	Proline	CH_2u	3.34	48.7	P	P	P	t
72	Scyllo-Inositol	CH	3.35	-	P	A	A	s
73	α-glucose	C4H	3.41	72.3	P*	P	P	t
74	β-glucose	C4H	3.42	72.3	P*	P	P	t
75	Taurine	CH_2-SO_3-	3.42	37.9	*	P	P	t
76	Proline	γCH_2d	3.42	48.7	P	P	P	t
77	β-glucose	C5H	3.46	78.6	*	P	P	t
78	β-glucose	C3H	3.48	78.2	*	P	P	t
79	Myo-Inositol	C1H,C3H	3.53	74.1	P	P	P	dd
80	Choline	βCH_2 1,3CH_2O	3.53	70.1	P	P	P	m
81	Glycerol	Hu	3.56	65.1	P	P	P	dd
82	Glycine	αCH	3.56	44.2	P	P	P	s
83	PCho	βCH_2	3.57	69.3	P	P	P	t
84	Threonine	αCH	3.58	63.1	P	P	P	d
85	Glycogen	C2H	3.61	71.8	A	P	A	dd
86	Valine	αCH	3.61	63.2	P	P	P	d
87	MI	C4H,C6H 1,3CH_2O	3.61	75.1	P	P	P	t
88	Glycerol	H	3.63	65.1	P	P	P	dd
89	Glycogen	C4H	3.63	77.1	A	P	A	q
90	GPCho	βCH_2	3.67	68.6	P	*	P	m
91	Isoleucine	αCH	3.67	62.1	P	P	P	m
92	α-glucose	C3H	3.69	75.5	P	P	P	t

(*continued on page 80*)

TABLE I. (continued)

S.No	Metabolite	Group	^{1}H Shift	^{13}C Shift	Human Brain	Human Liver	Human Pancreas	Multiplicities
93	Glycogen	C5H,C6H	3.71	61.2	A	P	A	dd
94	Leucine	αCH	3.73	56.2	P*	P	P	t
95	β-glucose	C6Hd	3.73	63.5	P	P	P	dd
96	Glutamate	αCH	3.75	57.2	P	P	P	t
97	Alanine	αCH	3.76	53.4	P	P	P	q
98	α-glucose	C6Hu	3.77	63.4	P*	P	P	m
99	Lysine	αCH	3.77	56.2	P	P	P	t
100	Glutamine	αCH	3.77	56.9	P	P	P	t
101	Ethanolamine	CH_2-OH	3.78	71.8	P	P	P	t
102	Glycerol	CH(OH)	3.78	74.9	P*	P	P	m
103	α-glucose	C5H	3.82	73.9	P	P	P	m
104	α-glucose	C6H d	3.83	63.4	P*	P	P	m
105	Serine	αCH	3.83	59.2	P	A	P	dd
106	Arginine	αCH	3.86	56.6	P*	P	P	dd
107	Aspartic Acid	αCH	3.89	55.0	P	P	P	dd
108	β-glucose	C6H	3.91	63.5	P	P	P	dd
109	Creatine	CH_2	3.92	56.5	P	P	P	s
110	Tyrosine	αCH	3.92	58.7	P	P	P	dd
111	Serine	βCHu	3.93	62.8	P	A	P	dd
112	Serine	βCHd	3.96	62.9	P	A	P	dd
113	Glycogen	C3H	3.96	73.8	A	P	A	dd
114	Aspargine	αCH	3.98	54.0	P	P	P	dd
115	Phenylalanine	αCH	4.00	58.2	P	P	P	dd
116	Myo-Inositol	C2H	4.04	74.8	P	P	P	t
117	Choline	αCH_2	4.05	58.8	P	P	P	m
118	Uridine(Ribose)	αCH	4.05	-	A	A	P	
119	Tryptophan	αCH	4.05	-	A	P	P	dd
120	Tryptophan	αCH	4.06	-	A	P	P	dd
121	Glyceryl in TriGlycerides	CH_2OR	4.11	-	P	P	P	
122	Lactate	CH	4.11	71.1	P	P	P	q
123	Proline	αCH	4.12	63.8	P	P	P	t
124	PCho	αCH_2	4.17	60.7	P	P	P	t
125	Threonine	βCH	4.25	68.7	P	P	P	m
126	GPCho	αCH_2	4.28	56.6	P	P	P	t
127	Glyceryl in TriGlycerides	CH_2OR	4.31	-	P	P	P	
128	NAA	αCH	4.39	56.2	P	A	A	dd
129	β-glucose	C1H	4.64	98.7	P	P	P	d
130	α-glucose	C1H	5.23	94.8	P	P	P	d
131	Tri-Glycerides	CHOR	5.24	-	P	P	P	
132	Fatty acids(b)	(2)CH	5.32	132.5	P*	P	P	m
133	Fatty acids(b)	(1)CH	5.33	130.6	P*	P	P	m
134	Glycogen	C1Hα	5.41	100.2	A	P	A	d
135	Uracil	C5H	5.79	88.2	A	P	A	d
136	Uridine(Ribose)	C1H	5.89	89.2	A	A	P	d
137	Tyrosine	CH 3,5	6.88	118.4	P*	P	P	d
138	Tyrosine	CH 2,6	7.17	133.1	P*	P	P	d

TABLE I. (continued)

S.No	Metabolite	Group	^{1}H Shift	^{13}C Shift	Human Brain	Human Liver	Human Pancreas	Multiplicities
139	Tryptophan	CH6	7.19	-	A	P	P	t
140	Phenylalanine	CH 2,6	7.31	132.1	P*	P	P	m
141	Phenylalanine	C4	7.38	130.1	P*	P	P	m
142	Phenylalanine	CH 3,5	7.42	131.8	P*	P	P	m
143	Tryptophan	CH7	7.53	-	A	P	P	d
144	Uracil	C6H	7.53	141.8	A	P	A	d
145	Tryptophan	CH4	7.72	-	A	P	P	d
146	Uridine(Ribose)	C5H	7.88	142.1	A	A	P	d

u, up-field; d, down-field
A=Absent, P=present, P* = The cross peaks were not observable in the HSQC Spectrum

Human Liver

The one dimensional spectrum of human liver tissue specimen from trauma cases was quite similar to that of pancreas; the basic difference observed was the presence of glycogen and uracil. With each metabolite having its specific correlation pattern, the COSY spectrum of liver (supplementary material) was very much similar to that of pancreas with additional cross peak due to C4H and C1Hα group of glycogen being observed at 3.63 and 5.41 ppm confirming the presence of glycogen in liver tissue specimen (10). The COSY plot also helped in final confirmation of uracil with its C5H and C6H groups showing a distinct cross peak at 5.79 and 7.53 ppm. The HSQC spectrum of liver was also very much similar to that of pancreas with additional ^{1}H-^{13}C peaks of glycogen due to C1Hα group being observed at 5.41 and 100.2 ppm and few additional peaks of glucose being observed compared to that of pancreas; the reason could be that the liver plays a major role in the regulation of glucose metabolism and supplies glucose to other organs.

Human Brain

The one-dimensional spectra of human brain tissue followed a very similar pattern as that observed in pancreas, but certain differences were observed in both one and two dimensional spectra of brain compared to that of pancreas. Doublets due to CH_3 groups of lactate and alanine were readily assigned, triplets due to CH_2 group of taurine at 3.42 ppm, CH group of α-glucose and glutamine at 3.82 and 3.77 ppm. Similar to the singlets observed in one dimensional spectra of pancreas of acetate, acetoacetate, creatine, choline/glycerophosphocholine/phosphocholine, two additional singlets were identified in the spectra of human brain. Singlet due to the methyl group of N-acetylaspartate (NAA) at 2.02 ppm and CH group of scyllo-inositol at 3.35 ppm was observed in brain tissues. Doublet of doublet of aspartate and β-glucose at 3.89 and 3.73 ppm were similar to that of pancreas, while an overlapped doublet of doublet of citrate and NAA at about 2.71 ppm was observed in brain, this was clearly resolved in the two-dimensional COSY spectrum (supplementary material). Quartet due to CH group of lactate, multiplets of GABA, glutamate, glutamine and resonance assignments of myo-inositol were similar to that of pancreas.

The two-dimensional COSY spectrum of human brain was also very much similar as that of pancreas except for a few minor differences. Distinct cross peak due to the β-CH_2 and α-CH group of NAA was observed in the COSY spectra (supplementary material) at 2.49 and 4.39 ppm. Similarly, the same pattern for the assignments of α-hydroxyvalerate and oxo-leucine was observed in the tissue specimen of brain as that observed in pancreas. The HSQC cross peak pattern was very much similar to that of pancreas except that additional peaks of NAA and C2H, C4H and C6H groups of myo-inositol were observed in brain. The ^{1}H-^{13}C cross peaks of tyrosine and phenylalanine in the range of 6.0 to 7.0 ppm were not observed in the HSQC spectra of human brain while they were observed in pancreas (Table I) thus indicating its low concentration in the brain tissue specimen.

Uridine involved in the biosynthesis of polysaccharides was observed only in pancreas, while scyllo-inositol, a cyclohexanehexol stereoisomer, is observed only in brain while it was not observed in liver and pancreas. Similarly, N-Acetylaspartate (NAA) a neuronal marker was only observed in brain tissue specimens. It is synthesized in neurons from the amino acid aspartate and acetyl-coenzyme A. Previous studies have shown extracellular N-acetylaspartate depletion in traumatic brain injury (20).

Presence of prominent resonances of glycogen in liver was due to the fact that carbohydrate reserves are mainly stored as glycogen in humans and it is particularly abundant in liver reaching concentrations up to 100–500 mmol/kg (21). As observed from the one and two dimensional plots, the presence of tyrosine and phenylalanine were significantly lesser in concentration in brain tissues as compared to liver and pancreas tissues. The breakdown of glucose or glycogen in anaerobic conditions results in the production of lactate resulting in intense signal in all the three tissue specimens as is clearly observed in both the one and two dimensional spectra.

Tryptophan is an essential amino acid which has profound effects on a number of metabolic pathways in the whole body system, particularly in the nervous system. Reason for its observance in the liver could be because it is metabolized principally in the liver, and in pancreas it may be due to high enzymatic activity. Whereas, in brain tissue specimens it was not observed inspite of breach in the blood brain barrier, probably due to its very low concentration in the blood.

In the one-dimensional ^{1}H NMR spectra Figure 1a–c of all the three sets of tissue samples, the resonances obtained from valine, leucine and isoleucine appear as a single broad line due to lipid signal in the range 0.91–1.5 ppm. The CPMG spectra provided the assignments of the methyl signals of the above mentioned cytosolic amino acids Figure 2a–c. Although the histological analysis of the tissues confirmed to be normal, which was free from any malignancy and infection, the additional presence of α-hydroxyisovalarate and α-hydroxybutarate (22) in the tissue specimen indicated dysfunction of certain enzymes involved in amino acid synthesis due to trauma induced metabolic changes in the tissues. Since in traumatic tissues, there is deprivation of oxygen, earlier studies carried out on infants suffering asphyxiation has demonstrated an elevated level of Lac/Cr ratio when compared to normal controls (23) using *in-vivo* MR spectroscopy. Similarly, our results also indicate an increase in Lac/Cr ratio (1.57 Mean ± 0.12 SD) thus indicating hypoxic state of the brain tissue specimens. The presence of strong lactate signal in all tissue specimens may be attributed to trauma induced de-vitalization of tissues (anaerobic metabolism). Regarding pancreas and liver tissue specimens, the Lac/Cr ratio was found to be 9.51 Mean ± 0.56 SD and 37.5 Mean ± 1.5 SD. To the best of our knowledge there is

no report existing regarding the Lac/Cr ratio in pancreas and liver using NMR spectroscopy. The presence of α-hydroxyisovalarate and α-hydroxybutarate along with high concentration of the lactate may be utilized in distinguishing the traumatic tissues with healthy and diseased ones. Quantitation is not possible as the external reference TSP binds with the macromolecules in the tissue samples. Although in certain other methods like the ERETIC Method (24) off resonances signal is generated for quantification purpose but that requires additional hardware modification. Nevertheless, the ratio of various metabolites may be used in order to distinguish tissue types so that it may be translated in *in-vivo* spectroscopy.

Conclusions

After a through study of identification of metabolites in human organ of brain, liver and pancreas from trauma cases it is possible to conclude that all assignments have characteristic properties. Although the assignments of brain and liver are previously known, additional assignment of α-hydroxyisovalarate and α-hydroxybutarate have been characterized for the first time in all three tissue specimens. Using earlier work on metabolite characterization of other tissue specimens, the characterization of various metabolites of pancreas have been carried out, which to the best of our knowledge has not been reported earlier.

The importance of the work lies in the fact that characteristic fingerprints of different human organ tissues (pancreas, brain and liver) from trauma cases have been studied which can identify and distinguish between metabolic differences from other tissue specimens like diseased states like cancer, tumor etc or non-diseased/healthy tissues. Since few tissue specimens have been analyzed, more studies on traumatic tissues of these organs will be needed in order to substantiate our findings.

The facility at SAIF, of Central Drug Research Institute, Lucknow, India for providing the NMR data is gratefully acknowledged.

Supplementary Material

The COSY, HSQC spectra (along with expansions) of a human brain and liver tissue specimen have been provided as Supplementary Material.

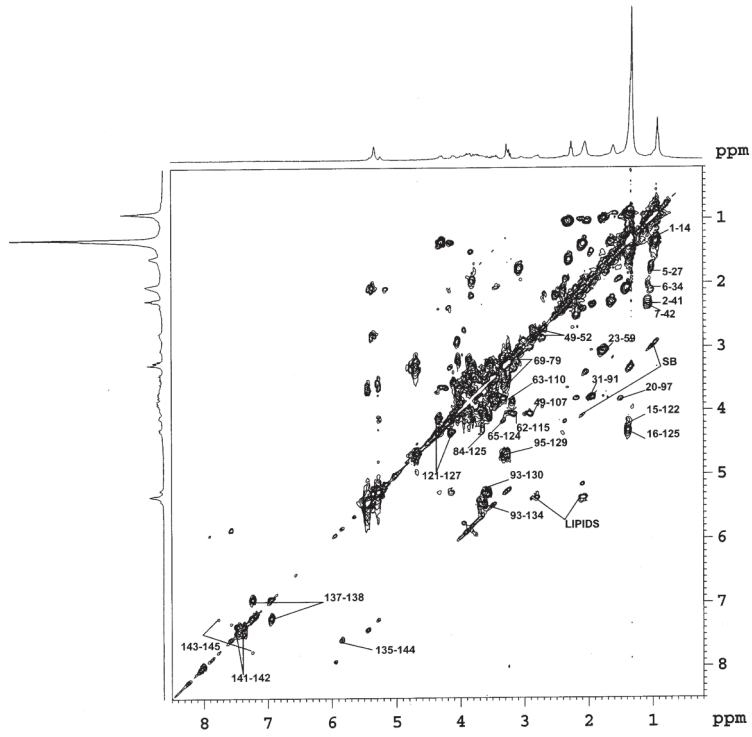

FIGURE S-1. The COSY spectrum of the liver tissue specimen with labeled assignments of the metabolites as given in the Table I, see page 78.

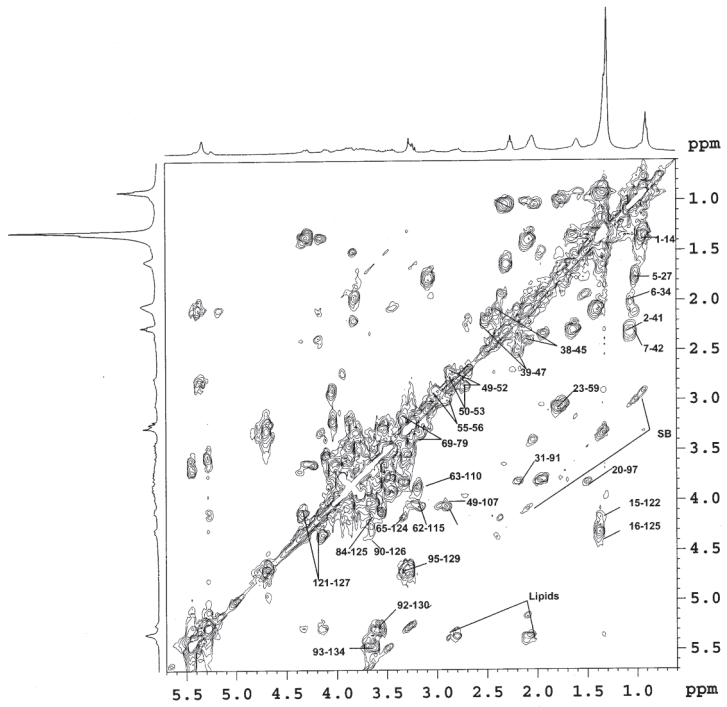

FIGURE S-1a. Expansions of the COSY spectrum of the liver tissue specimen (0.2–5.8 ppm). The detailed labeled assignments are given in Table I, see page 78.

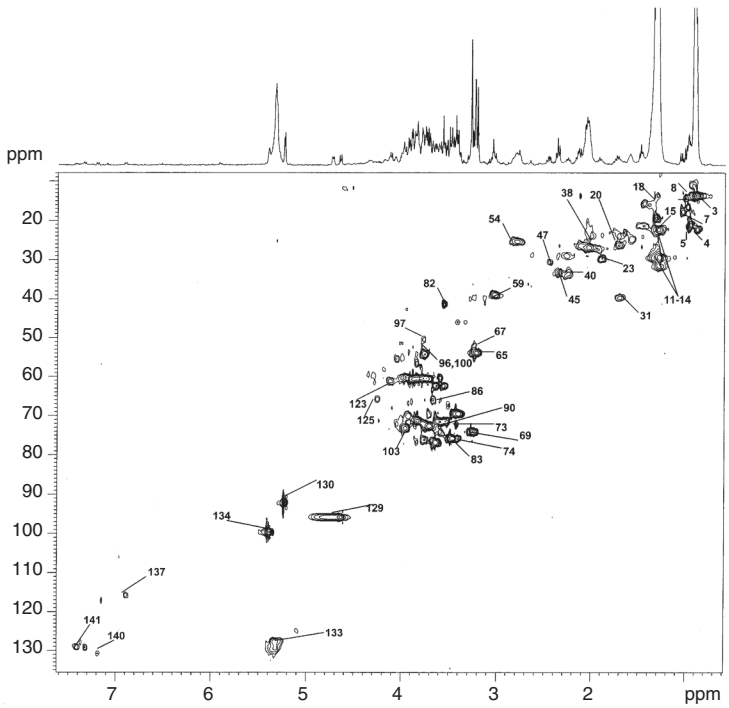

FIGURE S-2. The ^{1}H-^{13}C HSQC spectrum of the liver tissue specimen, highlighting the resonance assignments in the F1 dimension (^{13}C) and in the F2 dimension (^{1}H). The labeled assignments are as given in Table I, see page 78.

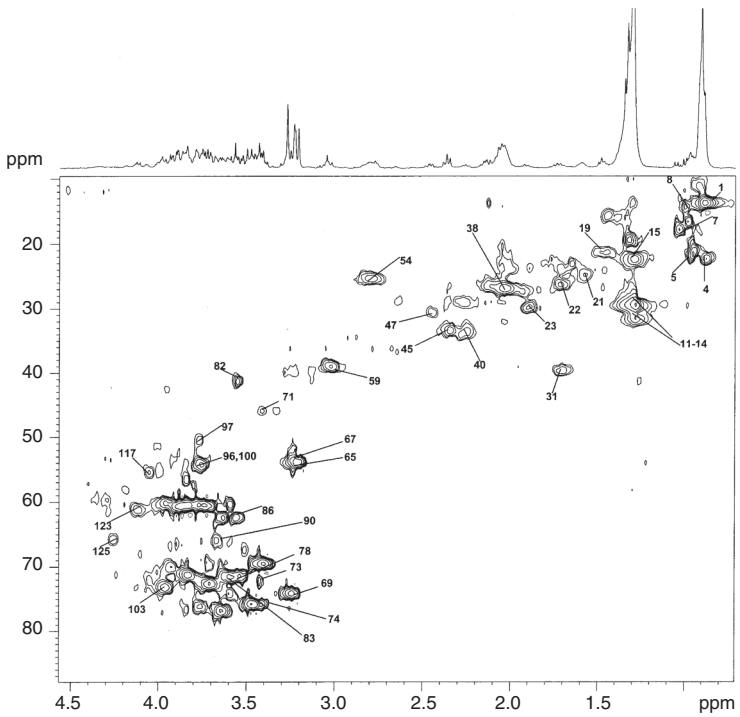

FIGURE S-2a. Expansion of the ^{1}H-^{13}C HSQC spectrum of the liver tissue specimen, highlighting the resonance assignments between 9.0–133.0 ppm in the F1 dimension (^{13}C) and 0.55–5.22 ppm in the F2 dimension (^{1}H). The labeled assignments are as given in Table I, see page 78.

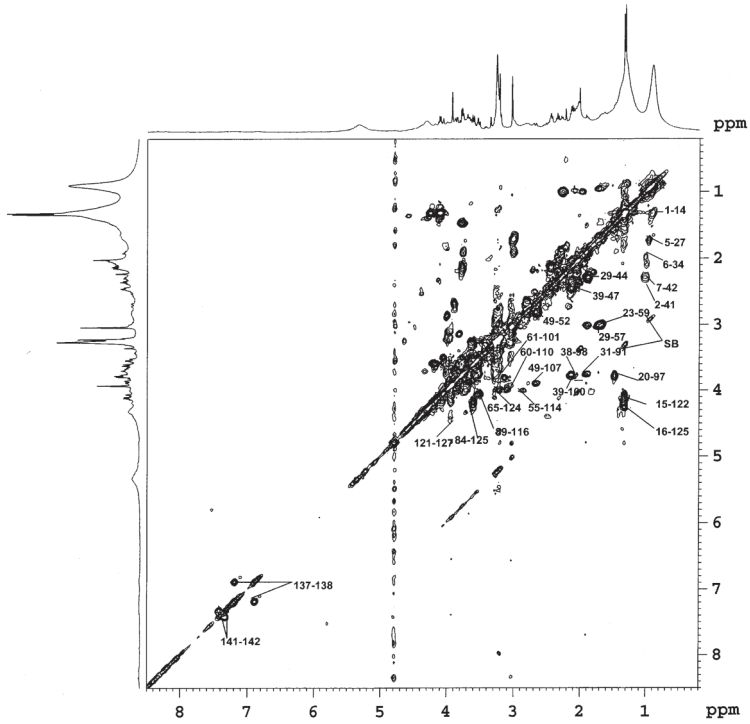

FIGURE S-3. The COSY spectrum of the brain tissue specimen with labeled assignments of the metabolites as given in the Table I, see page 78.

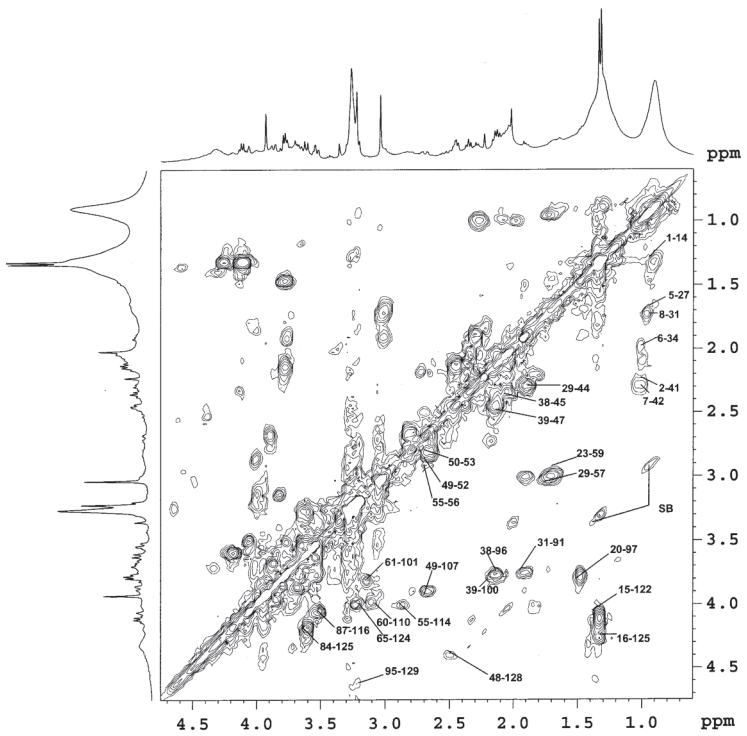

FIGURE S-3a. Expansions of the COSY spectrum of the brain tissue specimen (0.2–5.8 ppm). The detailed labeled assignments are given in Table I, see page 78.

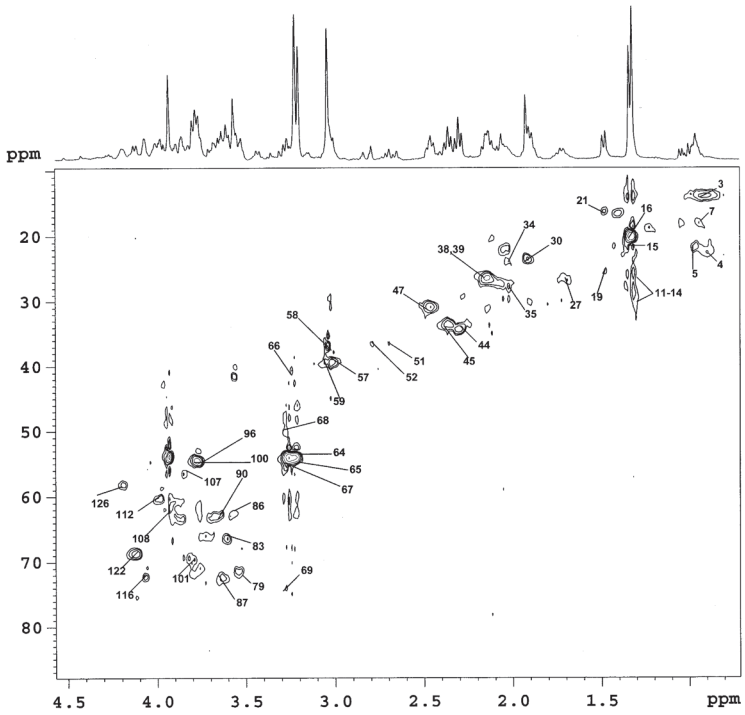

FIGURE S-4. The ^{1}H-^{13}C HSQC spectrum of the of the brain tissue specimen, highlighting the resonance assignments in the F1 dimension (^{13}C) and in the F2 dimension (^{1}H). The labeled assignments are as given in Table I, see page 78.

References

1. Duarte, I.F., Stanley, E.G., Holmes, E., Lindon, J.C., Gil, A.M., Tang, H., Ferdinand, R., McKee, C.G., Nicholson, J.K., Melendez, H.V., Heaton, N., Murphy, G. (2005) *Anal. Chem.* 77, 5570–5578.
2. Ratai, E.M., Pilkenton, S., Lentz, M.R., Greco, J.B., Fuller, R.A., Kim, J.P., He, J., Cheng, L.L., Gonzalez, R.G. (2005) *NMR Biomed.* 18, 242–251.
3. Barton, S.J., Howe, F.A., Tomlins, A.M., Cudlip, S.A., Nicholson, J.K., Bell, B.A., Griffths, J.R. (1999) *Magnetic Resonance Materials in Physics, Biology and Medicine* 8, 121–128.
4. Cheng, L.L., Chang, I.W., Louis, D.N., Gonzalez, R.G. (1998) *Cancer Research* 58, 1825–1832.
5. Denkert, C., Budczies, J., Kind, T., Weichert, W., Tablack, P., Sehouli, J., Niesporek, S., Könsgen, D., Dietel, M., Fiehn, O. (2006) *Mass Spectrometry* 66, 10795–10804
6. Tomlins, A.M., Foxall, P.J.D., Lindon, J.C., Lynch, M.J., Spraul, M., Everett, J.R., Nicholson, J.K. (1998) *Anal. Commun*. 35, 113–115.
7. Schenetti, L., Mucci, A., Parenti, F., Cagnoli, R., Righi, V., Tosi, M.R., Tugnoli, V. (2006) *Concepts Magn. Reson.* 28, 430–443.
8. Taylor, J.L., Wu, C.L., Cory, D., Gonzalez, R.G., Bielecki., A., Cheng, L.L. (2003) *Magn. Reson. Med.* 50, 627–632.
9. Sjobakk, T.E., Johansen, R., Bathen, T.F., Sonnewald, U., Juul, R., Torp, S.H., Lundgren, S., Gribbestad, I.S. (2008) *NMR Biomed.* 21, 175–85.
10. Granados, B.M., Onleon, D.M., Martinez-Bisbal, M.C., Rodrigo, J.M., Olm, J., Liuch, P., Ferrandez, A., Bonmati, L.M., Celda, B. (2006) *NMR Biomed*. 19, 90–100.

11. Swanson, M.G., Zektzer, A.S., Tabatabai, Z.L, Simko, J., Jarso, S., Keshari, K.R., Schmitt, L., Carroll, P.R., Shinohara, K., Vigneron, D.B. and Kurhanewicz, J. (2006) *Magn. Reson. Med.* 55, 1257–1264.
12. Lyng, H., Sitter, B., Bathen, T.F., Jensen, L.R., Sundfor, K., Kristensen, G.B. and Gribbestad, I.S. (2007) *BMC Cancer* 7, 1–12.
13. Cheng, L.L., Anthony, D.C., Comite, A.R., Black, P.M., Tzika, A.A. and Gonzalez, R. (2000) *Neuro-Oncology* 2, 87–95.
14. Viant, M.R., Lyeth, B.G., Miller, M.G., Berman, R.F. (2005) *NMR Biomed*. 18, 07–516.
15. Govindaraju, V., Young, K., Maudsley, A.A. (2000) *NMR Biomed.* 13, 129–153.
16. Sitter, B., Sonnewald, U., Spraul, M., Fjosne, H.E. and Gribbestad, I.S. (2002) *NMR Biomed*. 15, 327–337.
17. Martinez-Bisbal, M.C., Marti-Bonmati, L., Piquer, J., Revert, A., Ferrer, P., Llacer, J.L., Piotto, M., Assemat, O. and Celda, B. (2004) *NMR Biomed*. 17, 191–205.
18. Bell, J.D., Sadler, P.J. (1999) *Encyclopedia of Magnetic Resonance*. John Wiley and Sons: New York. 2, 989–1001.
19. Cheng, L.L., Newell, K., Mallory, A.E., Hyman, B.T., Gonzalez, R.G. (2002) *Magn. Reson. Imaging* 20, 527–533.
20. Shulman, R.G., Rothman, D.L. (2005) *Metabolomics by in vivo NMR.* John Wiley and Sons: New York, pp 24
21. Antonio, B., Jon, S., Axel, P., Salvatore, R., Neil, K., Martin, S., Barbara, T., Vagnozzi, Roberto, V., Stefano, S., Angela Maria, A., Francesco, B., Giuseppe, G. (2006) *J. Neurochem*. 96, 861–869.
22. Lindon, J.C., Nicholson, J.K., Everette, J.R. (1999) *Ann. Rep. NMR Spectros*. 38, 1–88.
23. Hanrahan, J.D., Sargentoni, J., Azzopardi, D., Manji, K., Cowan, F.M., Rutherford, M.A., Cox, I.J., Bell, J.D., Bryant, D.J., Edwards, A.D. (1996) *Pediatric Res.* 39, 584–590.
24. Silvestre, V., Goupry, S., Trierweiler, M., Robins, R., Akoka, S. (2001) *Anal. Chem.* 73, 1862–1868.

Received January 29, 2009;
accepted April 13, 2009.

Physiol. Chem. Phys. & Med. NMR (2008) *40*: 89–113

A Historically Significant Study that at Once Disproves the Membrane (Pump) Theory and Confirms that Nano-protoplasm Is the Ultimate Physical Basis of Life — Yet so Simple and Low-cost that it Could Easily Be Repeated in Many High School Biology Classrooms Worldwide

Gilbert N. Ling and Margaret M. Ochsenfeld

Damadian Foundation for Basic and Cancer Research
Tim and Kim Ling Foundation for Basic and Cancer Research
110 Marcus Drive, Melville, NY 11747
Email: gilbertling@dobar.org

In 1889 Abderhalden reported his discovery that there is no (or as shown later, little) sodium ion (Na^+) in human red blood cells even though these cells live in a medium rich in Na^+. History shows that all major theories of the living cell are built around this basic phenomenon seen in all the living cells that have been carefully examined. One of these theories has been steadily evolving but is yet-to-be widely known. Named the association-induction hypothesis (AIH), it has been presented thus far in four books dated 1962, 1984, 1992 and 2001 respectively. In this theory, the low Na^+ in living cells originates from (i) an above-normal molecule-to-molecule interaction among the bulk-phase cell water molecules, in consequence of (ii) their (self-propagating) polarization-orientation by the backbone NHCO groups of (fully-extended) cell protein(s), when (iii) the protein(s) involved is under the control of the *electron-withdrawing cardinal adsorbe*nt (EWC), ATP. A mature human red blood cell (rbc) has no nucleus, nor other organelle. 64% of the rbc is water; 35% belongs to a single protein, hemoglobin (Hb). This twofold simplicity allows the concoction of an ultra-simple model (USM) of the red blood cell's cytoplasmic protoplasm, which comprises almost entirely of hemoglobin, water, K^+ and ATP. Only in the USM, the ATP has been replaced by an artificial but theoretically authentic EWC, H^+ (given as HCl). To test the theory with the aid of the USM, we filled dialysis sacs with a 40% solution of pure (ferri-) hemoglobin followed by incubating the sacs till equilibrium in solutions containing different amounts of HCl (including zero) but a constant (low)

concentration of NaCl. We then determined the equilibrium ratio of the Na^+ concentration inside the sac over that in the solution outside and refer to this ratio as q_{NaCl}. When no H^+ was added, the q_{NaCl} stayed at unity as predicted by the theory. More important (and also predicted by the theory,) when the right amount of H^+ had been added, q_{NaCl} fell to the 0.1- 0.3 range found in living red blood (and other) cells. These and other findings presented confirm the AIH's theory of life at the most basic level: in the *resting living state*, microscopic, or *nanoprotoplasm*, is the ultimate physical basis of life. (See Post Script on page 111.)

IN 1834 Felix Dujardin introduced what was eventually known as protoplasm[1]. Five years later, Theodor Schwann (and Mathias Schleiden) announced the Cell Theory[2,3]. Less well known is the fact that Schwann also introduced the essence of the membrane pump theory as a part of his Cell Theory. That is, cells are membrane-enclosed cavities filled with clear liquid water[2a], and that the cell membrane has *metabolische Kraft* (metabolic power) that controls the chemical makeup of the fluids inside and outside the cell[2b].

In contrast, Max Schultze pronounced in 1861 that a living cell is "a membrane-less lump of protoplasm containing a nucleus"[4]. Continuing this line of thinking, Thomas Huxley came to the conclusion that protoplasm is the physical basis of life[5] and communicated this idea to a lay audience in an Edinburgh church. Huxley's speech was breathtaking from start to finish; notwithstanding, it had a disconcerting flaw. Since protoplasm was then characterized as a semi-fluid, sticky and transparent substance, it did not match the more rigid and darker nucleus. If the nucleus is not a part of the physical basis of life, what is it? Then again, not all living cells possess a nucleus.

The mature mammalian red blood cell, for example, has no nucleus; nor could the best microscope available then reveal the presence of an enclosing cell membrane. Therefore, the very existence of mature mammalian red blood cells suggested that, at their simplest, living cells are lumps of protoplasm without a nucleus or cell membrane.

In 1889, Emil Abderhalden discovered something crucial that challenged the view of membrane-less red blood cells[6]. Abderlalden found no sodium ion (Na^+) inside the red blood cells even though the blood plasma, in which the red blood cells spend their lives, contain a great deal of Na^+. The question arose, if the red blood cell has no enclosing membrane, what would prevent Na^+ from becoming equally distributed inside and outside the cell? In years to come, further investigations revealed that there is some Na^+ in red blood cells. Nevertheless, a strongly asymmetrical distribution of Na^+ exists not only in red blood cells but in virtually all types of living cells carefully examined as exemplified by the human red blood cell, the frog muscle and the squid axons (Table I.)

TABLE I. The water and Na^+ concentrations in three of the most extensively studied types of living cells and the Na^+ concentrations in their respective blood plasma.

	H_2O (%)	$[Na]_{in}$ (mM)	$[Na]_{ex}$ (mM)	q_{NaCl}	ref.
nerve axon (squid)	86.5	50	440	0.114	7
muscle cell (frog)	77.4	16.9	104	0.163	8, 9
mature red blood cells (human)	65	18	135	0.133	10

Doubt about the existence of a cell membrane was laid to rest not long after the invention in 1931 of the electron microscope by Knoll and Ruska[11]. Its much higher magnifying power enabled biologists to establish that the red blood cell[12] — like other cell types studied[13] — does indeed possess a (vanishingly thin) cell membrane. In the decades following, the membrane pump theory rose to the peak of its popularity. Meanwhile, interest in the protoplasm concept steadily declined.

In an article entitled *Meaninglessness of the Word Protoplasm*[14], microbiologist Hardin showed that between 1926 and 1951 citation in the *Biological Abstract* of the word, protoplasm, had plummeted 77% (p.118.) In recent years, Encyclopedia Britannica Online has repeated Hardin's message. "As the cell has become fractionated into its component parts, protoplasm, as a term no longer has meaning."[15] In the US at least, biology textbooks at both the high school and college level teach the membrane pump theory exclusively; they rarely if at all mention the word protoplasm[9, 9a, 16]. However, a scattering of cell physiologists worldwide believe that the rejection of protoplasm may be a painful but passing episode in history.

Ling, for example, suggested that the real cause of the dwindling popularity of the protoplasm concept could be that the relevant parts of physics, chemistry and biology needed to give a more cogent definition of protoplasm and move the concept forward were still things of the future[16]. With time the relevant branches of knowledge attained the needed maturity one by one.

Arriving on the scene at just the right time, Ling was able to put together in 1962 an elementary unifying theory of the living phenomena in a volume entitled "A Physical Theory of the Living State: the Association-Induction Hypothesis"[17–22].

The association-induction (AI) hypothesis grew up in the light of critical knowledge denied earlier investigators. That includes the knowledge on protein structure and the new branch of physics called statistical mechanics. From a historic perspective, however, the AI hypothesis is without question the heir to what Dujardin, von Mohl, Schultze, Huxley and others introduced in mid-19th century. Another 45 years were to elapse before a new name, nano-protoplasm, was coined[23] to replace what was once referred to as a *biological fixed charge system*[18a] or *an elementary living machine*[17a].

Protoplasm re-defined

The long-range goal of the AI Hypothesis is to interpret all macroscopic cell physiological manifestations in terms of the properties and activities of microscopic molecules, atoms, ions, and electrons. Thus, in the latest version of the AI Hypothesis, what Thomas Huxley called the physical basis of life is a specific but highly prominent example of macroscopic protoplasm[23]. Other varieties of macroscopic protoplasm make up respectively the cell nuclei, the cell membrane and other sub-cellular structures. Despite their great diversity in form and function, all macroscopic protoplasms have one thing in common. They all comprise a vast number of similar microscopic units called nano-protoplasm[23]. Accordingly, nano-protoplasm — rather than a specific kind of prominent macroscopic protoplasm — is the smallest unit of life and hence its ultimate physical basis[23].

In introducing a more detailed description of a typical nano-protoplasm, we start out with a single mature human (or mammalian) red blood cell — to be referred to henceforth as a rbc. The electron-microscopic cross-section of two such rbc's is shown in Figure 1. Note that they have no nucleus, nor sub-cellular organelles of any other kind. Consequently, the inside of a rbc is essentially homogeneous. Furthermore, cytologists of the past had demonstrated that a rbc could be cut into tiny pieces without spilling its intracellular protein, hemoglobin[24]. Armed with these relevant insights and an imaginary knife, we cut a rbc into smaller and smaller pieces until each piece contains just one single hemoglobin molecule — and more as indicated next.

Water makes up 64% of the rbc's total weight. Of the 36% solid, *97%* belongs to a *single* protein, hemoglobin[10]. Thus, water and hemoglobin together make up more than 98% of the total weight of mature mammalian red blood cells. Thirty percent (30%) of the remaining 1.1% solid is K^+. Even less belongs to organic substances including about 5 mM of {2,3-diphophoglycerate (2,3-DPG)[25] *plus* adenosine triphosphate (ATP.)[26]} All told, what is still unaccounted for is not more than 1% of the total weight of a rbc.

From all these facts and numbers, one can estimate what is in each of the smallest microscopic lumps of rbc cytoplasm that we carved out from a rbc. Thus, in addition to one hemoglobin molecule, there are also some 7000 water molecules, 20 K^+ and one (2,3 DPG + ATP.) Together, they make up a *nano-protoplasmic (NP) unit.* And it can be represented by a formula: $(Hb)_1\ (H_2O)_{7000}\ (K^+)_{20}\ (ATP\ or\ 2,3\text{-}DPG)_1$. (For a general formula for all nano-protoplasms, see ref. 23, p.124.) The molar concentration of these NP units in a rbc is equal to that of hemoglobin at approximately 5 mM. Assumed spherical in shape, each rbc NP unit measures 6.8 nanometers in diameter[23].

The next section addresses the crucial question: How does a nano-protoplasm unit differ from a random mixture of the same chemical makeup and nano-metric dimensions?

Life and death at their most basic level

Unlike most objects in the dead world, nano-protoplasm can exist, in two alternative discrete states under the same atmospheric pressure and at the same temperature. An illustration of the "core structure" of a nano-protoplasm unit in its (lasting) *resting living state* is shown in the right-hand side picture of Figure 2. Another illustration of the core structure of either a nano-protoplasm unit in its (transient and reversible) *active living state* or one that is in its (irreversible) *dead state* is shown on the left of Figure 2[18a,20a,21d,22a]. In the resting living state, all the components of the core structure are directly or indirectly in contact with one another spatially (association) and electronically (induction.) In the active or dead state, the two major components, water and K^+ are set free mostly if not

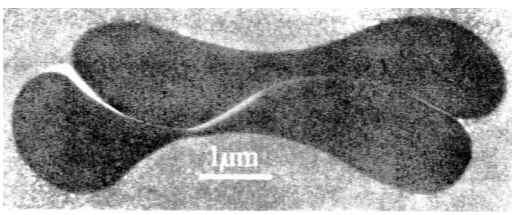

FIGURE 1. An electron micrograph of the cross section of two mature human red blood cells (in blood plasma). Cryofixed, freeze-dried and imbedded in Lowicryl. (Gift of Dr. Ludwig Edelmann)

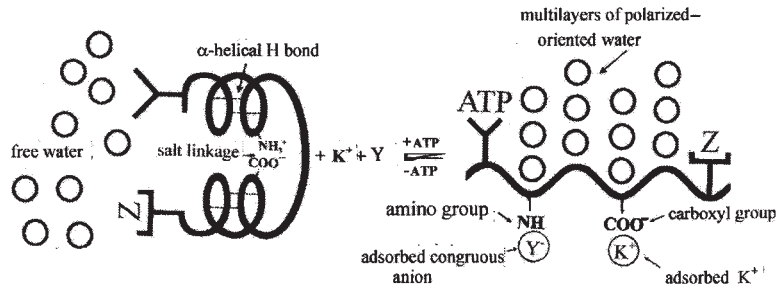

FIGURE 2. Diagrammatic illustration of the all-or-none transition between the folded and the fully-extended state of the core structure of a nano-protoplasmic unit.

totally[17c, 18e, 21g, 23c]. Thus, *it is the pervasive spatial and electronic connectedness that sets apart nano-protoplasm in its resting living state from a random mixture of similar chemical composition and miniscule dimension.*

While existence in the resting living state defines *living*, momentary reversible transitions between the resting and active living, state underlies *life activities.* As a rule, transitions in life activities are all-or-none; or, in the language of the AI Hypothesis, *auto-cooperative*[18b,21a,23e,27]. Center stage in these transitions is the auto-cooperative transition of the protein component of the nano-protoplasm between the folded *α-helical conformation* and the *fully extended conformation,* as diagrammatically illustrated in Figure 2.

Another player in the maintenance of two discrete living states and hence the auto-cooperative transition between them is the *salt-linkage*[28,29a]. Salt linkages are formed one on one between an equal number of fixed cations like the *ε-amino and guanidyl groups* and fixed anions like the *β-, and γ-carboxyl groups.* (See Figure 2 left.)

Neither the α-helical structure, nor the salt linkages — nor the *self-assembling* microscopic NP units making up macroscopic protoplasm — are joined together permanently. Rather, the structural connections in living protoplasm are *dynamic* — like that of a flock of wild geese in their migratory flight.

Nano-protoplasms are similar and different. Three major sources of their diversity are: (i) the amino acid composition-and-sequence of the protein(s) in the NP unit as defined by their respective genes; (ii) prosthetic groups, enzyme sites etc. that the protein may or may not carry and (iii) the location of the nano-protoplasmic (NP) cationic unit in the cell.

On the other hand, what make different nano-protoplasms (and hence different macroscopic protoplasm) similar are the shared components of the "core structures" of nano-protoplasm. They include: (1) a lengthy and highly polarizable polypeptide chain, serving as the highway of information and energy transmission; (2) close to the information highway, an abundance of fixed anionic β-, and γ-carboxyl groups carried respectively on short side chains of aspartic and glutamic residues; (3) the even more abundant peptide iminocarbonyl groups (CONH) — right on the information highway, the polypeptide chain; (4) the fixed cationic groups, including e-amino, guanidyl and (cationic) imidazole groups, which roughly match in total number the total number of fixed anions; (5) alternative partners for adsorption on these ubiquitous functional groups including K^+ (or another cation) for the carboxyl groups[29] and water molecules for the backbone carbonyl

groups; (6) adenosine triphosphate (ATP), the controlling *principal cardinal adsorbent* and specific sites on the protein that adsorb ATP, as well as *auxiliary cardinal site(s)* that adsorb other controlling agent(s) denoted by the symbol, Z (See Figure 2 right.)

ATP as the principal electron-withdrawing cardinal adsorbent

As a generic name for drugs, hormones, ATP , Ca^{++} and other agents that exercise powerful influence on the nano-protoplasm at extremely low concentration, are what we call *cardinal adsorbents* [17b,21e,23a]. As a rule, they act as the on-and-off switch of the all-or-none transitions of the nano-protoplasm between two discrete states. To serve that function, they adsorb onto (and desorb from) *specific cardinal sites* on the nano-protoplasmic protein. Depending on the consequence of their respective electronic impact on the protein, each cardinal adsorbent belongs to one of three categories: *the electron-indifferent cardinal adsorbent* or EIC, the *electron-donating cardinal adsorbent* or EDC, and the *electron withdrawing cardinal adsorbent* or EWC.

The most pervasive and powerful EWC is ATP. In conjunction with other auxiliary adsorbents or agents, ATP plays a critical role in maintaining (reversibly) the nano-protoplasm in *its resting living state* through its adsorption on a specific cardinal site. As such, its action can reach over long distances. ATP is unusual in yet another way. It can be rapidly removed through the action of a specific enzyme called ATPase. It can also be rapidly replenished through the activities of other enzymes of one kind or another.

In the original AI Hypothesis, two types of long-distance operations of ATP and other agents were presented. They are respectively called the (static) *direct F-effect*[17d, 21j] — a combination of direct or D-effect, transmitted through space and inductive or I-effect transmitted through intervening atoms, — and the i*ndirect F-effect*[18c]. The direct F-effect is local and static in action; its name remains unchanged though often replaced by the predominant inductive or I-effect alone. In contrast, the dynamic and far-reaching indirect F-effect has been renamed *AI cascade mechanism* {where the letter A and I used here stand for the (close-contact) *association* and the electronic *induction* respectively}[23b,17e].

It is the AI cascade mechanism that provides the means for the (ideally) non-attenuating, one-on-many, from-here-to-there influence of the cardinal adsorbent. In its mode of operation, the AI cascade mechanism resembles a falling domino chain — in that the energy that topples the first domino is the same as the one that topples the last domino, regardless how far apart they are. (See also ref. 17k, 21i.) (Regrettably, space limitation does not permit even a brief sketch of a more detailed account of the AI cascade mechanism. The interested reader may want to consult earlier presentations[17e] or a recent downloadable pdf version[23b].)

By the same token, it is the AI cascade mechanism that makes a *gang* of cooperatively linked sites behave as if it were a single site[17e]. It is this AI cascade mechanism that produces the across-the-board *uniform* rise or fall of the *c-values* of the β-, and γ-carboxyl groups and of the *c-value analogue* of backbone carbonyl groups along the lengths of the polypeptide chain. What is a c-value? What is a c-value analogue? What roles do their perturbations play in the phenomena of living and life activities? The answers follow next.

The effective electron density of a singly-charged carboxyl oxygen atom of, say a β-, and γ-carboxyl group, is expressed in Ångstrom units and called *the c-value*[18d, 21b,17i]. The-

oretical computations made in the late 1950's showed that variation of the c-value could decide adsorption preferences on these negatively charged functional groups[17g,18f]. Thus, according to what we now call the **c-scheme**, at low c-value, K^+ is preferred over Na^+; at high c-value, the reverse is the case. As a pervasive EWC, ATP adsorption on its special cardinal site — in conjunction with auxiliary agents of various kinds — keeps all the nano-protoplasmic β-, and γ-carboxyl groups at a low c-value. That is why K^+, and not Na^+, is adsorbed on these anionic sites and accumulates in the nano-protoplasm maintained at its resting living state as shown in Figure 2 right[29].

However, at both low and high c-value, H^+ is preferred over most other mono-valent cations often by a high margin[17g,18f]. Keep this in mind, as it will appear again in new experimental studies to be presented on later pages.

Similarly, the *c-value analogue* of the backbone peptide carbonyl group represents the effective electron density of the dipolar carbonyl group (CO)[18d, 21c], and as such it has a parallel capacity like that of the c-value. Based on the comprehensive and mutually consistent work of three groups of scientists on the "α-helical potential" of amino acid residues in proteins (Chou & Fasman, Tanaka & Scheraga and Garniere *et al*), Ling introduced in 1980 the theoretical concept later named the **c-analogue scheme**[30,17j,21k]. According to this scheme, at high c-value analogue, the peptide carbonyl group prefers to engage in α-helical H-bonds. On the other hand, at low c-value analogue, the peptide group prefers to assume the fully extended conformation. As such, they adsorb, polarize and orient multilayers of water molecules according to the *polarized-oriented multilayer or POM theory* of cell water[31,32].

The POM theory, short for the "polarized-oriented multilayer theory" of cell water and model systems — for some time also called the PM theory — was added to the *AI Hypothesis proper* in 1965 to explain the exclusion from the living cells[31](Table I) of (hydrated) Na^+ — i.e., Na^+ plus its more or less permanently attached coat of water molecules in an aqueous environment. As illustrated in the right hand side picture of Figure 2, all the water molecules in the nano-protoplasm in its resting living state adopt the dynamic structure of polarized-oriented multilayers. In this polarized-oriented water, the average water-to-water interaction energy is stronger than in normal liquid water—with important consequences[33,34,35]. Thus, it would take more energy to excavate a hole in the polarized-oriented water to accommodate a large hydrated Na^+ than the energy recovered in filling up the hole left behind in the normal liquid water from where this Na^+ came.

Accordingly, to move such a Na^+ (and its companion Cl^-) from the normal water outside a living cell into the polarized-oriented water inside a living cell entails extra energy expenditure. The Boltzmann distribution law then dictates that, at equilibrium, less Na^+ (and its companion anion, Cl^-) would be found inside the cell water than in the external-bathing medium[36]. This then constitutes the important *volume component* of the solute exclusion mechanism against large solutes like hydrated Na^+ (and Cl^-) but with less or no expulsive impact on smaller solutes like urea, for example, according to what has become known as the *size rule*[33,34,37,17f].

As mentioned above, ATP adsorption on the nano-protoplasmic protein exerts a pervasive and far-reaching electron-withdrawing effect. At the lowered c-value thus achieved, the β-, and γ-carboxyl groups favor K^+ over Na^+ adsorption *via* what is known as the ***c-scheme***. Similarly, the lowered c-value analogue of backbone carbonyl groups keeps the polypeptide chain in the fully extended state *via* the **c-analogue scheme**. Take away the

ATP and the system reverts in an all-or-none manner to the doubly folded state as shown in Figure 2 on the left, and in the process, liberates all or virtually all its adsorbed water and K^+ [17c, 21g, 23c, 38]. With that, the nano-protoplasm's ability to exclude Na^+ also disappears.

An *ultra-simple model* of the core structure of nano-protoplasm

The utter simplicity of the chemical makeup of the rbc's cytoplasmic NP unit offers an unusual opportunity. It makes it feasible to construct an *ultra-simple model* (USM) of the core structure of a NP unit from *pure chemicals exclusively.* On the vast collection of these models in say 0.4-ml of the mix in a dialysis sac, we can test the theory how its real-life counterpart works. If the ultra-simple model (USM) can indeed reproduce what the theory has predicted, we know that it is the pure chemicals we put together and nothing beyond them that did the job.

Philosophically, this new USM approach could offer the cell physiologist a way out of the inherent trouble of there being too many inseparable participants within the living cell being studied. Remember Occam's Razor, *One should not increase, beyond what is necessary, the number of entities required to explain anything.* For only when dealing with *all* the essential entities — and when they are only a few of them — can we keep our eyes on the *total* picture all the time and avoid being sidetracked into pursuing more and more (on less and less — ultimately to nowhere.)

However, given the advantage of reducing the number of entities involved, the full potential of a test with an ultra-simple model could be reached only when the physiological trait chosen for study is *critically important* and *it is shared by all or virtually all living cells***.**

To reach that goal, we believe that no other physiological manifestation could come close to the (reversible) *maintenance of Na^+ (as chloride) in the cell water at a level much lower than that in the surrounding medium* (Table I.)

The entire history of cell physiology[39] testifies to the veracity of this belief. To the best of our knowledge, all the major theories of the living cell were built around the critical phenomenon of Na^+ exclusion. They include Boyle and Conway's sieve version of the membrane theory[40], the pump version of the membrane theory once wrongly attributed to R.Dean[41], but truly due to Theodor Schwann as pointed out earlier, Troshin's sorption theory[42] and Ling's association-induction hypothesis[18].

With our strategy outlined, we proceed to test our theoretical concept of pervasively connected nano-protoplasm as the ultimate physical basis of life. First, we outline how we carried out the studies under Materials and Methods and attach it at the end of the Results and Discussion sections, which are presented in two parts labeled respectively R and D part 1 and R and D part 2. However, make sure to read the Materials and Methods section first.

Results and Discussion

R and D part 1

As described under Material and Methods, we incubated dialysis sacs (filled with initially a 40% hemoglobin solution) in solutions containing the same low concentration of NaCl

but different amounts of HCl. After equilibrium was reached, we determined the equilibrium distribution ratio of Na^+ or q_{NaCl} of the water inside each sac and plotted the result in Figure 3 as six bar graphs.

The first bar graph on the right came from ultra-simple models in which the final equilibrium pH of the bathing medium averaged 7.1. After correcting for a small amount of adsorbed Na^+ in the sacs, we obtained an *equilibrium distribution coefficient* of NaCl or q_{NaCl} of 1.0 within error of ± 0.06. This unity q_{NaCl} shows that at neutral pH, the water in this ultra-simple model does not exclude NaCl. As such, this finding agrees with the unity q-value demonstrated earlier for sucrose and other small and large non-electrolytes in similar neutral USM of hemoglobin systems[37]. The finding also agrees with the theoretical prediction mentioned earlier that in the absence of ATP or an alternative effective EWC, hemoglobin exists in the introverted doubly folded state (Figure 2 left.) And in that state, the hemoglobin exercises virtually no influence on the physical state of the bulk-phase water. (However, see ref. 43 and 44 for more on the subject.)

The five short bar graphs in Figure 3 tell an entirely different story. Here, the right amount of H^+ had been added and it has caused the q_{NaCl} to fall consistently to between 0.1 and 0.3. As such, it ***quantitatively*** matches the q_{NaCl} found in most if not all healthy resting living cells (Table I.)

Two conclusions can be drawn from this quantitatively exact matching. *First*, it contradicts the membrane pump theory for the maintenance of low Na^+ level in living cells. *Second*, it affirms the AI hypothesis that nano-protoplasm is the seat of basic physiological functions exemplified by Na^+ exclusion.

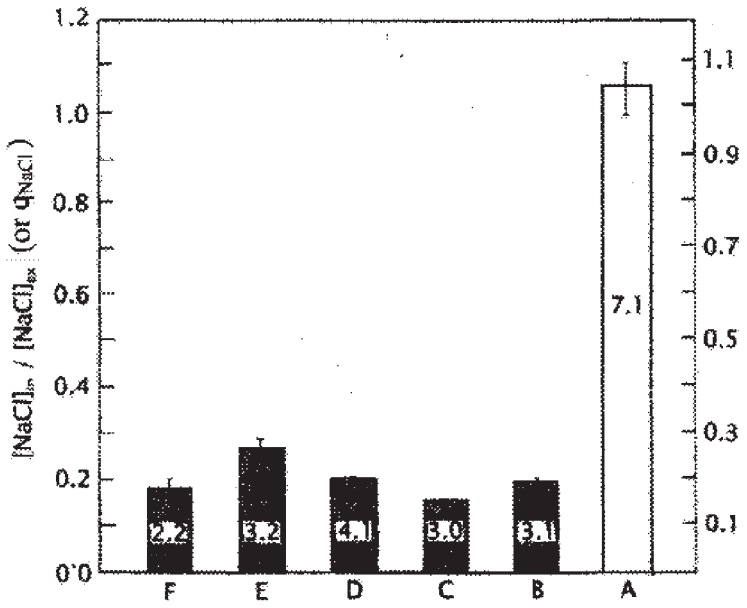

FIGURE 3. The *equilibrium distribution ratio* of NaCl, or q_{NaCl} of ultra-simple models of red blood cell cytoplasmic nano-protoplasm (A) not treated with HCl; (B, C, D, E, F) treated with appropriate amount of HCl. Numbers in bar graphs indicate equilibrium pH of the media bathing that particular set of dialysis sacs.

Thus, the data summarized in Figure 3 provides yet a fourth set of evidence against the membrane pump theory of Na^+ exclusion, — in addition to three other sets published earlier, which are: i) energy insufficiency[18e, 45, 16]; ii) intact membrane without cytoplasm does not work[46,47,48]; iii) cytoplasm without functional membrane (and pump) does work[49,17m].

The new data presented here suggests once more that the low Na^+ level in living cells does not come from an impermeable cell membrane barrier, nor from the ceaseless activity of (postulated) sodium pumps in the cell membrane. Indeed, the new evidence is so plain, that one doubts that any one with an open mind could miss what the data tell. *Not a trace of the cell membrane nor postulated pumps exists in the USM preparation that has quantitatively reproduced the 0.1–0.3 q_{NaCl} seen in most living cells*.

Of far greater significance, this concordance between the experimental and real life q_{NaCl} fulfills what we set out to do. Namely, proving that a mix of four pure chemicals — hemoglobin, water, NaCl and HCl — can indeed reproduce not only qualitatively but *quantitatively* one of the most fundamental physiological attributes shared by living cells. What is more, it can be turned on or off by the introduction or removal of the agent, HCl.

Having completed part 1 of our Result and Discussion, we begin R and D part 2 with a brief introduction.

R and D part 2

The addition of HCl to a mix of three pure chemicals and the conversion of normal liquid water in that mix into one that exhibits a 0.1 to 0.3 q_{NaCl} are by themselves totally unconnected events. The only logical connection between them comes from the AI Hypothesis. From a broad perspective, the quantitative confirmation of a predicted result implies that all the interweaving steps giving rise to the predicted results have already been confirmed. However, in dealing with a science as complex as cell physiology, a deeper look into the validity of each of the intervening (three) step sequence is a must. Indeed, to do that is the purpose of the second part of our study that has yielded R and D part 2.

In the **first step** of the three-step sequence, the right amount of the *premiere* EWC, H^+ given in the form of HCl binds onto appropriate sites on the hemoglobin in the ultra-simple model.

In the **second** step, this binding of the EWC, H^+, lowers the *c-value analogue* of local backbone carbonyl groups of the hemoglobin molecules — *via* the direct F-effect. The local c-analogue fall then sets in motion the complex third step**.**

In the **third step,** an auto-cooperative transition takes place producing in an all-or-none manner the following trio of interlocking changes: (a) converting contiguous NHCO groups from their original high c-analogue to low c-analogue — *via* the *AI cascade mechanism*; (b) converting sections of the hemoglobin chains from their original a-helical folded conformation to the fully extended conformation with the backbone NHCO groups exposed — *via* the *c-analogue scheme*; (c) converting a large number of free water molecules to the state of multi-layer polarization and orientation — on the exposed NHCO groups of the fully-extended hemoglobin chains — to assume the dynamic structure distinguished by a 0.1-0.3 q_{NaCl}.

Before going into our next section, we point out that there are already repeatedly confirmed evidence in support of step 2 and step 3c. Thus in regard to step 2, there are mutually supportive evidence that the step 2 inductive effect can be launched by the formation of new ionic or H-bonds as in the more familiar formation of new covalent

bonds[21m]. In addition, four sets of independent evidence exist demonstrating that the direct F-effect can effectively transmit through a length of the polypeptide chain plus segments of saturated hydrocarbon chains[17d, 21j]. In reference to step 3c, one may mention the following: Proteins which may for structural reasons as in gelatin (i.e., high contents of non-helical forming proline and hydroxyproline residues)[50] or in response to denaturants (e.g., NaOH, guanidine HCl, urea) exist in the fully-extended conformation[51]. In that case, they have been shown to adsorb at the physiological relative vapor pressure (0.9969) enough water molecules that match the living cells in amount[52] and in the extents of exclusion of sucrose, free amino acids and Na_2SO_4 — with the exception of NaCl[53].

Accordingly, the subject matter that most urgently calls for confirmation include: (i) identifying H^+ (of the HCl added) as the true causal agent that brings about the q_{NaCl} fall from unity to 0.1-0.3; (ii) determining the nature and number of the binding sites for H^+; (iii) establishing the role of the AI cascade mechanism in creating the low q_{NaCl} observed; and (iv) verifying the way an effective EWC actually transforms a protein like hemoglobin from its α-helical folded conformation to the fully extended conformation (that produces the low q_{NaCl} in the bulk-phase water the extended protein chain adsorbs, polarizes and orients.)

We end this introduction with a question, How did we find "just the right amount of HCl" — as pointed out earlier — to produce the five short bar graphs of Figure 3?

Just right amount of HCl

Once more, we repeat**.** We incubated dialysis sacs (containing initially a 40% hemoglobin solution) in solutions containing the same concentration of NaCl but different amounts of HCl. After equilibrium was reached, we determined the q_{NaCl} of the water inside each sac and plotted their averages against the final pH's of their respective bathing solutions in Figure 4.

The data demonstrate that as the amount of HCl added increased step by step, both the pH and the q_{NaCl} fell steadily to lower and lower values — until the pH reached a value of 2.2. From this point on, further addition of HCl continued to lower the pH but not the q_{NaCl}. Instead, the q_{NaCl} started to rise with further HCl addition. Seen as a whole, the curve has the shape of an asymmetrical U. As such, it comprises three distinct segments designated 1, 2 and 3 respectively, counting from the high pH end. A minimum of q_{NaCl} occurs at pH 2.2. The amount(s) of HCl needed to create this minimum in this, and in other companion sets of studies, are referred to as the "right amount of HCl" used to produce the five short bar graphs in Figure 3.

The specific set of data shown in Figure 4 was obtained with the Na-electrode after incubation of the sacs at around 9° C. Two additional full sets of data were obtained after incubation of sacs at 25° C with the radioactive tracer method and they produced similar asymmetrical U-shaped curves. However, the minimums occurred at pH closer to 3 than 2. Notwithstanding, the values of the q_{NaCl} measured at or near these pH's also fall between 0.1 and 0.3 and are among those shown as short bar graphs in Figure 3.

In what follows, we will pursue further what underlies the data presented in Figure 4 in two sections. We begin with a section on the "*falling limb"* (Segment 1 and 2) on the right of the asymmetrical U-shaped curve. After that, we will continue with a section on the *minimum* and the *rising limb* of the curve to the left of the minimum at pH 2.2 (Segment 3.)

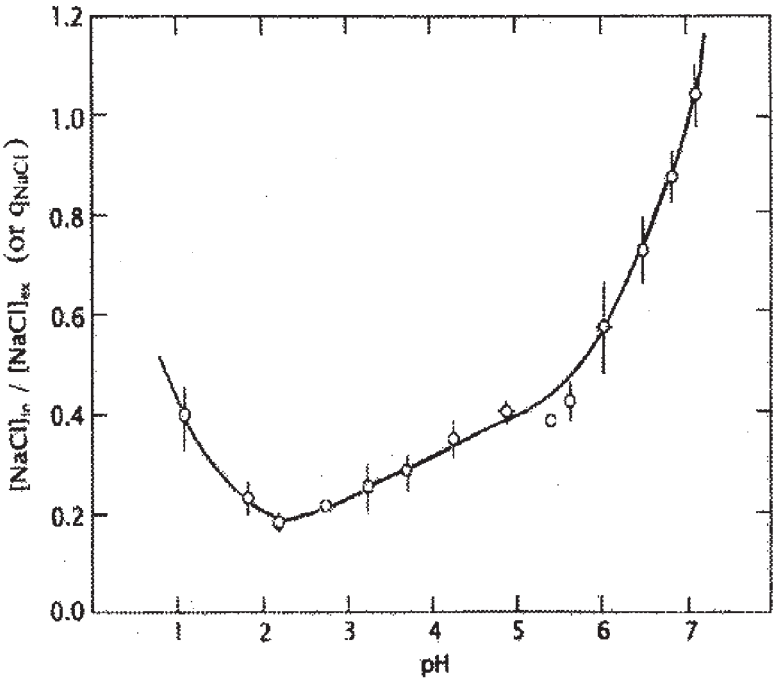

FIGURE 4. The *equilibrium distribution ratio* of NaCl, or q_{NaCl} of ultra-simple models of red blood cell cytoplasmic nano-protoplasm in dialysis sacs treated with different amounts of HCl. Data plotted against the final pH of the bathing solution.

What underlies the falling limb?

From the formula of rbc cytoplasmic NP unit given earlier, one can deduce that each *principal cardinal adsorbent* (ATP or 2,3-DPG) — and its supporting auxiliary agents — keeps 7000 water molecules in its dynamic structure that produces a q_{NaCl} of 0.13 (Table I.) Frog muscle contains 5 mM ATP[17c] but little or no 2,3-DPG. 78% of its total weight is water[8]. Accordingly, each ATP molecule (and its auxiliary helpers including creatine phosphate and K^+)[21h] controls more than 8000 water molecules. (For other evidence of the far reach of another cardinal adsorbent, see ref. 17n.)

Of course, our present study did not use ATP as the principal cardinal adsorbent. Instead, we chose an artificial but theoretically authentic EWC, H^+. As shown above, when enough H^+ had been added, it can also produce a q_{NaCl} to match those seen in living red blood cells or frog muscle under the domination of their natural principle EWC, ATP.

Thus, unlike ATP, which has just one (principal) cardinal site on each hemoglobin molecule, H^+ can bind onto a multitude of sites on a nano-protoplasmic protein molecule. Bovine hemoglobin, for example, carries three kinds of acidic functional groups that bind H^+ between pH 7.0 and 1.0. They comprise 34 imidazole groups (pK_a 6.0), 64 β-, and γ-carboxyl groups (pK_a 4.0) and 4 α-carboxyl groups (pK_a 2.0)[54]. Given their different pK_a values, one expects that as more and more HCl is added, H^+ would bind onto the imidazole groups before binding onto the β-, and γ-carboxyl groups. From the more or less

steady fall of q_{NaCl} between pH 7 and 2.2, one draws the tentative conclusion that the q_{NaCl} of the bulk phase water falls in a more or less unchanging direction each time another H^+ binds onto one of these three types of acidic groups. Put simply, the impacts produced on the q_{NaCl} by different (bound) H^+ add up *via* what is known as the *additivity principle* to be described below.

Experimentally, one can also roughly estimate how many water molecules each bound H^+ controls with the help of another parameter, $(1 - q_{NaCl})$. For a q_{NaCl} equal to, say 0.2, $(1 - q_{NaCl})$ would be 0.8. As a *working hypothesis* — but not so literally in the latest version of the definitive theory, so far published only in parts [33, 34, 35, 43] — a $(1- q_{NaCl})$ equal to 0.8 could be seen as indicating that 80% of the bulk-phase water has completely lost its natural solvency for Na(Cl), leaving completely unchanged the remaining 20% in its normal solvency for Na(Cl).

By taking also into account the equilibrium water content (not shown) and the $(1 - q_{NaCl})$ calculated, one can estimate the minimum number of water molecules made "non-NaCl-solvent" at different points along the q_{NaCl} vs. pH curve of Figure 4, counting the right-hand most point as point 1. Thus, at point 5, the number of water molecules made "non-NaCl-solvent" by each H^+ bound is 500. In contrast, the additional number of water molecules made "non-NaCl-solvent" by each additional H^+ bound between point 5 and point 11 averages only 66.

The large difference between these two numbers (500 and 66) suggests that each of these two averages cover a wide spread of numbers. Thus at pH above 6.5, the number of water molecules made "non-NaCl-solvent" by each H^+ bound could exceed substantially 500. And, at pH below 4.0, the number could fall substantially below 66. It is the lowest below 66-number that would set the limit of water molecules made non-NaCl solvent by each H^+ adsorption *via* the direct F-effect alone. Anything above that lowest number could only have come about *via* the AI cascade mechanism. All told, it is clear that most of the water polarized and oriented got there by way of the AI cascade mechanism.

In summary, one may say that the falling limb of the q_{NaCl} vs. pH plot in Figure 4 is a profile of the all-or-none transition from the active living (or dead) state back to the resting living state in "slow motion." Only in this slow motion version with the binding of a large number of H^+ to the same protein are details of the progress of the transition of the protein revealed that would be hard to detect when there is only a single cardinal site adsorbing a single cardinal adsorbent (ATP) — as is the case in the real-life nano-protoplasm. This is just another example of the bonuses from studying an ultra-simple model.

What lies behind the q_{NaCl} minimum and its secondary rise?

If H^+ alone determines c-value analogue of all the backbone carbonyl groups and the dynamic water structure, one would expect the q_{NaCl} to continue its decline with further HCl addition until a constant q_{NaCl} value is reached and then stays unchanged from there on with still more HCl addition. That the q_{NaCl} in fact exhibits a *minimum* followed by a rise suggests that some other player(s) might have entered the arena. What could that player be?

A moment of reflection provides an answer. That new player could only be the chloride ion (Cl^-) that was added systematically with H^+ in the form of HCl since nothing else was added.

As mentioned earlier, H^+ is very strongly bound to fixed anions[17g, 18f, 23f]. Accordingly, H^+ would have no trouble displacing and thus liberating the fixed (and some free) cation

originally bound to a fixed anion in the salt linkages they formed together (as illustrated in Figure 2 left.) In contrast, the Cl^- is by itself too weakly bound[55] to compete against and displace a fixed anion in a salt linkage. However, given the opening provided by the spearhead effect of H^+, it will now seize the opportunity to bind itself onto the liberated fixed cation. Put differently, Cl^- introduced as NaCl, for example, will not be able to displace the fixed anion of a salt linkage and becomes adsorbed on the liberated fixed cation as the study of Carr has shown[55]. Only the Cl^- introduced as HCl can bind onto the fixed cations.

(The experimentally established Cl^- binding further affirms the theoretical conclusion that for statistical mechanical reasons given, fixation of ionic sites on protein chains propels counter-ions to engage in close-contact association with fixed ions[56, 29]. This point known as the *principle of enhanced counter-ion association with site fixation* is made here in anticipation of the traditional aversion to the concept of ionic association among some influential protein chemists.)

Furthermore, there is another principle introduced in the AI Hypothesis that comes into play here. It is the *additivity principle*[18c] mentioned a few paragraphs above. As an example, we can say that the effective electron density of each backbone peptide carbonyl group expressed as its c-value analogue is determined not only by the intrinsic value of that group alone. Rather, it is that, *plus* the algebraic sum of the inductive effects of all other near and far linked groups and their respective adsorbents — according to the distance of separation between the inducing group and the target group and the target group's polarizability. Armed with this *additivity principle*, we examine next how adsorbed Cl^- could affect the q_{NaCl}.

Like its counterpart H^+, a Cl^- is also an uncomplicated single atom. However, unlike H^+, which carries a *positive* electric charge and acts as a *bona fide* EWC, a Cl^- carries a *negative* electric charge and acts as a *bona fide electron-donating* agent, or EDC. The adsorption of a Cl^- would therefore in theory produce a direct F-effect on the hemoglobin molecule opposite to that produced by H^+.

Now is the time to put this train of theoretical speculations and deductions to a test. To that end, we studied the (equilibrium) binding of both H^+ and Cl^- (added together as HCl) on a bovine hemoglobin solution, at a concentration of 19.2%. The results are shown in Figure 5. Note that before the H^+ binding curve (labeled A) reaches its maximum at pH 2.0, it too comprises two distinct segments — like the q_{NaCl} curve shown in Figure 4. However, there is also a difference. In Figure 4, Segment 1 has a higher slope than Segment 2; the opposite is the case of curve A in Figure 5. We will return to this subject shortly.

Since the midpoint of Segment 1 in Figure 5 is close to the pK_a of the imidazole groups (6.0), it confirms our earlier speculation that Segment 1 of Figure 4 originates from the binding of H^+ (alone) on the imidazole groups of the hemoglobin molecule. From the existing points in Figure 5, one can draw a curve. And from that curve, we then roughly extrapolate to a maximum of between 10 and 20 (averaging 15) moles of H^+-binding imidazole groups per mole of hemoglobin (or rbc NP unit) as the pH approaches zero. Subtracting this estimated 15 moles/ mole from the maximum of 92 moles/mole of the H^+-binding curve at a pH of about 2, we obtain a figure of 77 which is not too far from the total number of β-, and γ-carboxyl groups at 69 moles/ mole of hemoglobin[54]. This and a midpoint close to the pK_a of the β-, and γ-carboxyl groups (4.0) confirms our second

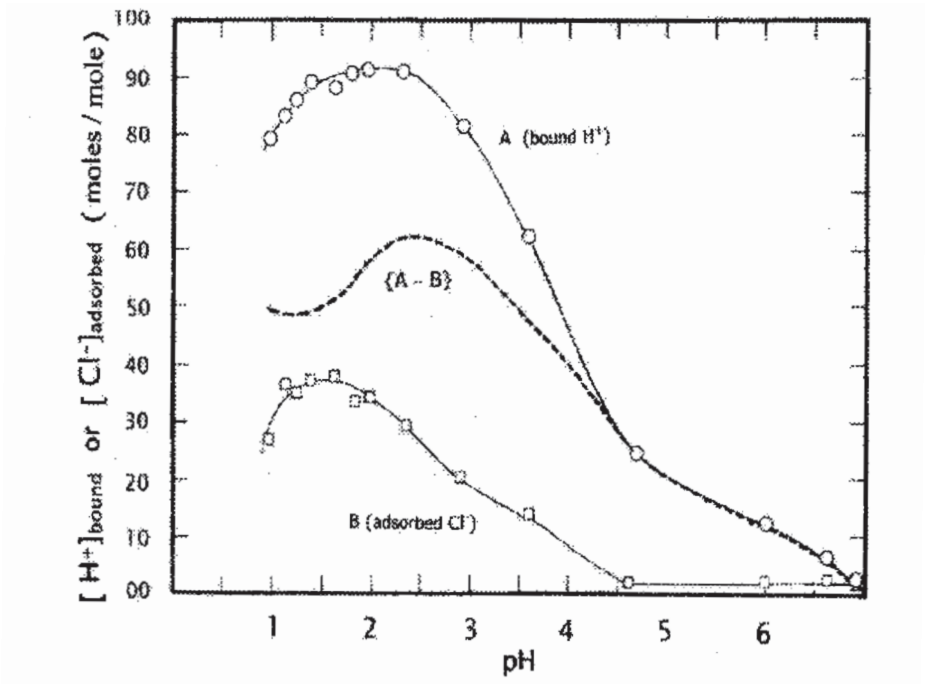

FIGURE 5. The binding of hydrogen ions (curve A) and adsorption of chloride ions (curve B) by 19.2% aqueous solution of bovine hemoglobin when different amounts of HCl were added to the bathing solutions. Curve labeled {A – B} is obtained by subtracting point by point Curve B from Curve A.

tentative assignment of Segment 2 in Figure 4 to originate mostly from the binding of H^+ on the β-, and γ-carboxyl groups.

The lower-most curve in Figure 5 is labeled B; it represents the Cl^- binding curve. Note that there is little binding of Cl^- from the HCl added until the pH has reached about 4.5. This shows that under the condition of the experiment, the Cl^- ion does not bind onto cationic imidazole groups at all. Instead, for the reason given above, they readily bind onto the (liberated) fixed cations when the pH falls below 4.5.

The absence of Cl^- binding at pH between pH 7 and 4 is important on two accounts. (1) It shows that we were right in attributing (without proof up to this moment) that the impact of HCl on the q_{NaCl} (as shown in Figure 3) to be caused by its H^+ component alone as an EWC. Now that we do have proof, it would be fitting to count this as an additional piece of supportive evidence that ATP, which acts like H^+, is also an EWC. (2) It explains why Segment 1 in Figure 4 has a higher slope than Segment 2. In Segment 1, H^+ acts alone in reducing q_{NaCl}, while in Segment 2, the *electron-withdrawing* influence of bound H^+ is counteracted and thus reduced by the simultaneous adsorption of the *electron-donating* Cl^-.

We turn next to what happens after the pH has fallen below 4.5. From there on down, Cl^- binding is on the rise. To better visualize its overall impact on q_{NaCl}, we began by making a simple assumption. That is, the electron withdrawing impact on q_{NaCl} created by the

binding of each H^+ is equal to, but opposite in direction to that produced by the binding of each Cl^-. (Space limitation forbids telling more about the detailed reasoning that led us to make this assumption.)

Based on this assumption, we subtracted point by point curve B from curve A and plotted the difference as the dashed line labeled {A – B.} Since we know in theory at least that H^+ binding lowers the q_{NaCl}, while Cl^- binding raises it, the theoretical prediction of the overall effect of H^+ and Cl^- binding together is revealed as the curve {A – B} *turned upside down*. And this upside down {A – B} curve also has the shape of an asymmetrical U with a minimum at pH between 2 and 3. In other words, the upside-down {A – B} curve in form replicates the observed q_{NaCl} vs. pH curve in Figure 4. A positive causal relation between the binding of both H^+ and Cl^- and q_{NaCl} is thus substantiated experimentally.

Additionally, we also begin to understand a little more about the fine structure of the asymmetric U-shaped curve of Figure 4. Thus, a minimum occurs at pH 2.2 because just before the pH has fallen to this value, the H^+ binding has already attained its full maximum while the Cl^- binding curve still has a way to go before reaching *its* maximum. Since H^+ binding lowers q_{NaCl} while Cl^- binding raises it, it is at this pH that q_{NaCl} sinks to its minimum.

As the pH falls still further below 2.2, q_{NaCl} begins to rise again (Segment 3), because the Cl^- binding continues to increase while the H^+ binding had ceased to increase and is beginning to decrease.

The parallelism between the inverted {A – B} curve in Figure 5 and the q_{NaCl} curve in Figure 4 affirms the 3 step scheme presented at the outset of R and D part 2. Regrettably, however, it does not tell us explicitly about the intermediate step 3b, i.e., the transformation of the protein from the folded α-helical conformation to the fully extended conformation. Indeed, step 3b tells us that in theory the percentage of the protein that stays in the α-helical conformation at each final pH value should also follow the inverted {A – B} curve and it too should show a minimum near pH 2 — just like that of the q_{NaCl} vs. pH curve shown in Figure 4. It was thus with great joy that we came upon belatedly a 19-year old paper telling us something about just that.

Predicted unfolding of α-helical fold and reversal retroactively affirmed

In 1990 Goto, Takahashi and Fink reported their study on the folding and unfolding of β-lactamase, cytochrome c and apomyoglobin in response to HCl[57]. They showed that increasing HCl caused all three proteins to undergo progressive loss of their α-helical content, reaching a maximum of unfolding at pH 2, or put differently, reaching a *minimum* of folding at pH 2. From there on, further pH decrease brought on by the addition of still more HCl caused the proteins to refold again. They then showed that the rise of α-helical content below pH 2 was caused by the binding of Cl^- to (each of) the protein under study.

In short, Goto and his coworkers had retroactively confirmed what the *c- analogue scheme* described as step 3b has predicted. And, we repeat that *pari passu* with the change of q_{NaCl} with the addition of HCl, the α-helical content follows a similar asymmetrical U pattern with a minimum at the pH close to 2. Thus, just as the data shown in Figure 4 provides a direct link between H^+ and Cl^- binding and the lowering of q_{NaCl}, Goto *et al*'s work establishes a direct link between H^+ and Cl^- binding and the unfolding of the α-helical conformation of the proteins that precedes and is instrumental in the lowering of q_{NaCl},

Materials and Methods

In our ultra-simple model (USM), we chose the hydrogen ion or H^+ as the principal cardinal adsorbent. It is the smallest atom minus its electron or a proton carrying a single positive electric charge. As such, H^+ is, in theory, our premiere authentic EWC (and will be used from now on as a standard EWC.) We chose H^+ as the principal cardinal adsorbent in our ultra-simple model over say, ATP, because our evidence that ATP is an EWC are entirely empirical — strong and consistently so as they are [17h, 21f, 58]. Since K^+ is not included in the makeup of the USM, H^+ would also substitute for K^+ in its role as the partners of fixed anions as shown in Figure 2 right (See below.)

Experimentally, we began by preparing a 40% solution of (exhaustively dialyzed) *pure* bovine methemoglobin (ferri-hemoglobin) (Sigma Chemical Co, St Louis, Mo., Catalogue No. H-2625, H-2500.) 0.4 gram portions of the 40% hemoglobin solution were steadily but forcefully injected through a catheter into bubble-free dialysis sacs made from quarter-inch Spectra Por 2 dialysis tubing (cut off point: 12,000-14,000 Daltons.) The bathing solutions of a fixed volume in which the filled sacs were incubated contained a constant concentration of 20 mM (or 10 mM) NaCl but varying initial concentration of HCl, ranging from 0 to 200 mM.

Hermetically sealed in paraffin film (*Parafilm*), each screw-capped glass tube containing the bathing solution and one or more dialysis sacs was then shaken for 5 or 7 days in a constant temperature water bath maintained at 25°C or in a refrigerator kept at about 9°C. This is 15 to 21 times longer than that required for the NaCl to reach diffusion equilibrium (i.e., 8 hours, from time course study.) Inclusion of the antiseptic thymol in trial runs, showed that in its absence, the systems studied were not adversely affected by microbial or fungal contamination.

During the incubation, the sacs, especially those exposed to a higher concentration of HCl, gained varying amount of water — reaching equilibrium in 4 days. Meanwhile, the contents of these sacs exposed to the higher concentrations of HCl, turned into a stiff gel, which could keep their shape after the dialysis sac membrane has been peeled off.

We used two methods of assaying the Na^+ concentrations. In the experiments to be described in detail, we employed a Na^+-selective combination glass electrode purchased from Thomas Scientific Co., of Philadelphia (Cat. #4230819.) In supportive experiments using radioactive Na-22 labels, we followed the detailed procedure given by Ling and Hu in 1988[37]. For pH and chloride ion measurements, we used respectively a Fisher glass membrane electrode (Catalog. # 315-75) and an Orion chloride ion electrode, Model 94-17A.

In the H^+ and Cl^- binding studies, the hemoglobin solution was not kept inside dialysis sacs, its hemoglobin concentration therefore stayed unchanged at 19.2%. This particular concentration of hemoglobin was chosen to approximate the hemoglobin concentration in the swollen dialysis sacs with final pH substantially below neutrality for reason that would become self-evident later. In this H^+ and Cl^- binding studies, we deliberated upon but decided against adding NaCl to the 19.2% hemoglobin solution. See ref.59.

Our main findings were expressed quantitatively in terms of the ratio of the equilibrium NaCl concentration in the bulk-phase water in the sac over that in the bathing medium. This ratio is, of course, the (true) *equilibrium distribution coefficient* or q-value of Na^+ (as chloride) and will be represented by the symbol $q_{NaCl.}$ This symbol rather than the

original designation will be cited frequently in Results and Discussion without further explanation.

As mentioned above, we will present results of our experimental studies in two parts. The first part shows the result of our attempt to use an ultra-simple model to test the theory that nano-protoplasm is the physical basis of life. The second part describes what we found out in our efforts to understand how and why we got what we got in the first part. And then there is also something else we did not count upon at first but is just as exciting.

We thank Dr, Raymond Damadian and his Fonar Corporation for continued support. For their tireless assistance and inexhaustible patience, we thank our librarian, Anthony Colella and our Director of Internet Service, Michael Guarino. We thank Dr. Ludwig Edelmann for his invaluable gift of EM picture of two human red blood cells shown here as Figure 1 and Dr.Wei-hsiao Hu for a large amount of the work he did in the 1980's while a post-doctorate scholar in our laboratory in Philadelphia. Much of his work will be published later; it encompasses another new and enticing subject, diversity of dynamic water structure.

References

1. Dujardin, F. *Annales des science naturelles: partie zoologique*, 2nd Sér. **4**, 343–377 (1835).
2. Schwann, T. *Mikroscopische Untersuchungen ηber die übereinstimmung in der Struktur und dem Wachstum der Thiere und Pfanzens* (Engelmann, Leipzig, 1839).
2a. Ibid p. 175. (p. 177 in ref. 3)
2b Ibid p. 197. (p. 197 in ref. 3)
3. Smith, H. *Microscopical Researches into the Accordance in the Structure and Growth of Animals and Plants,* (Siedenheim Society, 1847). (Reprinted by Kraus Reprint Co., New York, 1969).
4. Schultz, M. *Das Protoplasma der Rhizopoden und der Pflanzenzellen: ein Beitrag zur Theorie der Zellen* (Engelmann, Leipzig, 1863).
5. Huxley, T.H. On the physical basis of life. *Fortnightly Review* **5**, 129–145 (1869).
6. Abderhalden, E. *Zur quantitative Vergleich. Analyse des Blutes. Zs. Physiol. Chem.* **25**, 65–115 (1898).
7. Hodgkin, A.L. *The Conduction of the Nervous Impulse* (Liverpool Univ. Press, 1971). p. 28, Table 2.
8. Ling, G.N. What determines the normal water content of a living cell? *Physiol. Chem. Phys. & Med. NMR* **36**, 1–19 (2004). Also available at <http://www.physiologicalchemistryand physics.com/pdf/PCP36-1_ling.pdf>. Or, go to www.gilbertling.com, choose volume and article from drop-down list and click.
9. Ling, G.N. In response to an open invitation for comments on AAAS Project 2061's Benchmark Books on Science. Part 1. Documentation of serious errors in cell biology. *Physiol. Chem. Phys. & Med. NMR* **38**, 55–76 (2006). Also available at www.physiologicalchemistry andphysics.com/pdf/PCP38-55_ling.pdf Or, go to <www.gilbertling.com>, choose volume and article from drop-down list and click.
9a. Ibid p. 75, Endnote 1.
10. Ponder, E. *Hemolysis and Related Phenomena*, (Grune and Stratton, New York, 1948, 1971) pp.119–121.
11. Molecular Expression: Science, Optics and You. Timeline-Ernst Ruska. <http:micro.magnet. fsu.edu/optics/timeline/people/ruska/html>
12. Marchesi, V.T. and Palade, G. E. *J. Cell. Biol*. **35**, 385–404 (1967).
13. Jain, M. K. *The Bimolecular Lipid Membrane* (van Nostrand, 1972). p. 11, Figure 1–4.
14. Hardin, G. Meaninglessness of the word protoplasm. *Scientific Monthly* **82**, 112–120 (1956).

15. "Cell" Encyclopedia Britanica, 2009 Encyclopedia Online. 10 March, (2009) http://search.eb.com/eb/article 37477
16. Ling, G.N. History of the membrane (pump) theory of the living cell from its beginning in mid-19th century to its disproof 45 years ago — though still taught worldwide today as established truth. *Physiol. Chem. Phys. & Med. NMR* **39**, 1–67 (2007). Also available at <www.physiologicalchemistryandphysics.com/pdf/PCP39-1_ling.pdf>, Or, go to <www.gilbertling.com>, choose volume and article from drop-down list and click.
17. Ling, G. N. *Life at the Cell and Below-Cell Level: The Hidden History of a Fundamental Revolution in Biology* (Pacific Press, New York, 2001).
17a. Ibid pp. 152–153.
17b. Ibid p. 167.
17c. Ibid p. 184.
17d. Ibid p.161, Figure 46.
17e. Ibid pp.171–175.
17f. Ibid p. 93.
17g. Ibid p. 141.
17h. Ibid pp. 169–170.
17i. Ibid p. 140.
17j. Ibid pp. 143–148.
17k. Ibid p. 157.
17m. Ibid pp. 52–54 Figure 8.
18. Ling, G. N. *A Physical Theory of the Living State: the Association-Induction Hypothesis* (Blaisdell Publishing Co., Waltham, MA., 1962).
18a. Ibid p. 53, 163.
18b. Ibid p. 103.
18c. Ibid pp. 95–97, pp.111–120.
18d. Ibid. p. 57 Figure 4.2.
18e. Ibid p.189.
18f. Ibid p.77.
19. Ling, G.N. *In Search of the Physical Basis of Life* (Plenum Publ., New York, 1984) http://www.gilbertling.org/lp6c.htm.
20a. Ibid p. 324.
21. Ling, G. N. *A Revolution in the Physiology of the Living Cell* (Krieger Publishing Co., Malabar, FL, (1992).
21a. Ibid p. 138.
21b. Ibid p. 126–127, Figure 6–7.
21c. Ibid p. 147.
21d. Ibid p.184.
21e. Ibid p.144.
21f. Ibid pp.180–182.
21g. Ibid p. 189.
21h. Ibid p.196.
21i. Ibid p.146.
21j. Ibid pp. 132, Figure 6–11.
21k. Ibid pp. 118–121. Table 6.2.
21m. Ibid pp. 112–126.
22. Ling, G.N. A new model of the living cell: a summary of the theory and recent experimental evidence in its support. *Intern. Rev. Cytology* **24**, 1–61 (1969).
22a. Ibid p.47.
23. Ling, G.N. Nano-protoplasm: the ultimate unit of life. *Physiol. Chem. Phys. & Med. NMR* **39**, 111–234 (2007). Also available at <www.physiologicalchemistryandphysics.com/ pdf/PCP39-111_ling.pdf> Or, go to <www.gilbertling.com>, choose volume and article from drop-down list and click.

23a. Ibid p.136.
23b. Ibid p.137.
23c. Ibid p.172.
23d. Ibid pp. 147–152.
23e. Ibid p.142.
23f. Ibid p.176.
24. Best, C.H. and Taylor, N.B. *The Physiological Basis of Medical Practice,* 4th ed. (William & Wilkins, Baltimore, 1945). p. 7, col. 2.
25. Benesch, R.E. and Benesch, R. The mechanism of interaction of red cell organic phosphates with hemoglobin. *Adv. Prot. Chem*. **28**, 211–237 (1974).
26. Nakao, M., Nakao, T. Yamazoe, S and Yoshikawa, H. Adenosine triphosphate and shape of erythrocytes. *J. Biochem.* **49,** 487–492 (1961).
27. Ling, G.N. The theory of allosteric control of cooperative adsorption and conformation change: a molecular model of physiological activities according to the association-induction hypothesis. In *Cooperative Phenomena in Biology* (ed. George Karremann, Pergamon Press, New York, 1980).
28. Speakman, J.B. and Hirst, M.C. *Nature* **128**, 1073–1074 (1931).
29. Ling, G.N. An updated and further developed theory and evidence for the close-contact one-on-one association of nearly all cell K^+ with β-, and γ-carboxyl groups of intracellular proteins. *Physiol. Chem. Phys. & Med. NMR* **37**, 1–88 (2005). Also available at http://www.physiologicalchemistryandphysics.com/pdf/PCP37-ling.pdf Or, go to <www.gilbertling.com>, choose volume and article from drop-down list and click.
29a. Ibid p.46, Endnote 2.
30. Ling, G.N. The role of induction effect in the determination of protein structure. *Physiol. Chem. Phys. & Med. NMR* **18,** 3–16 (1986). Also available at <http://www. physiological-chemistryandphysics.com/pdf/PCP18-3__ling.pdf>. Or, go to <www.gilbertling.com>, choose volume and article from drop-down list and click.
31. Ling, G.N. The physical state of water in living cells and model systems. *Ann. N.Y. Acad. Sci.* **125**, 401–417 (1965).
32. Ling, G.N. A convergence of experimental and theoretical breakthroughs affirms the PM Theory of dynamically structured cell water on the theory's 40th birthday. In *Water and the Cell* (eds. Gerald H. Pollack, Ivan L. Cameron and Denys Wheatley, Springer, Dordrecht, the Netherlands, 2006).
33. Ling, G N. A quantitative theory of solute distribution in cell water according to molecular size. *Physiol. Chem. Phys. & Med. NMR* **25**, 145–175 (1993). Also available at <http://www.physiologicalchemistryand physics.com/pdf/PCP25-45_ling.pdf> Or, go to <www.gilbertling.com>, choose volume and article from drop-down list and click.
34. Ling, G N. Predictions of polarized multilayer theory of solute distribution confirmed from a study of the equilibrium distribution in frog muscle of twenty-one nonelectrolytes including five cryoprotectants. *Physiol. Chem. Phys. & Med. NMR* **25**, 177-208 (1993). Also available at <http://www.physiologicalchemistryand physics.com/pdf/PCP25-177_ling.pdf>, Or, go to <www.gilbertling.com>, choose volume and article from drop- down list and click.
35. Ling, G. N. A new theoretical foundation for the polarized-oriented multilayer theory of cell water and for inanimate systems demonstrating long-range dynamic structuring of water molecules. *Physiol. Chem. Phys. & Med. NMR* **35**: 91–130 (2003). Also available at <http://www.physiologicalchemistryandphysics.com/pdf/PCP35-91_ling.pdf>. Or, go to <www.gilbertling.com>, choose volume and article from drop-down list and click.
36. http://www.faqs.org/theories/Bo-Bu/Boltzmann-s-Distribution-Law.html
37. Ling, G.N. and Hu, W. Studies on the physical state of water in living cells and model systems. X. The dependence of the equilibrium distribution coefficient of a solute in polarized water on the molecular weights of the solute: experimental confirmation of the "size rule" in model systems. *Physiol. Chem. Phys. & Med. NMR* **29**, 293–307(1988). Also available at <http://www.physiologicalchemistryandphysics.com/pdf/PCP29-293_ling_hu.pdf>. Or, go to <www.gilbertling.com>, choose volume and article from drop-down list and click.

38. Ling, G.N. and Walton, C.L. What retains water in living cells? *Science* **191**: 293–295 (1976).
39. Ling, G. N. History of the membrane (pump) theory of the living cell from its beginning in mid-19th Century to its disproof 45 years ago — though still taught worldwide as established truth. *Physiol. Chem. Phys. & Med. NMR* **39**: 1–67 (2003). Also available at <http://www.physiologicalchemistryandphysics.com/pdf/PCP39-1_ling.pdf>. Or, go to <www.gilbertling.com>, choose volume and article from drop-down list and click.
40. Boyle, F.J. and Conway, E.J. Potassium accumulation in muscle and associated changes. *J. Physiol*. (London) **100**, 1–63 (1941).
41. Dean, R.B. Theories of electrolyte equilibrium in muscle. *Biol. Symp*. **3**, 331–348 (1941).
42. Troshin, A.S. *Problems of Cell Permeability*. (transl. M.G. Hell and W.F. Widdas, Pergamon, 1966).
43. Ling, G.N. How much water is made "non-free" by 36% native hemoglobin? *Physiol. Chem. Phys & Med. NMR* **36**, 143–158 (2004). http://www.physiologicalchemistryandphysics.com/pdf/PCP36-143_ling.pdf Or go to <www.gilbertling.com>, choose volume and article from drop-down list and click.
44. Ling, G.N. What befalls the protein and water in a living cell when the cell dies? *Physiol. Chem. Phys & Med. NMR* **37**, 141–158 (2004). http://www.physiologicalchemistryandphysics.com/pdf/PCP37-141_ling.pdf . Or go to <www.gilbertling.com>, choose volume and article from drop-down list and click.
45. Ling, G. N. Debunking the alleged resurrection of the sodium pump hypothesis. *Physiol. Chem. Phys & Med. NMR* **29**, 123–198 (1997). Also available at http://www.physiologicalchemistryandphysics.com/pdf/PCP29-ling.pdf. Or go to <www.gilbertling.com>, choose volume and article from drop-down list and click.
46. Ling, G.N. and Negendank, W. Do isolated membranes and purified vesicles pump sodium? A critical review and reinterpretation. *Persp. Biol. Med*. **23**: 215–239 (1980).
47. Brinley, F.J. and Mullin, L. J. Sodium extrusion by internally dialyzed squid axons. *J. Gen. Physiol*. **52**, 181–211 (1968).
48. http://www.gilbertling.org/lp6a.htm.
49. Ling, G.N. Maintenance of low sodium and high potassium levels in resting muscle cells. *J. Physiol* (London) **280**, 105–123 (1978).
50. Ling, G.N., Ochsenfeld, M.M., Walton, C. and Bersinger, T. J. Mechanism of solute exclusion from cells: the role of protein-water interaction. *Physiol. Chem. Phys.***12**, 3–10 (1980). Also available at <http://www.physiologicalchemistryandphysics.com/pdf/PCP12-3_ling_ochsenfeld_walton_bersinger.pdf>. Or go to <www.gilbertling.com>, choose volume and article from drop-down list and click.
51. Ling, G.N. and Ochsenfeld, M.M. The physical state of water in living cells and model systems. XII. The influence of the conformation of a protein on the solubility of Na^+ (sulfate), sucrose, glycine and urea in the water in which the protein is also dissolved. *Physiol. Chem. Phys. & Med NMR* **21**, 19–44 (1989). Also available at <http://www.physiologicalchemistryandphysics.com/pdf/PCP21-19_ling_ochsenfeld.pdf>. Or, go to <www.gilbertling.com>, choose volume and article from drop-down list and click.
52. Ling, G.N. and Hu, W.X. Studies on the physical state of water in living cells and model systems. VIII. Water vapor sorption on proteins and oxygen-containing polymers at physiological vapor pressure: presenting a new method for the study of vapor pressure at close to and including saturation. *Physiol. Chem. Phys. & Med. NMR* **19**, 251–269 (1987). Also available at <http://www.physiologicalchemistryandphysics.com/pdf/PCP19-251_ling_hu.pdf>. Or, go to <www.gilbertling.com>, choose volume and article from drop-down list and click.
53. Ling, G.N., Walton, C. and Bersinger, T. J.. Reduced solubility of polymer-oriented water for sodium sulfate, amino acids, and other solutes normally maintained at low levels in living cells. *Physiol.Chem.Phys.* **12**, 111–138 (1980). Also available at <http://www.physiologicalchemistryandphysics.com/pdf/PCP12-111_ling_walton_bersinger.pdf>. Or, go to <www.gilbertling.com>, choose volume and article from drop-down list and click.

54. Dayhoff, M.O. *Atlas of Protein Sequence and Structure* (National Biomedical Research Foundation, Washington, D.C., 1972).
55. Carr, C.W. Studies on the binding of small ions on protein solutions with the use of membrane electrodes II. The binding of chloride ions in solution of various Proteins. *Arch. Biochem. Biophys*. **46,** 417–423 (1953).
56. Ling, G.N. The role of phosphate in the maintenance of the resting potential and selective ionic accumulation in frog muscle cells. *Phosphorus Metabolism* Vol. II, 748–795 (W.D. McElroy and B. Glass, eds., Johns Hopkins University Press, Baltimore, Md., 1952).
57. Goto, Y. Takahashi, N. and Fink, A.L. Mechanism of acid-induced folding of proteins. *Biochem*. **29**, 3480–3488 (1990).
58. Ling, G.N. Oxidative phosphorylation and mitochondrial physiology: a critical review of chemiosmotic hypothesis and reinterpretation by the association-induction hypothesis. *Physiol. Chem. Phys. & Med. NMR* **33**, 29–96 (1981). pp. 86–87. Also available at <http://www.physiologicalchemistryand physics.com/pdf/PCP33-29_ling..pdf>. Or, go to <www.gilbertling.com>, choose volume and article from drop-down list and click.
59. We decided not to add NaCl to the 19.2% hemoglobin solution for the H^+ and Cl^- binding studies for several reasons. Two will be cited here. First, the contents of the dialysis sacs, which produced the data of Figure 4, are highly variable and often much lower than the initial concentrations due to the low q_{NaCl} — known only after the experimental data are in. This has made it hard to decide before the experiment what and which concentration of NaCl to duplicate. Second, as shown by Carr[55], in the form of NaCl, Cl^- does not bind onto hemoglobin significantly Thus, whatever concentration of NaCl we may choose to add, it could not conceivably give us any tangible benefit.

Received September 11, 2009;
accepted September 25, 2009.

Post Script

In order to reach a larger numbers of scientists, teachers and others directly or indirectly involved with biomedical science, we submitted this manuscript on August 6, 2009 to the Nature magazine of Great Britain — though it bore at that time a different title: *A Test of the Theory of Microscopic- or Nano-protoplasm as the Physical Basis of Life.*

Our article was promptly rejected without an explanation. Since we believe that this paper is of major historic importance, its offhand rejection represents an event that many would have believed impossible in the 21st century. To help them to understand the true situation, we decided that it would be worthwhile to reproduce below both our introductory letter to Nature's Editor-in-Chief, Dr. Philip Campbell and Nature's unsigned summary response.

We also decided to keep the manuscript in the format Nature requires. We made this decision to add another reminder of the major efforts long past due to improve our science education worldwide — of not only the practicing scientists themselves but all the others entrusted with the awesome responsibility of making critical decisions in science. Over time their decisions may have profound influence on the future of not only pure science itself but the future of humanity which needs trustworthy basic science more than ever (See also references 9 and 48.)

August 4, 2009

Dr. Philip Campbell,
Editor-in-Chief
Nature Magazine
Macmillan Building
4 Crinan Street
London N1 9XW

Dear Dr. Campbell:

I (and co-author) submit the enclosed article for consideration of publication in Nature. I made this choice for three reasons.

First, the results of the critical test conducted clearly and unequivocally show that Thomas Huxley was correct in advocating that life has a physical basis — despite the fact that most bio-medical scientists and teachers have rejected the concept in recent times for what I believe to be wrong reasons. In addition, the publication of our article in Nature would be a triumphant sequel to what the journal's founder, Sir Joseph Lockyer printed in the very first issue of your journal, his article, *Protoplasm at the Antipodes.* Since Sir Lockyer was also the first Editor-in-Chief and apparently wrote the overall objective of the journal still being printed on current issues, I can cite his words in persuading you to accept our article for publication in Nature.

Second, the work described is highly unusual in combining unprecedented *incisiveness* and utter *simplicity.* In one stroke, it has once again disproved the membrane pump theory (of the living cell) and establishes the alternative theory called the association-induction hypothesis — in a manner so plain that an average high school student would have no problem understanding its essence (if not all the details) in one reading.

Third, given the wide circulation your journal enjoys, the publication of our article in Nature could be, from a historical point of view, the first step in giving *all the young people of the world a uniting, shared purpose*. That is, to seek the one and only *truth* by way of the one and only *scientific method* and relying on the one and only *honesty* to make certain that the theory thoroughly refuted by objective evidence be promptly abandoned by all involved. In its place, the alternative theory that has been confirmed by overwhelming evidence be promptly and universally adopted and taught — until new evidence points to a still better theory. Failing that, we should continue to develop this established theory to serve as part of the established knowledge on which to build an ever better place for all humanity and other living creatures that share our planet to live and prosper in.

For your convenience, I am enclosing a copy of my fourth book, "Life at the Cell and Below-Cell Level." Skimming through the Preface of the book alone will give you an overall perspective far beyond what I can write here. I may also mention that very recently two Russian scientists at the Pavlov Institute of Physiology and the Leningrad Institute of Cytology have combined their resources in translating this book into Russian. The initial response has been very encouraging. Next I return to our submission and your standard procedure for deciding which paper to publish and which to reject: the peer review system.

In my opinion, the conventional peer review system is fundamentally not a good thing but perhaps tolerable for a science like astronomy, which has seen its revolutionary struggles centuries ago. For a science like cell physiology whose major progress still lies in the future, peer review is as tolerable as cyanide pills. However, if you are not allowed, or do not want to review our paper personally and if you have trouble finding *truly* qualified peers — for cause, see p.8 of www.gilbertling.org, on the front page of which are titles of (downloadable) relevant recent publications — I enclose the names and addresses of three world-class scientists who are men of high integrity and qualified to review our article.
Finally, I want to explain why I submit the article directly to you. It is too serious an event to be trusted to anyone else I know. True, you are an astronomer and not a cell physiologist. That is a distinct advantage I count upon. You have no peers to fear. The scientific issues involved are simple enough for any intelligent and fair-minded person to handle. After all, Sir Joseph Lockyer was also an astronomer. That did not prevent him from judiciously evaluating and supporting Thomas Huxley' work on protoplasm.

Sincerely yours,
Gilbert Ling, Ph.D.

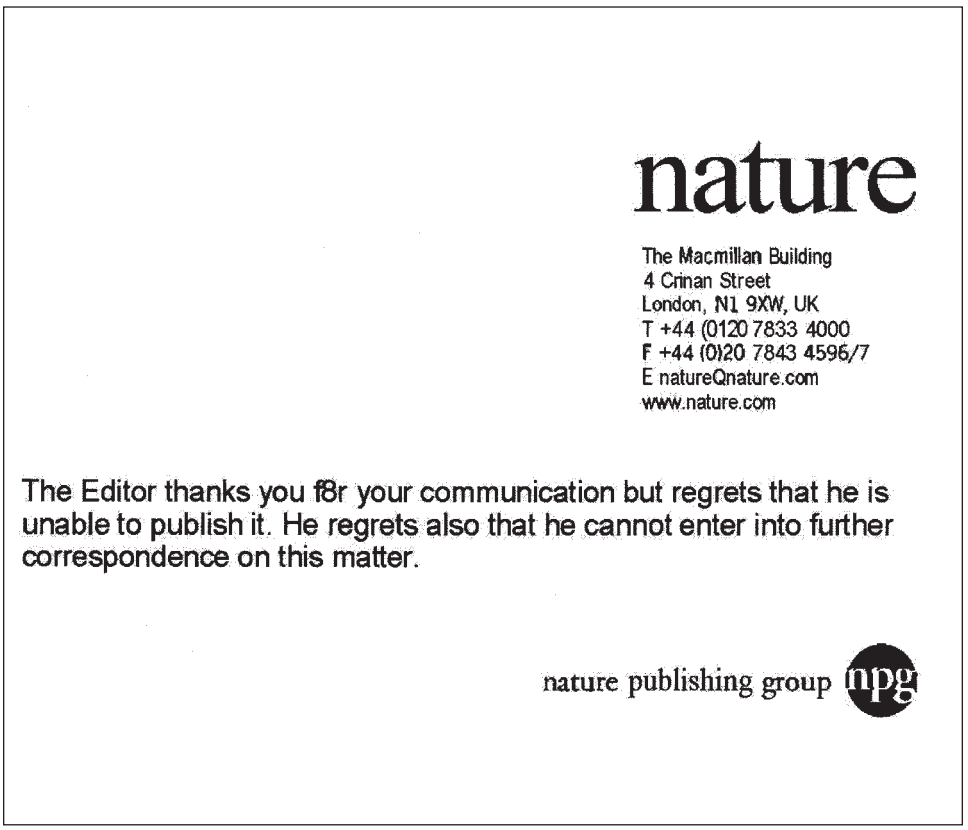

nature

The Macmillan Building
4 Crinan Street
London, N1 9XW, UK
T +44 (0120 7833 4000
F +44 (0)20 7843 4596/7
E natureQnature.com
www.nature.com

The Editor thanks you f8r your communication but regrets that he is unable to publish it. He regrets also that he cannot enter into further correspondence on this matter.

nature publishing group npg

Physiol. Chem. Phys. & Med. NMR (2008) *40*: 115–118

A Preliminary Report on the Survival of Fully-hydrated Living (Cancer) Cells to Liquid Helium Exposure

Gilbert N. Ling and Margaret M. Ochsenfeld

Damadian Foundation for Basic and Cancer Research, Fonar Corporation,
110 Marcus Drive, Melville, NY 11747
Email: gilbertling@dobar.org

Abstract: Fully-hydrated Ehrlich carcinoma ascites cells under the protective action of DMSO fully survived exposure to near-absolute zero temperature provided by liquid helium.

KEY WORDS: association-induction hypothesis, AI hypothesis, Bradley isotherm, cell water, DMSO, fully-hydrated cells, idealized NP system, liquid helium temperature, NaCl exclusion, non-freezing water, polarized-oriented multilayer theory, PM theory, POM theory, 0°K.

THE YEAR 1965 saw the addition to the theory of the living cell called the association-induction hypothesis (Ling 1962; 1997; 2001), the *polarized-oriented multilayer* (POM, or PM) theory of cell water. The POM theory was introduced to explain the low level of sodium ion (Na^+) as chloride (and other solutes like sucrose) in cell water (Ling 1965.) To achieve that end, the theory contends that all or virtually all cell water in living cells is polarized and oriented by the cell proteins. For many years afterwards, Bradley's multilayer adsorption isotherm has offered important support for the POM theory (Bradley 1936.) Notwithstanding, this and other then-existing theories had limitations. Thus, they could not provide key quantitative insights needed, including the depth of multilayers that can be so polarized (and oriented) by the polar surfaces (Ling 2003.)

By taking a short cut, Ling derived a new theoretical foundation for his POM theory of cell water and inanimate systems demonstrating long range dynamic structure. The theory began by defining and calling a checkerboard of positively- and negatively charged sites of a rigorously defined geometry and dimension as an *idealized NP system.* The theory then shows that under idealized conditions — including 0°K temperature, freedom from any kind of disturbance etc. — the propagated polarization-orientation of bulk-phase water molecules produced by such an idealized NP system could proceed *ad infinitum.*

In addition, the theory predicts that water so polarized and oriented would not freeze at any attainable low temperature. This prediction was confirmed retroactively some fifty years before when Canadian chemists, Giguère and Harvey discovered unintentionally that thin films of water held between polished silver chloride lenses — which possess crystal structure nearly ideal as defined in the new theory — would not freeze at liquid nitrogen temperature (–196°C or 77° K.) (Giguère and Harvey 1956)

Following the introduction of the POM theory in 1965, unusual properties of water in the living cell and model systems beyond the low solvency for NaCl were examined one by one in the light of the new theory. (For a full list of these attributes, see Ling 1992, Table 5.5 on pp. 208–209.) One of these additional attributes is the demonstrated ability of living cells to survive freezing and thawing in liquid nitrogen when a *cryoprotective agent* like glycerol or dimethyl sulfoxide (DMSO) was added to the freezing medium (for review, see Smith 1961.) And in time, the predictions of the POM theory was confirmed not only for these two physiological manifestations — Na(Cl) exclusion and survival in freezing temperature — but for six other manifestations listed in the table quoted above as well.

Ling and Zhang studied the freezing and thawing behaviors of two categories of model systems referred to as the extrovert and introvert respectively (Ling and Zhang 1983.) Extrovert models include proteins that for structural reason, like gelatin, or in response to denaturants, like urea, exist in the *fully-extended* state and various linear oxygen carrying polymers including polyethylene oxide, polyvinylpyrrolidone. Introvert models include mostly what are often (erroneously) called "native" proteins. In most of our studies with a Perkin Elmer differential scanning calorimeter, the low temperature was provided by a mixture of dry ice and ethanol. In a smaller number of runs, we used liquid nitrogen. The lowest temperature reached in our runs was around 123° K.

From these model studies, Ling and Zhang confirmed most if not all of what was theoretically predicted. Thus, in solutions up to as high as 50% concentration, the six introrvert "native" proteins investigated demonstrated no detectable influence on either the freezing temperature of the bulk phase water or the width of its freezing peak — in a plot of heat absorption or release against increasing (or decreasing) temperature. In contrast, all the extrovert models uniformly demonstrate strong influence on the freezing (and thawing) pattern of the bulk-phase water. Thus with increasing polymer concentration, the freezing temperatures became steadily lower and the freezing peak became progressively wider — so that at the highest polymer concentration, the freezing peak disappeared altogether. The vanishing freezing peak shows that a state of non-freezing had been brought about by the extrovert models.

That extrovert models can lower the freezing temperature of the bulk phase water and make it unfreezable is important. It demonstrates that closer juxtaposition of water-polarizing and orienting sites enhances the stability of the dynamic polarized-oriented water. As such, it offers an explanation why glycerol, dimethyl sulfoxide (DMSO) and other cryoprotectants help to preserve living cells from fatal injury from freezing and thawing: Because these cryoprotectants as a rule form strong H-bonds with water molecules and by so doing further enhance the water-to-water interaction energy of the bulk phase water in the resting cell by the fully extended protein chains and make the cell water unfreezable. (See also Ling, Niu and Ochsenfeld 1993, pp. 193–195; Ling 2006)

That increasing the concentration of the extrovert models could cause non-freezing also offers an explanation why only after severely lowering of the water content (to 8%) could

the larvae of the West African beetle, *Polypedilum vanderplanki* survive exposure to liquid helium (Hinton 1960.)

The purpose of this preliminary study is to find out if living cells in their normal fully hydrated state could also survive exposure to liquid helium when the cells are under the protection of the cyoprotectant, DMSO (Lovelock and Bishop 1959.) If this proves successful, it would go one step further confirming the theory of non-freezability at *any* attainable low temperature when the bulk phase water is polarized and oriented like that in the idealized NP system.

Materials and Methods

Ehrlich carcinoma ascites cells were carried in ICR mice and routinely harvested 14 days after abdominal injection. The ascites fluid was mixed with Sigma RPMI 1640 medium before low speed (900 rpm) centrifugation and resuspension of the cells in similar medium and centrifugation a second time. 0.5 to 0.7 gram of the cell pellet was then suspended in 5 ml of a freezing medium (76% RPMI medium, 16% newborn calf serum and 8% DMSO.) The suspension was then further diluted with similar freezing medium by mixing 0.85 ml of the suspension in 20 ml of the freezing medium and 2 ml aliquots of the suspension placed in 2 ml sterile cryo-tubes. After 2 hours of gentle shaking in a refrigerator kept at about 9° C, the cryotubes containing the ascites cells were suspended over-night inside a standard 10 liter liquid nitrogen tank at about 13 inches below the top of the tank and about 6–7 inches from the surface of the liquid nitrogen beneath. The cells in the cyrotubes were then lowered into the liquid nitrogen.

To expose the ascites cells to near absolute zero temperature, we allowed liquid helium to flow over the cryotubes — containing the liquid-nitrogen frozen ascites cells — in a Dewar jar for a total duration of 5–10 minutes.

Results and Discussion

The viability of the ascites cells were examined after staining with erythrosin B. Sample cells taken before freezing in liquid nitoroten was 97.7% ; it fell to 81% after freezing in liquid nitrogen. Following the exposure to liquid helium, the viability stayed essentially unchanged at 86% survival.

Before exposing to the liquid helium, the ascites cells had been in liquid nitrogen four days at the temperature of –196° C or 77.2° K. Liquid heliium could provide a temperature of 1.9° K as it was maintained at the Large Hadron Colllider at CERN in Switzerland. The usually given value is 3 to 4° K. The temperature our samples sank to was unknown but it is certainly much lower than 77° K. The fact that the viability remained entirely undiminished by further lowering of temperature gives us the assurance that the theoretical prediction that living cells in the presence of cryoprotectant DMSO could indeed survive temperature close to the temperature of liquid helium and hence absolute zero.

We thank Dr. Raymond Damadian and the Fonar Corporation for their continued support.

References

Bradley, R.S. (1936) Polymolecular Adsorbed Films. Part II. The General Theory of the Condensation of vapors on finely divided solids. *J. Chem. Soc.* 1936: 1799–1804.

Giguère, P.A. and Harvey, K.B. (1956) On the infrared absorption of water and heavy water in condensed states. *Canad. J. Chem*. 34: 798–808.

Henniker, J.C. (1949) The depth of the surface zone of a liquid. *Reviews of Modern Physics* 21: 322–341.

Hinton, H.E. (1960) A fly larva that tolerates dehydration and temperture of –270 C to +102 C. *Nature* 188: 333–337.

Ling, G.N. (1962) *A Physical Theory of the Living State: the Association-Induction Hypothesis*, Blaisdell Publ. Co., Waltham, MA.

Ling, G.N. (1965) The physical state of water in living cells and in model systems. *Ann. N.Y. Acad. Sci.* 125: 401–417.

Ling, G.N. (1992) *A Revolution in the Physiology of the Living Cell,* R. Krieger Publ.Co., Malabar. FL

Ling, G.M\N. (1997) http://www.gilbertling.org

Ling, G.N. (2001) *Life at the Cell and Below-Cell Level: the Hidden History of a Fundamental Revolution in Biology,* Pacific Press, NY.

Ling, G.N. (2003) A new theoretical foundation for the polarized-oriented multilayer theory of cell water and for inanimate systems demonstrating long-range dynamic structuring of water molecules. *Physiol. Chem. Phys. & Med. NMR* 35: 93–130. Also available at: http://www.physiologicalchemistryandphysics.com/pdf/PCP35-91_ling.pdf Or go to www.gilbertling.org choose volume and article from drop-down list and click.

Ling, G.N. (2006) Chapter 1. A convergence of experimental and theoretical breakthrough affirms the PM theory of dynamically structured cell water at the theory's 40th birthday in: *Water and the Cell (Pollack, G.H., Cameron, I.L. and Wheatley, D.N., eds.) Springer Verlag, Berlin, New York.* Can also be reached by going to www.gilbertling.org and click the title on the front page of the website.

Ling, G.N. and Zhang, Z. (1983) Studies on the physical state of water in living cells and model systems. IV. freezing and thawing point depression of water by gelatin, oxygen-containing polymers and urea-denatured proteins. *Physiol. Chem. Phys. & Med. NMR* 15: 391–406. Also available at: http://www.physiologicalchemistryandphysics.com/pdf/PCP15-3911_ling_zhang.pdf Or go to www.gilbertling.org choose volume and article from drop-down list and click

Ling, G.N., Niu, Z. and Ochsenfeld, M. (1993) Predictions of polarized multilayer theory of solute distribution confirmed from a study of the equilibrium distribution in frog muscle of twenty-one nonelectrolytes including five cryoprotectants. *Physiol. Chem. Phys. & Med. NMR* 25: 177–208. Also available at: http://www.physiologicalchemistryandphysics.com/pdf/PCP25-177_ling_niu_cohsenfeld.pdf Or go to www.gilbertling.org choose volume and article from drop-down list and click.

Lovelock, J.E. and Bishop, M.W.H. (1959) Prevention of freezing damage of living cells by dimethyl sulfoxide. *Nature* 183: 1394–1395.

Smith, A. U. (1961) *Biological Effects of Freezing and Supercooling*, Williams and Wilkins, Baltimore.

Received August 5, 2009;
accepted September 10, 2009

Physiological Chemistry and Physics and Medical NMR
INDEX
Volume 40, 2008